

博士学位論文
Doctoral Dissertation

Searching for neutral lipid regulators in mammalian cells
from natural resources

北里大学大学院 薬学研究科 薬科学専攻 博士課程
微生物薬品化学
DP-20101 Elyza Aiman Azizah Nur

Table of Contents

Abbreviation table

I. Introduction	1
II. Main	10
Chapter I. Polyacetylenes from <i>Atractylodes</i> rhizome extract	11
1-1. Introduction of <i>Atractylodes</i> rhizome	11
1-2. Extraction and isolation of compounds from <i>Atractylodes</i> rhizome	12
1-3. Compound identification	14
1-4. Inhibition of neutral lipid synthesis	14
1-5. Discussion	16
1-6. Supplemental data	17
Chapter II. Terpendole congeners from <i>Volutella citrinella</i> BF-0440	25
2-1. Fungus BF-0440 strain identification	26
2-2. <i>V. citrinella</i> BF-0440 strain fermentation and isolation of compounds	26
2-3. Structure elucidation of new terpendole O	31
2-4. Structure elucidation of new terpendole N	38
2-5. Structure elucidation of new terpendole P	42
2-6. Other terpendole congeners identification	45
2-7. Inhibition of SOAT isozymes using SOAT1- and SOAT2-CHO cells	45
2-8. Discussion	47
2-9. Supplemental data	50
Chapter III. Screening for neutral lipid degradation potentiators	86
3-1. Establishment of cell-based lipid degradation assay for screening	86
3-2. Screening result for neutral lipid degradation potentiators from microbial sources	89
3-3. Purification and identification of active compounds	90

3-4. Effect of microbial potentiators on neutral lipid degradation in CHO-K1 cells	90
3-5. Discussion	91
3-6. Supplemental data	95
III. Summary	101
IV. Experimental Methods	105
V. Acknowledgments	123
VI. References	125

Abbreviation Table

ACC:	adrenocortical carcinoma
ADP:	adenosine diphosphate
BARS:	brefeldin A-induced ADP-ribosylated substrate
BRA:	brefeldin A
BSA:	bovine serum albumin
BV:	beauveriolide
CE:	cholesteryl ester
CETP:	cholesteryl ester transfer protein
CHO:	chinese hamster ovary
CoA:	coenzyme A
COSY:	correlation spectroscopy
CtBP1:	C-terminal-binding protein 1
CVD:	cardiovascular disease
DGAT:	diacylglycerol acyltransferase
DMSO:	dimethyl sulfoxide
DPA:	dinapinone A
EC ₅₀ :	a drug concentration causing 50% effect of biological activity
EDTA:	ethylenediamine tetraacetic acid
ER:	endoplasmic reticulum
ESI:	electrospray ionization
EtOAc:	ethyl acetate
EtOH:	ethanol
FBS:	fetal bovine serum
FDA:	food and drug administration
H:	human
HCC:	hepatocellular carcinoma
HDL:	high-density lipoprotein
HAM's F12:	ham's F12 nutrient mixture
HMBC:	heteronuclear multiple bond correlation
HMG-CoA:	3-hydroxy-3-methylglutaryl-coenzyme A

HSQC: heteronuclear single quantum correlation
HPLC: high performance liquid chromatography
IC₅₀: a drug concentration causing 50% inhibition of biological activity
i.d.: internal diameter
IR: infrared
LDL: low-density lipoprotein
M: molecular (adduct ion)
MeOH: methanol
Min: minute
MS: mass spectrometry
NAFLD: non-alcoholic fatty liver disease
NASH: non-alcoholic steatohepatitis
NMR: nuclear magnetic resonance
NOE: nuclear Overhauser effect
NOESY: nuclear Overhauser effect spectroscopy
NTD: *N*-terminal hydrophilic domain
ODS: octadecylsilyl
PBS: phosphate buffered saline
PCSK9: proprotein convertase subtilisin/kexin type 9
PDA: potato dextrose agar
PL: phospholipid
PPAR: peroxisome proliferator-activated receptor
ppm: parts per million
PPPA: pyripyropene
P/S: penicillin/streptomycin
R_f: relative to front
ROESY: rotating Overhauser effect spectroscopy
rpm: rotation per minute
S: supplemental
SDS: sodium dodecyl sulfate
SOAT: sterol *O*-acyltransferase
TG: triacylglycerol
TLC: thin layer chromatography

TM: transmembrane

Tris: 2-amino-2-hydroxymethyl-1,3-propanediol

UFLC: ultra-fast liquid chromatography

UV: ultra violet

V-ATPase: vacuolar adenosine triphosphatase

I. Introduction

Natural products, chemical substances derived from animals, plants and microbes, have historically been used as a rich source for drug discovery. These natural compounds formed by living systems are broadly classified into primary metabolites and secondary metabolites. Compounds that existed in all cells and play an important role in the metabolism and reproduction of those cells are known as primary metabolites. Nucleic acids and common amino acids and sugars fall into this category. On the other hand, secondary metabolites are compounds which not directly involved in biological phenomena, such as defensive substances, attractants and pheromones [1].

These secondary metabolites have been regarded as an important drug discovery source since ancient times. One of the most famous natural product discoveries is penicillin from the fungus, *Penicillium notatum* discovered by Fleming in 1929. The antibiotic streptomycin was discovered soon after penicillin was introduced into medicine. Waksman isolated streptomycin from soil actinobacterium *Streptomyces griseus* in 1943. Since penicillin and streptomycin were effective therapeutic drugs for infectious diseases, which were a serious problem at the time, a worldwide endeavor to discover new antibiotics from microorganisms happened between 1940 to 1970 [2]. Drug discovery from microorganisms had also evolved from infectious diseases to a wide range of biological activities, including cancer and metabolic diseases. Notably, dyslipidemia drugs such as lovastatin [3] from the fungus *Aspergillus terreus*, immunosuppressive drug cyclosporine [4] from fungus *Tolypocladium inflatum* and antiparasitic drug avermectin [5] from actinomycete *Streptomyces avermitilis*, which have diverse structures and bioactivities. Feher, *et al.* showed that natural products provide more structurally diverse compounds compared to the synthetic compounds [6]. A continued analysis of new drugs approved by the US Food and Drug Administration (FDA) from 1981 to 2019 [7], showed that more than 60% of those drugs (except biologicals and vaccines) were natural products or derivatives/modifications of natural products. These showed the importance of natural products especially microorganism as drug discovery resources.

Cardiovascular diseases remain the leading cause of disease burden in the world. Cardiovascular diseases (CVDs) are a group of disorders of the heart and blood vessels. The number of prevalent cases of all CVD nearly doubled from 271 million in 1990 to 523 million in 2019, and the mortality toll from CVD rose significantly from 12.1 million in 1990 to 18.6 million in 2019. There is an emergence of cardiovascular disease in developing countries such as Indonesia [8]. Listed as 10 most common diseases by

Indonesian Ministry of Health Information Center, the change to unhealthy lifestyle, lack of exercise and trend in junk food increased the prevalence of this disease [9]. Cardiovascular disease is the second leading cause of mortality in Japan, while the cerebrovascular disease is the fourth, accounting for roughly 25% of all deaths within this nation in 2015 [10].

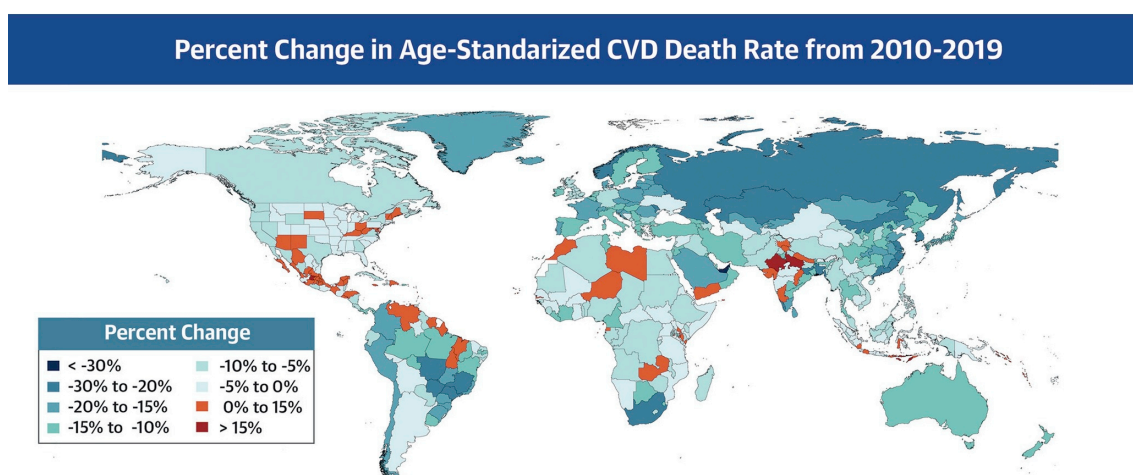


Figure 1. Global Burden of Cardiovascular Diseases, 2010–2019 [8].

Leading risk factors for cardiovascular diseases are high blood pressure, high low-density lipoprotein (LDL) cholesterol, low high-density lipoprotein (HDL) cholesterol, high triacylglycerides, diabetes, smoking and secondhand smoke exposure, obesity, unhealthy diet, and physical inactivity. Halting the rise in cardiometabolic risk factors is crucial to reduce the global burden of cardiovascular diseases [11, 12]. The basic treatment is the improvement of lifestyles such as diet and exercise therapy, but pharmacotherapy is needed if a sufficient effect cannot be obtained. Hyperlipidemia is critically involved in the progression of atherosclerosis and acute coronary syndromes, and prophylactic treatment has been carried out with the therapeutic goal of reducing low-density lipoprotein (LDL) in the blood [13-15]. The first-line drug, statin, works as 3-hydroxy-3-methylglutaryl CoA (HMG CoA) reductase inhibitor that blocks hepatic cholesterol synthesis to lower the serum low-density lipoprotein (LDL) level and retorted the progression to atherosclerosis [16-18]. Statins also decrease triglyceride levels in patients with hypertriglyceridemia [19]. Statins were developed from fungi-derived compactin [20] as a lead and are considered as one of the most important compounds in natural drug discovery. However, only 30-40% of statins treatments were reported to

suppress cardiovascular events (such as myocardial infarction and angina pectoris) [21]. Therefore, in general, it is used in combination with another drug with a different mechanism of action. There are drugs such as ion exchange resin preparation, cholestyramine [22] for lowering blood cholesterol, and ezetimibe [23] that suppress cholesterol absorption from the small intestine. Although the combination of statin, simvastatin and ezetimibe decrease LDL levels in blood, there is no significant difference observed in carotid intima thickening, a part of atherosclerosis development [24, 25]. Thus, the development of drugs having a different mechanism of action from statins has been actively conducted. Agents that targeted Proprotein Convertase Subtilisin/Kexin type 9 (PCSK9) [26] inhibits the degradation of LDL receptor leading to the decrease of blood LDL and inhibited Cholesteryl Ester Transfer Protein (CETP) [27] for mediating the exchange of cholesteryl esters and triacylglycerides between lipoprotein leading to the increase of high density lipoprotein (HDL) level in blood. PCSK9 inhibitors have been shown to be effective alone or in combination with statins [28]. However, because it is an antibody drug, the cost is relatively expensive, and the administration route is limited. In addition, since the CETP inhibitors were failing in phase III clinical trials [29], the prevention and treatment of atherosclerosis disease are still not sufficient with existing drugs alone. Underlying the process of most cardiovascular diseases, excessive accumulation of neutral lipids, cholesteryl ester (CE) and triacylglycerol (TG), can be built up in the endothelial cell, leading to plaque formation in the artery [30, 31]. Therefore, the inhibition of these neutral lipids might prevent/treat atherosclerosis.

Excessive accumulation of CE and TG *in vivo* has been shown to cause arteriosclerosis as well as fatty liver [32-34]. Fatty liver disease is an abnormal accumulation of CE and TG in the liver. It can be caused by alcohol and obesity as for non-alcoholic fatty liver. Among them, non-alcoholic fatty liver (NAFLD) has been increasing worldwide. NAFLD prevalence in Japan and Indonesia was estimated to be more than 30% [35]. In Japan, this number was increasing in 2003 from 12.6% before 1990 and 30.3% in 1998 [36].

The severe form of NAFLD, Non-Alcoholic Steatohepatitis (NASH), which is characterized by inflammation and fibrosis in addition to lipid accumulation in liver, can potentially progress to advanced liver disease, cirrhosis and hepatocellular carcinoma (HCC) [37]. Currently there are no biomarkers for NASH and an invasive liver biopsy is needed for diagnosis. As steatosis, lobular inflammation and hepatocellular ballooning

become the gold standard for diagnosing NASH, other histopathological features such as hepatocellular glycogenotic nuclei, lipogranuloma, and acidophil bodies can also be observed [38]. Up until now, the US Food and Drug Administration (FDA) has not approved any therapeutic agents for NAFLD/NASH and pharmacotherapy treatment are relatively limited. Pioglitazone, an antidiabetic drug which selectively stimulated the nuclear receptor peroxisome proliferator-activated receptor gamma (PPAR- γ), has been used by many clinicians, PPAR- γ -agonist showed an improvement to all histopathologic features of NASH. However, pioglitazone has not been studied further to patients with cirrhosis and its long-term administration has been associated to weight gain, postmenopausal bone loss and congestive heart failure. Vitamin E treatment showed an improvement in steatosis, inflammation and ballooning in nondiabetic NASH patients. There are several novel therapeutics in development for NASH, but they are still in phase 2 or planned to enter phase 3 of clinical trials [39]. With rapid disease progression, hard yet invasive diagnosis and limited therapeutic options, NAFLD/NASH remains as a big problem at present.

Against these backgrounds, our research group has been focusing on lipid metabolism for many years. Using various cells and enzyme assay systems, we discovered small molecules that control lipid metabolism from the secondary metabolites of microorganism. We found novel substances that have neutral lipid (CE or TG) accumulation inhibitory activity in cell based assay using mouse macrophages, such as beauveriolide III [40], phenochalasin A [41], and sespendole [42] (Figure 3). In particular, beauveriolide III has been demonstrated to be effective *in vivo* against arteriosclerosis model mice and has the potential to be a leading compound for the treatment of arteriosclerosis [40, 43]. The diacylglycerol acyltransferase (DGAT) inhibitors, roseline [44] and amidepsines [45], and sterol *O*-acyltransferase (SOAT) inhibitor, pyripyropenes [46] (Figure 3) were discovered in an assay system using rat liver microsomes.

In particular, SOAT has been expected as one of the molecular targets for the development of anti-hypercholesterolemia and anti-atherosclerosis agents. SOAT synthesized CE by introducing an acyl group to the hydroxyl group at the 3-position of cholesterol. SOAT plays important roles in mammals, for example, in the absorption of dietary cholesterol from the intestines, production of lipoprotein in the liver and formation of foam cells from macrophages in the arterial walls (Figure 2). Therefore, SOAT

inhibition is expected not only to lower plasma cholesterol levels, but also to have a direct effect on the arterial wall.

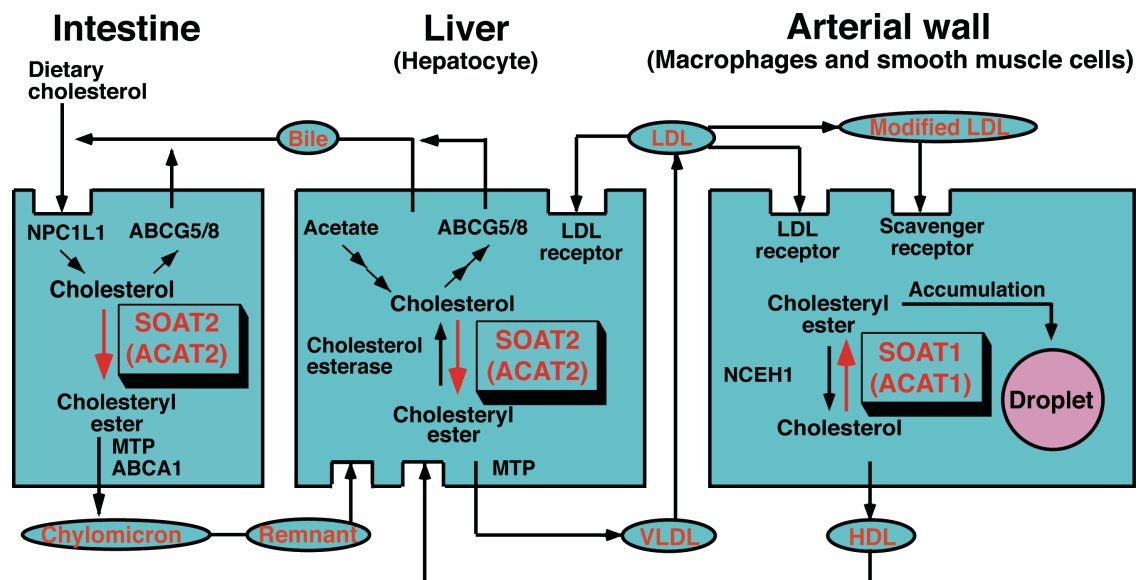


Figure 2. Functions of SOAT. There are two SOAT isozymes [47].

SOAT1 is ubiquitously expressed in most tissues and cells, including macrophages, smooth muscle cells and Kupffer cells. SOAT2 is exclusively expressed in the small intestine and liver.

Numerous pharmaceutical companies have been developing SOAT inhibitors since 1980s [48], but the development of synthetic SOAT inhibitors has been stopped due to side effect problems [49] and has not yet been put into practical use. Over years, along with the development of molecular biological research, SOAT was found to have two isozymes, SOAT1 and SOAT2 [50-53]. SOAT1 is expressed in almost all tissue and cells primarily in the Kupffer cells of the liver, in non-mucosal cell types in the intestine, and in kidney and adrenal cortical cells, whereas SOAT2 is absent from arteries but localized in the intestinal mucosal cells and hepatocytes [52]. Cholesterol esterification by SOAT2 supports separate functions compared to SOAT1, where SOAT1 appears to be responsible for maintaining cholesterol availability in cell membranes, SOAT2 has been shown to be involved in the absorption of dietary cholesterol [54, 55]. Human and mouse SOAT2 are about 40% identical to human SOAT1. Other characteristics of SOAT isozymes were listed in Table 1. Studies in mouse models of atherosclerosis showed reduced amounts of atherosclerosis when SOAT2 was deficient [56], while in SOAT1 deficient, atherosclerosis lesions were worsened and side effects such as dry eye and xanthomatosis

were observed [57-59]. Recently, gene depletion of SOAT2 in mice improves hepatic steatosis [60, 61].

Table 1. Characteristics of SOAT isozymes [47, 62-64].

Characteristics	SOAT1	SOAT2
Amino acids	550 (human, monkey), 540 (mouse)	550/522 (human), 526 (monkey), 540/525 (mouse)
Substrate specificity		
Sterol	Cholesterol, Oxysterols	Cholesterol, Oxysterols
Acyl-CoA	Long-chain fatty acid (16:0, 18:1, 18:2, 20:4)	Long-chain fatty acid (16:0, 18:1, 18:2)
Subunit	Dimer of dimer	Dimer of dimer
Distribution	All tissues and cells including macrophages and steroidogenic cells	Small intestine and liver
Location	Endoplasmic reticulum	Endoplasmic reticulum
Transmembrane domains (TMs)	9 (with 2 intracellular helices and 1 extracellular helices)	9 (with 2 intracellular helices and 1 extracellular helices)
Active site	Ser269 (human, monkey) or His460 (human)	Ser245 (human), Ser249 (monkey) or His434 (human)

On the other hand, SOAT1 inhibition gaining some attention as anti-cancer in recent years. Genetically silencing SOAT1 in glioblastoma suppressed its growth by blocking the lipogenesis in the cancer cells [65]. A dual SOAT inhibitor, nevanimibe, raised the possibility of targeted SOAT1 inhibition as a treatment for adrenocortical carcinoma (ACC). Nevanimibe is currently under clinical evaluation (Phase 2) for the treatment of ACC and congenital adrenal hyperplasia [66]. These results suggested the difference and selectivity importance of SOAT isozymes inhibitors.

Our research group has established cell-based assays using AC29 cells (SOAT-deficient CHO cells) expressing African green monkey SOAT1 (agmSOAT1-CHO) and SOAT2 (agmSOAT2-CHO) [67] also human SOAT1 (hSOAT1-CHO cells) and human SOAT2 (hSOAT2-CHO cells) to investigate the selectivity toward SOAT isozymes [68, 69]. To this day, beauveriolide III was discovered as a selective inhibitor for SOAT1 and pyripyropene A (PPPA) which has a meroterpene skeleton as selective inhibitor for SOAT2. We also discovered dual-type inhibitors with various skeletons such as a fatty chain, diketopiperazine, or indole diterpene skeleton (Figure 3) [70-77].

So far, the structure of SOAT localized in the endoplasmic reticulum membrane had not been defined. Very recently, three research groups have just reported the structure of human_SOAT1 [62, 63, 78] and human_SOAT2 [64] using cryo-electron microscopy.

hSOAT1 and hSOAT2 are dimer of dimers with N-terminal hydrophilic domain (NTD). Each monomer consists of nine transmembrane segments (TMs), three helices on intracellular side and one helix on the extracellular side, with cytosolic tunnel and transmembrane tunnel that connected to the catalytic site. In addition to that, a site with the allosteric activator, cholesterol, in each monomer was confirmed. Co-purification of SOAT2 with its selective inhibitor, PPPA, showed that PPPA selective binding sites in SOAT2 are distinct compared to dual inhibitor, nevanimibe. PPPA binds to Phe438, Gln488, and Val489 residues in SOAT2 which are all leucine in SOAT1 [64]. However, the purified SOAT1 and SOAT2 selectivity against PPPA were relatively smaller than our laboratory data which raised incredulity to the validity of the reported SOAT2 structure.

We also established a cell-based assay using CHO-K1 cells and discovered dinapinone A (DPA) and congeners from the culture broth of *Talaromyces pinophilus* FKI-3864[79-81]. Biaryl dihydronaphthopyranone atropisomers, dinapinone A1 (DPA1) and A2 (DPA2) (Figure 3) were originally discovered as inhibitors of neutral lipid. DPA2 showed potent inhibition of neutral lipid synthesis, while DPA1 showed almost no activity. Intriguingly, a 1:1 mixture of DPA1 and DPA2 was found to exhibit the most potent inhibition of neutral lipid synthesis [79, 80]. Further subsequent study of the mechanism of action revealed that instead of inhibiting the synthesis of neutral lipids, DPA promoted the neutral lipid degradation along with inducing autophagy [82].

Inhibitors of lipid synthesis primarily work as a preventive effect to stop or retard the progress of metabolic diseases in most cases. A number of inhibitors have been reported and practically used as preventive drugs. As a typical example, statins, HMG-CoA reductase inhibitors, block hepatic cholesterol synthesis to lower the serum low-density lipoprotein (LDL) level [16]. Conversely, potentiators of accumulated neutral lipid degradation are rarely discovered. Such potentiators will work as treatment drugs rather than preventive drugs to diseases involved in neutral lipid accumulation in the human body. Although discovering such potentiators seems to be more difficult and challenging than discovering inhibitors, our finding of dinapinones prompted us to establish an assay system and perform screening potentiators from microbial cultures.

Based on these backgrounds, this study focused on two main topics which are the search for neutral lipid synthesis inhibitors and degradation potentiators from natural resources. Using the established cell-based assay of CE and TG synthesis [68, 79], chapter I covers the study of new biological activity of known polyacetylenes isolated from

Atractylodes rhizome extract and chapter II covers the study of new terpendole congeners isolated from the culture broth of the fungus *Volutella citrinella* BF-0440. As a second topic, I conducted a cell-based assay system to evaluate neutral lipid (CE and TG) degradation and screened microbial culture broths for potentiators of neutral lipid degradation. Chapter III covers the assay establishment and the screening results for neutral lipid degradation potentiators.

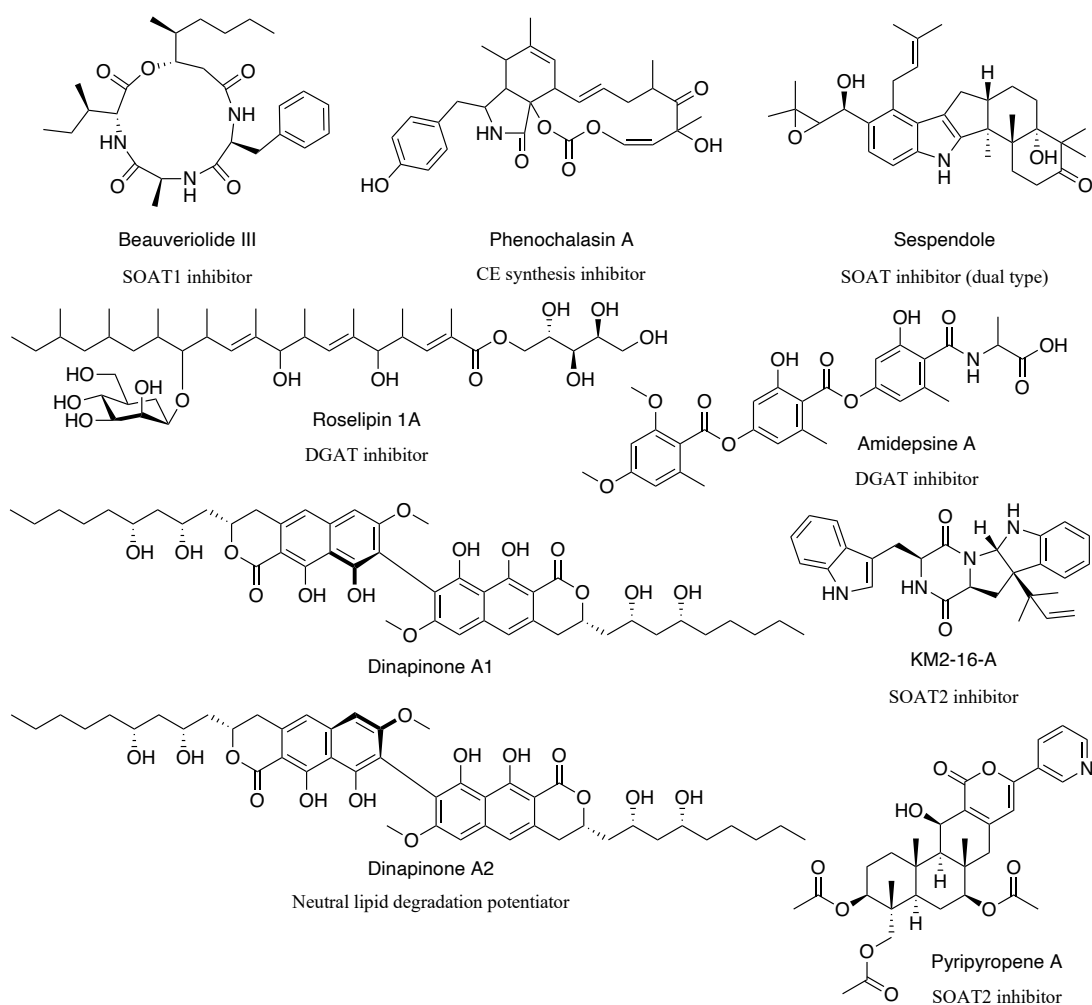


Figure 3. Microbial-derived neutral lipid regulators discovered in our laboratory.

II. Main

Chapter I

Polyacetylenes from *Atractylodes* rhizome extract

This chapter described the traditional herbal medicine, *Atractylodes* rhizome which was found to be active in the course of screening inhibitors of neutral lipid synthesis using CHO-K1 cells. From this rhizome extract, four known compounds, one sesquiterpene, atractylenolide III (**1**) and three polyacetylenes, 14-acetoxy-12-seneciolyloxytetradeca-2*E*,8*E*,10*E*-trien-4,6-diyn-1-ol (**2**), 14-acetoxy-12- α -methylbutyl-2*E*,8*E*,10*E*-trien-4,6-diyn-1-ol (**3**) and 14-acetoxy-12- β -methylbutyl-2*E*,8*E*,10*E*-trien-4,6-diyn-1-ol (**4**) were isolated (Figure 1-1). These compounds inhibited sterol *O*-acyltransferase (SOAT) isozymes, leading to the inhibition of CE synthesis in CHO-K1 cells. This study described the extraction, purification, identification of **1–4** as bioactive compounds and first reported SOAT inhibitory activities of **1–4**.

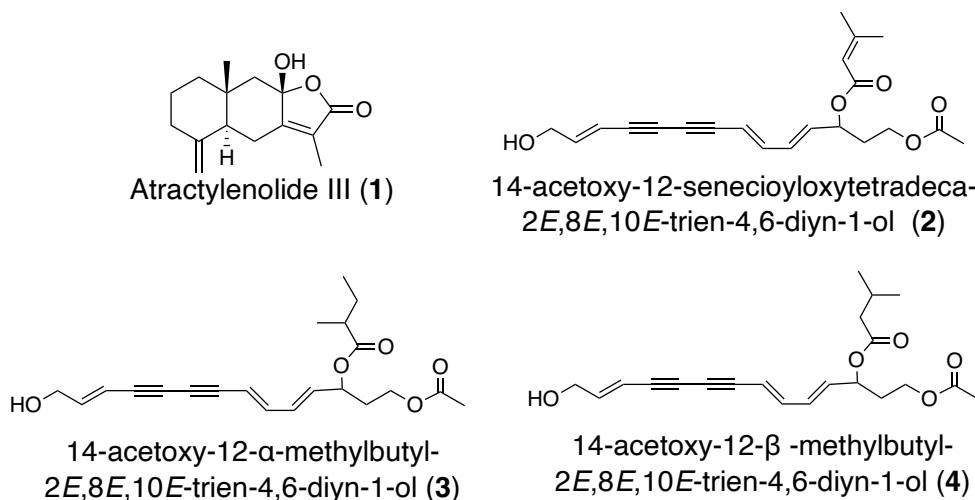


Figure 1-1. Structures of sesquiterpene **1** and polyacetylenes **2–4** isolated from *Atractylodes* rhizome.

1-1. Introduction of *Atractylodes* rhizome

Atractylodes rhizome (Figure 1-2), as described in the Japanese Pharmacopoeia 18th edition (JP18), was prepared from two plants, *Atractylodes japonica* Koidzumi ex Kitamura and *Atractylodes macrocephala* Koidzumi (*Atractylodes ovata* De Candolle). Both crude drugs are used as a diuretic, a stomachic, an anti-sudorific, and an anti-

inflammatory agent [83]. Dried *Atractylodes* rhizome used in this study was purchased from Jilin Aodong Medicine Industry Group Co., Ltd (Zhejiang Province, China). Additionally, known compounds **1–4**, isolated from *Atractylodes* rhizome in this study, have several biological activities, including gastroprotective effects [84], anti-cancer activity [85, 86] anti-inflammatory activity [87], and immunomodulatory activity [88].

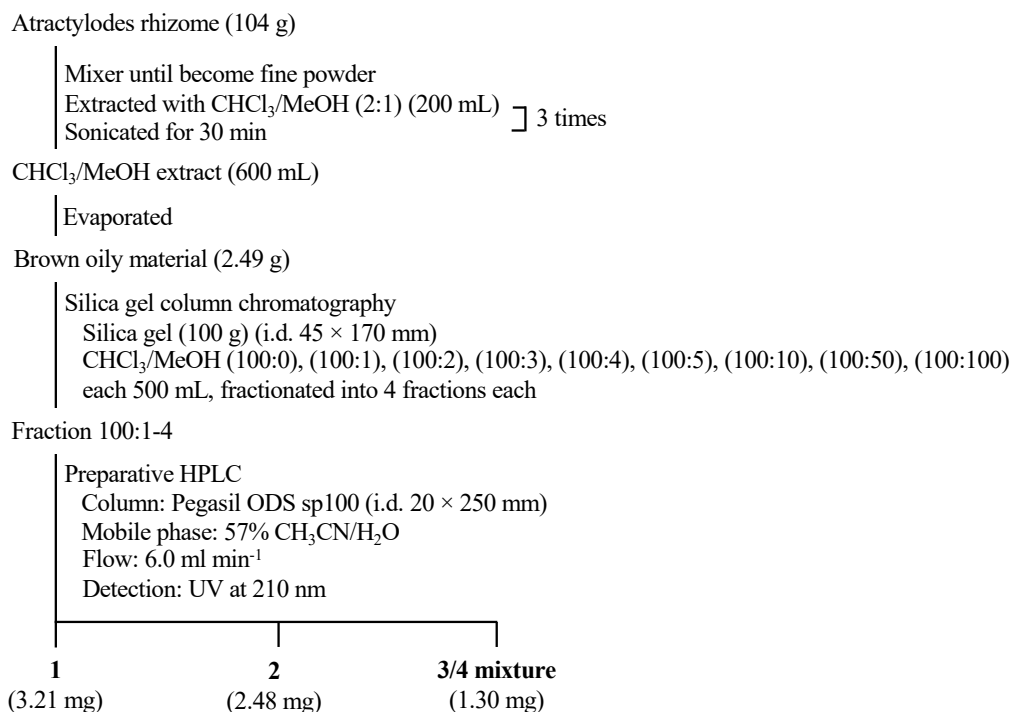


Figure 1-2. Dried *Atractylodes* rhizome

1-2. Extraction and isolation of compounds from *Atractylodes* rhizome

Extraction and isolation steps of compounds was shown in Scheme 1-1. Purchased dried *Atractylodes* rhizome (104 g) was treated with 2:1 CHCl_3 –MeOH (200 mL, three times), and the extract was concentrated to remove CHCl_3 –MeOH. Extracts were concentrated *in vacuo* to dryness, yielding a brown, oily material weighing 2.49 g. The material was dissolved in CHCl_3 , applied to a silica gel column (100 g), and eluted stepwise with 100:0, 100:1, 100:2, 100:3, 100:4, 100:5, 100:10, 100:50, and 100:100 (v/v) CHCl_3 –MeOH solvent [500 mL \times nine fractions for each solvent]. The fourth fraction of 100:1 (17.4 mg) showing the activity was obtained as an active fraction and concentrated to yield brown oily materials. The materials were purified by preparative high-performance liquid chromatography (HPLC; column, Pegasil ODS SP100 i.d. 20 \times 250 mm; mobile phase, 57% $\text{CH}_3\text{CN}/\text{H}_2\text{O}$ isocratic; flow rate, 6.0 mL min^{-1} ; detection, UV at 210 nm). Under these conditions, atractylenolide III (**1**) [89-91], 14-acetoxy-12-seneciolyloxytetradeca-2*E*,8*E*,10*E*-trien-4,6-diyn-1-ol (**2**) [92, 93], and a mixture of 14-acetoxy-12- α -methylbutyl-2*E*,8*E*,10*E*-trien-4,6-diyn-1-ol (**3**) and 14-acetoxy-12- β -methylbutyl-2*E*,8*E*,10*E*-trien-4,6-diyn-1-ol (**4**) [91-94] were eluted as the peaks with retention times of 29, 48, and 51 min, respectively (Figure 1-3). Although the last peak at 51 min was isolated as a single peak, this was determined to be a mixture of known compounds **3** and **4** from ^1H -NMR analysis. Each active fraction was collected and

concentrated *in vacuo* to dryness to yield **1** (3.21 mg), **2** (2.48 mg), and **3/4** mixture (1.30 mg), all as pale-yellow oils.



Scheme 1-1 Extraction and isolation steps of compounds from Atractylodes rhizome

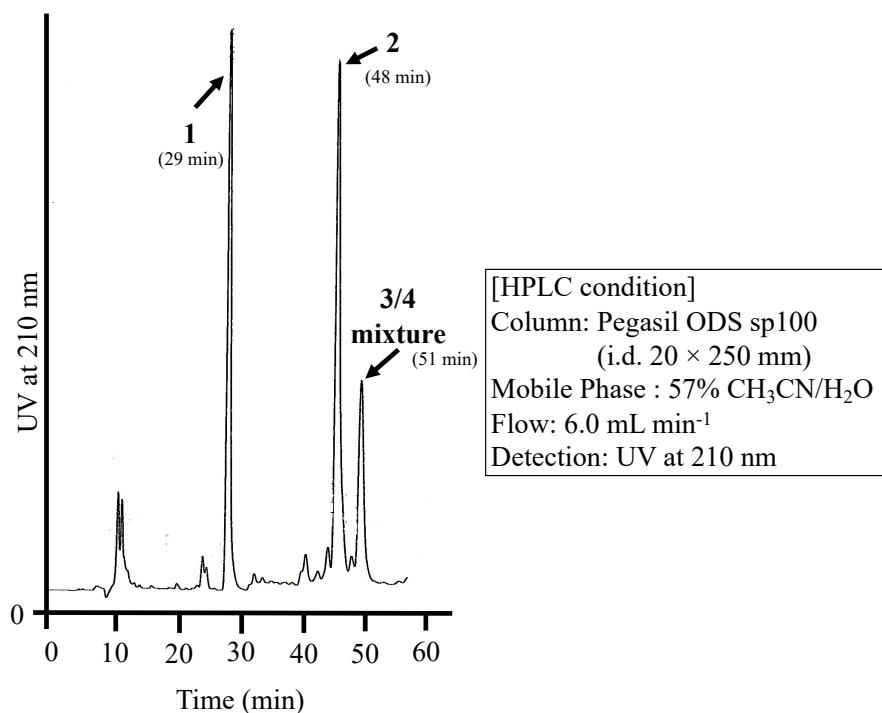


Figure 1-3. Preparative HPLC chromatogram of fraction 100:1-4

1-3. Compound identification

Compound identification of **1–4** was performed based on spectral data, including UFLC chromatogram and UV spectrum, ¹H-NMR, ¹³C-NMR, 2D NMR and MS (Supplemental Figures 1-1~1-8 and Supplemental Tables 1-1~1-3), and the search results of chemicals searching platform, SciFinder Scholar. Compounds **1** and **2** were identified as sesquiterpene, atractylenolides III and polyacetylene, 14-acetoxy-12-seneciolyoxytetradeca-2*E*,8*E*,10*E*-trien-4,6-diyn-1-ol, respectively. The last peak was identified as a mixture of known polyacetylenes compounds, 14-acetoxy-12- α -methylbutyl-2*E*,8*E*,10*E*-trien-4,6-diyn-1-ol (**3**) and 14-acetoxy-12- β -methylbutyl-2*E*,8*E*,10*E*-trien-4,6-diyn-1-ol (**4**) from NMR analysis. We tried to separate and purify them by several HPLC columns (pengasil ODS, Develosil C30 UG50, pegasil C4 and Cosmosil Cholesterol columns), but all in vain. Other researchers also reported the difficulty of their purification [87, 93]. The ratio of **3** and **4** was 3:2 based on ¹H-NMR and ¹³C-NMR data (Supplemental Figures 1-7~1-8). The configuration of C-12 in **2–4** and C-2'' in **3** were hard to be decided.

1-4. Inhibition of neutral lipid synthesis

The effects of **1–4** on synthesis of the main neutral lipids, namely, [¹⁴C]CE and [¹⁴C]TG from [¹⁴C]oleic acid, were examined in intact CHO-K1 cells using an established method [79, 82]. Under this condition, the polyacetylenes, **2** and **3/4** mixture, selectively inhibited [¹⁴C]CE synthesis with IC₅₀ values of 35.4 μ M and 10.2 μ M, respectively (Table 1-1 and Supplemental Figure 1-9). In contrast, **1** showed weak inhibition of [¹⁴C]CE synthesis (IC₅₀ = 73.5 μ M). Additionally, the cytotoxicity of these compounds was far less than [¹⁴C]CE inhibition in CHO-K1 cells. Thus, we investigated the mode of action of **1–4** during selective inhibition of [¹⁴C]CE synthesis.

Table 1-1. Inhibitory activity against neutral lipid synthesis in CHO-K1 cells of **1–4**

Compound	IC ₅₀ (μ M) ^a		Cytotoxicity
	[¹⁴ C]CE synthesis	[¹⁴ C]TG synthesis	
1	73.5	>195	>195
2	35.4	>136	111
3/4 mixture	10.2	>135	49.4

^a n \geq 3.

In the cellular [^{14}C]CE synthesis pathway, SOAT, the final enzyme in the pathway, is one potential target. Accordingly, the examination of effects of **1–4** on SOAT activity. When microsomes prepared from CHO-K1 cells were used as an enzyme source, SOAT activity was inhibited by **2** ($\text{IC}_{50} = 29.0 \mu\text{M}$) and **3/4** mixture ($\text{IC}_{50} = 11.6 \mu\text{M}$). In contrast, **1** showed weak SOAT inhibition with an IC_{50} value of $211 \mu\text{M}$. These data indicate that **1–4** inhibit SOAT activity, and that polyacetylenes **2–4** were more potent than sesquiterpene **1** (Table 1-2). Furthermore, there are two SOAT isoenzymes, SOAT1 and SOAT2, that have distinct functions and expression patterns in mammals, including humans [54]. Our group has established cell-based and enzyme-based assays using hSOAT1-CHO cells and hSOAT2-CHO cells to investigate the inhibitor selectivity toward SOAT isozymes [68, 69]. As shown in Table 1-3, **2** inhibited the both SOAT isozymes ($\text{IC}_{50} = 32.8 \mu\text{M}$ for hSOAT1, and $36.2 \mu\text{M}$ for hSOAT2), and the **3/4** mixture also inhibited both isoenzymes ($\text{IC}_{50} = 42.5 \mu\text{M}$ for hSOAT1, and $50.5 \mu\text{M}$ for hSOAT2) in the cell-based assay. On the other hand, **1** showed weak SOAT1 and SOAT2 inhibition. These results correlated with those showing selective [^{14}C]CE synthesis inhibition in CHO-K1 cells. Furthermore, in this enzyme-based assay using microsomes prepared from hSOAT1-CHO or hSOAT2-CHO cells, these compounds showed correlate IC_{50} values against both isozyme activities (Table 1-3). Interestingly, the inhibitory activities of **1–4** in cell-based assay were weaker than those measured in enzyme-based assay. These differences may be due to low permeability of the plasma membrane.

Table 1-2. Effect of **1–4** on SOAT activity using microsomes from CHO-K1

Compound	$\text{IC}_{50} (\mu\text{M})^a$
1	211
2	29.0
3/4 mixture	11.6

^a $n \geq 3$.

Table 1-3. Effect of **1–4** on [¹³C]CE synthesis in cell-based and enzyme-based assays in hSOAT1-CHO and hSOAT2-CHO cells

Compound	IC ₅₀ (μM) ^a			
	Cell-based assay		Enzyme-based assay ^b	
	hSOAT1-CHO cells	hSOAT2-CHO cells	hSOAT1	hSOAT2
1	174	187	55	100
2	32.8	36.2	4.7	11
3/4 mixture	42.5	50.5	2.3	13

^a n ≥ 3. ^b Enzyme source: microsomes from hSOAT1- and hSOAT2-CHO cells.

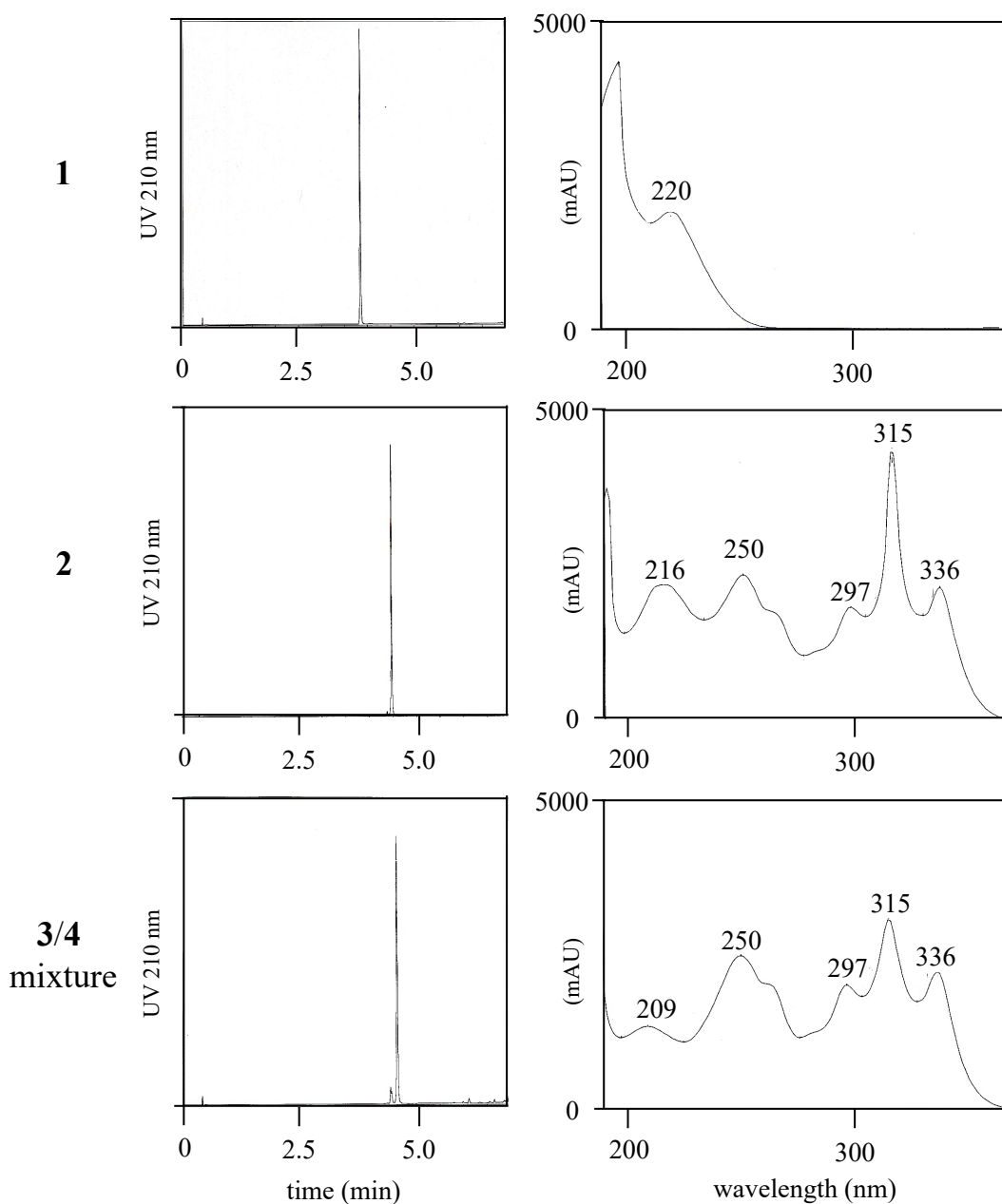
1-5. Discussion

Atractylodes rhizome contains diverse chemical compounds such as polyacetylenes, sesquiterpenes, and essential oils, and those compounds are thought to exert the pharmacological effect of the rhizomes. Of those compounds, polyacetylenes and sesquiterpenes most occurred in Atractylodes rhizome. From activity-guided isolation, one sesquiterpene (**1**) and three polyacetylenes (**2–4**) compounds were found to moderately inhibit both SOAT1 and SOAT2 activity.

Neutral lipids, mainly CE and TG, are stored as cytosolic lipid droplets. Subsequently, this study investigated the effect of **1–4** on lipid droplet accumulation in intact CHO-K1 cells according to a previously described method. Accumulated lipid droplets in their cytosol were observed microscopically after Oil Red O staining, **1–4** had insignificant effects on lipid droplet accumulation even at concentrations greater than 100 μM (data not shown). While **1–4** selectively inhibited CE synthesis, they did not affect the accumulation of lipid droplets, which could be rich in TG. These results agreed with those showing a slight increase in TG accumulation by CHO-K1 cells (Supplemental Figure 1-9).

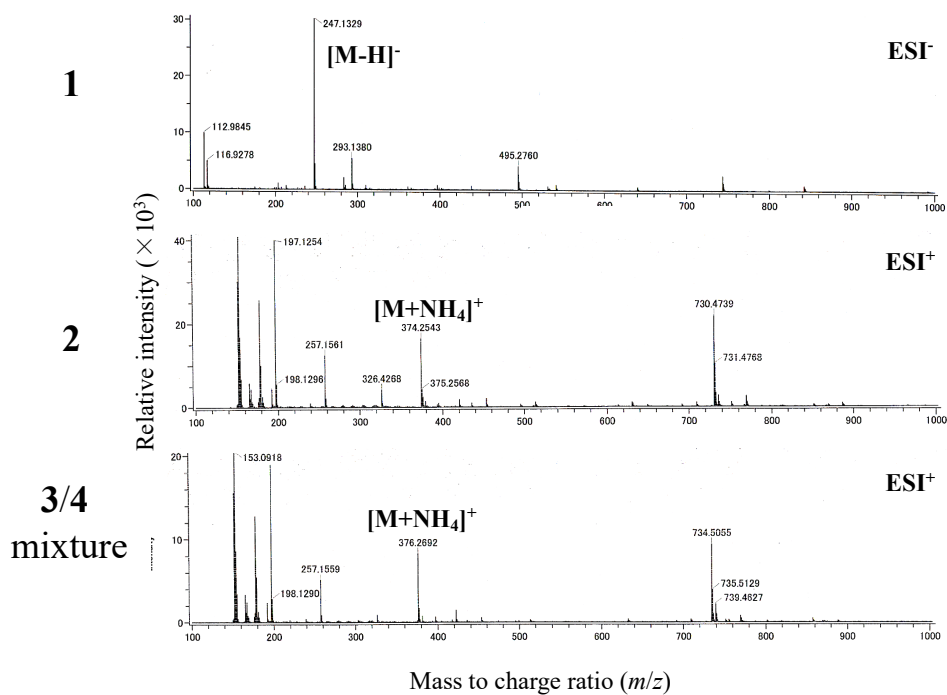
In conclusion, Atractylodes rhizome has been used as a traditional herbal medicine in China, Japan, and Korea. Our findings indicate that its ingredients may show therapeutic potential content as anti-hypercholesterolemia and anti-atherosclerotic agents.

1-6. Supplemental data

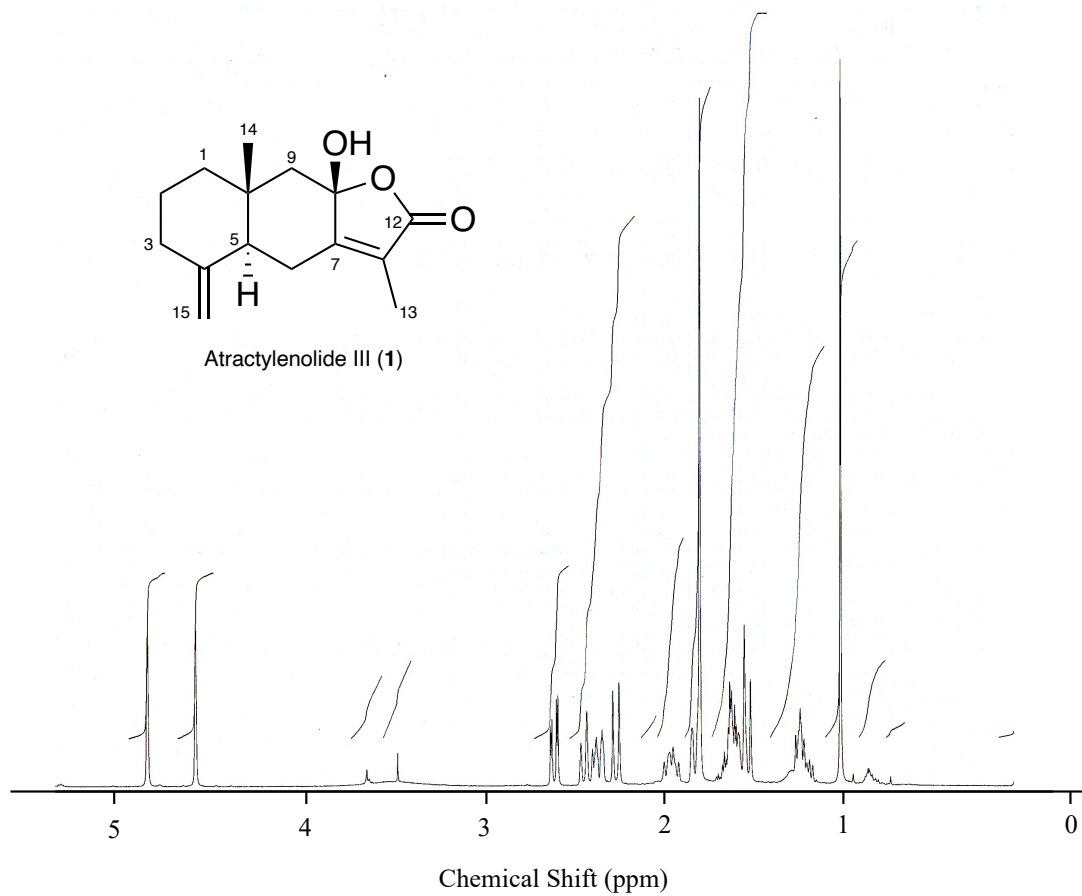


Supplemental Figure 1-1. Chromatogram and spectrogram of **1–4** analyzed by UFLC.

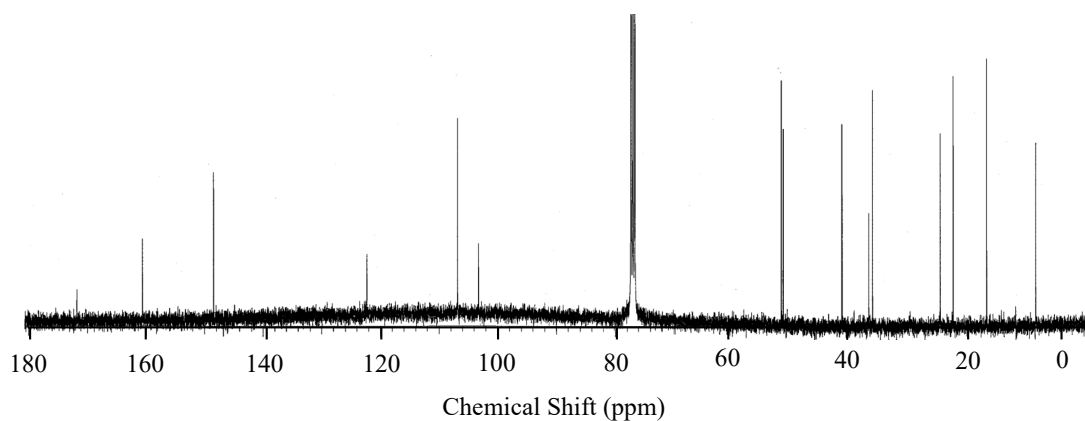
Compound **1**, **2**, and **3/4** mixture (1 μg) were diluted in MeOH and analyzed in UFLC system under the following condition (column, Shimpak XR-ODS (i.d. 2.0×75 mm); eluent, 6 minutes linear gradient from 5-95% $\text{CH}_3\text{CN}/\text{H}_2\text{O}$ -0.1% H_3PO_4 then 1 minute isocratic 95% $\text{CH}_3\text{CN}/\text{H}_2\text{O}$ -0.1% H_3PO_4 ; flow, 0.55 mL min^{-1} ; detection, UV at 210 nm).



Supplemental Figure 1-2. MS spectra of **1–4**



Supplemental Figure 1-3. ^1H -NMR spectrum of **1** (400 MHz in CDCl_3)

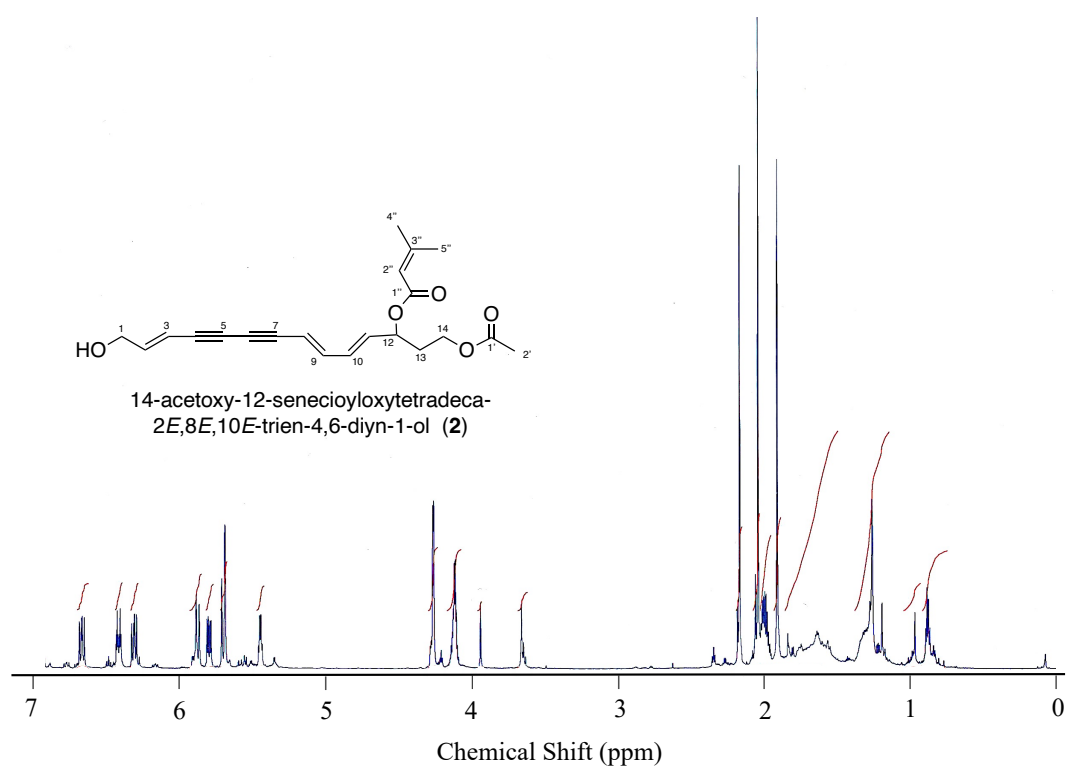


Supplemental Figure 1-4. ^{13}C -NMR spectrum of **1** (100 MHz in CDCl_3)

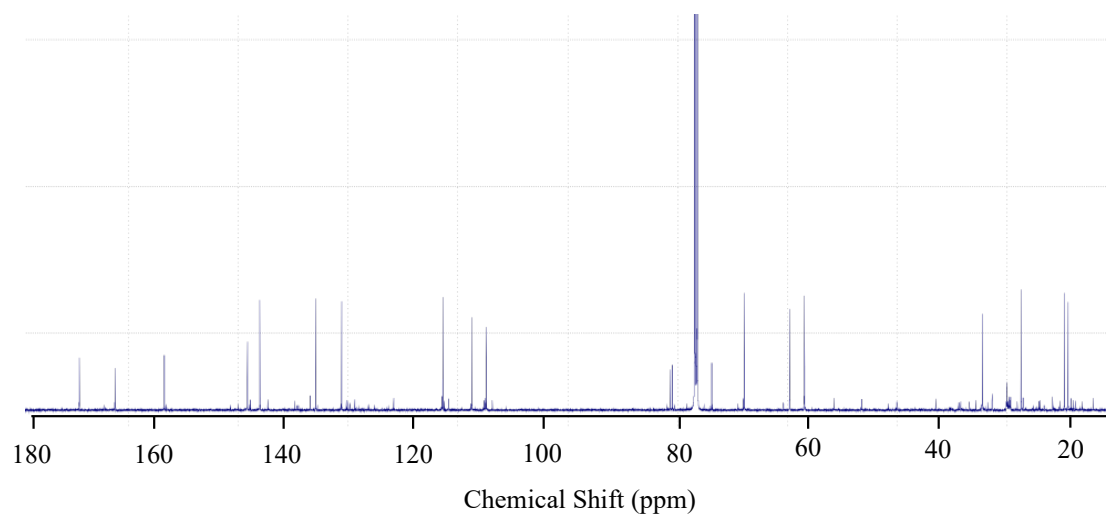
Supplemental Table 1-1. ^1H - and ^{13}C -NMR chemical shift of **1** in CDCl_3 .

Position	$\delta_{\text{C}}^{\text{a}}$, type	$\delta_{\text{H}}^{\text{b}}$ (multi, J Hz)
1	41.3, CH_2	1.24 (m), 1.61 (m)
2	22.3, CH_2	1.63 (m), 1.64 (m)
3	36.1, CH_2	1.96 (m), 2.37 (m)
4	148.6, C	-
5	51.7, CH	1.84 (br. s)
6	24.7, CH_2	2.45 (d, 13.4), 2.6 (dd, 2.8, 13.4)
7	161.3, C	-
8	103.9, C	-
9	51.1, CH_2	1.57 (d, 13.6), 2.26 (d, 13.6)
10	36.7, C	-
11	121.9, C	-
12	172.9, C	-
13	8.2, CH_3	1.80 (s)
14	16.6, CH_3	1.02 (s)
15	106.8, CH_2	4.59 (s), 4.85 (s)

^{13}C (100 MHz) and ^1H (400 MHz) NMR spectra were taken on an NMR 400 MHz spectrometer (Agilent). Chemical shifts are shown with reference to $^{\text{a}}\text{CDCl}_3$ as δ 77.0, $^{\text{b}}\text{CDCl}_3$ as δ 7.26. Multiplicity of signals as follows: s = singlet, d = doublets, dd = double doublets, m = multi. Coupling constants (Hz) were determined by the ^1H - ^1H decoupling experiments.



Supplemental Figure 1-5. ¹H-NMR spectrum of **2** (900 MHz in CDCl₃)

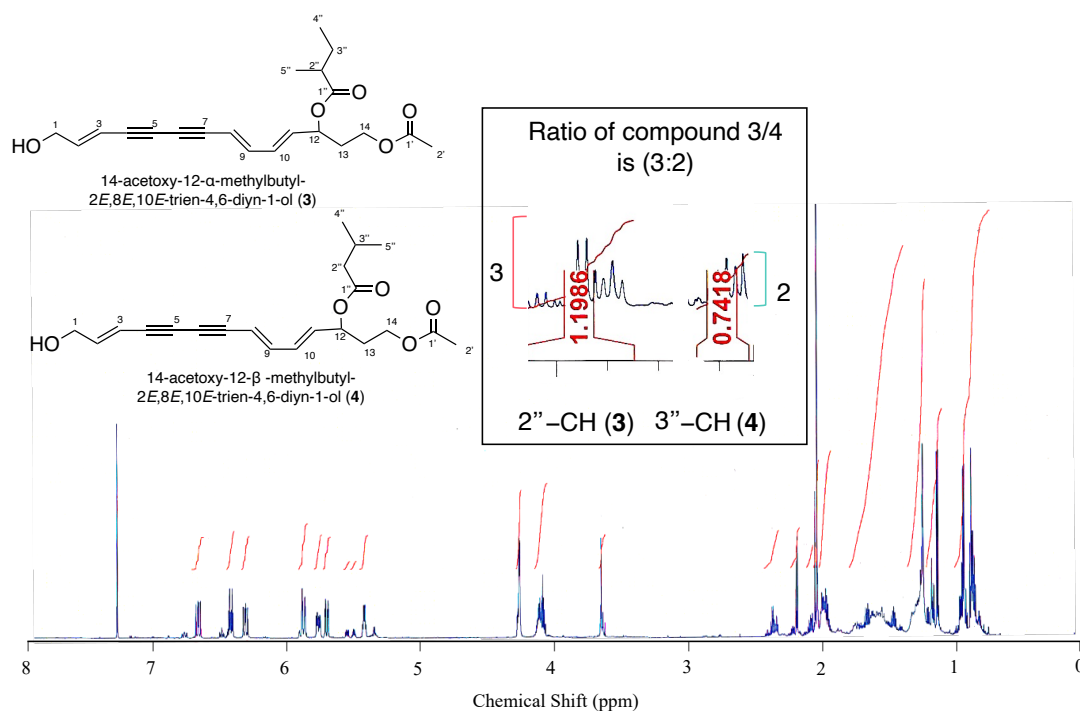


Supplemental Figure 1-6. ¹³C-NMR spectrum of **2** (225 MHz in CDCl₃)

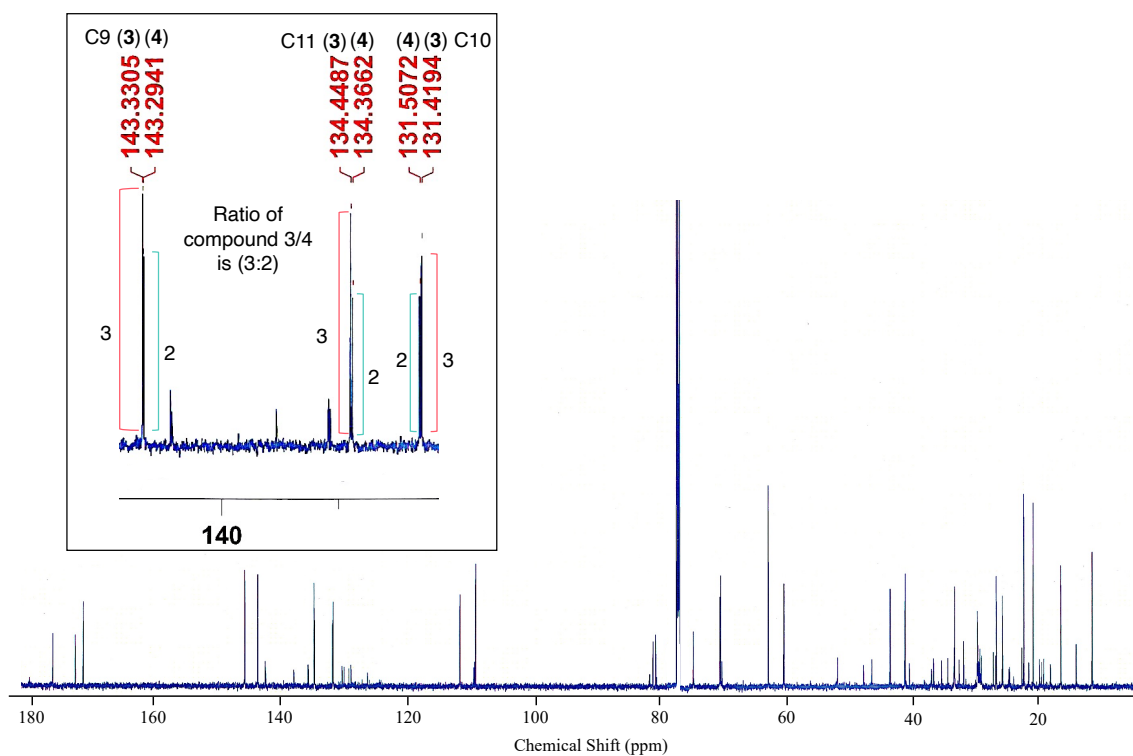
Supplemental Table 1-2. ¹H- and ¹³C-NMR chemical shift of **2** in CDCl₃.

Position	δ _C ^a , type	δ _H ^b (multi, J Hz)
1	62.7, CH ₂	4.25 (d, 5.4)
2	145.3, CH	6.40 (dt, 5.4, 18.0)
3	108.9, CH	5.86 (d, 18.0)
4	80.8, C	-
5	74.6, C	-
6	76.8, C	-
7	80.6, C	-
8	111.1, CH	5.69 (d, 16.9)
9	143.4, CH	6.65 (dd, 12.4, 16.9)
10	130.9, CH	6.30 (dd, 12.4, 17.1)
11	134.9, CH	5.78 (dd, 7.5, 17.1)
12	69.6, CH	5.43 (q, 7.5)
13	33.3, CH ₂	1.98 (m)
14	60.4, CH ₂	4.10 (m)
1'	170.9, C	-
2'	20.8, CH ₃	2.03 (s)
1''	165.5, C	-
2''	115.5, CH	5.67 (s)
3''	158.0, C	-
4''	20.2, CH ₃	2.15 (s)
5''	27.4, CH ₃	1.91 (s)

¹³C (225 MHz) and ¹H (900 MHz) NMR spectra were taken on an NMR 900 MHz spectrometer (Bruker). Chemical shifts are shown with reference to ^aCDCl₃ as δ 77.0, ^bCDCl₃ as δ 7.26. Multiplicity of signals as follows: s = singlet, d = doublets, dd = double doublets, dt = double triplets, m = multi, q = quartet. Coupling constants (Hz) were determined by the ¹H-¹H decoupling experiments.



Supplemental Figure 1-7. ^1H -NMR spectrum of **3/4** mixture (900 MHz in CDCl_3)

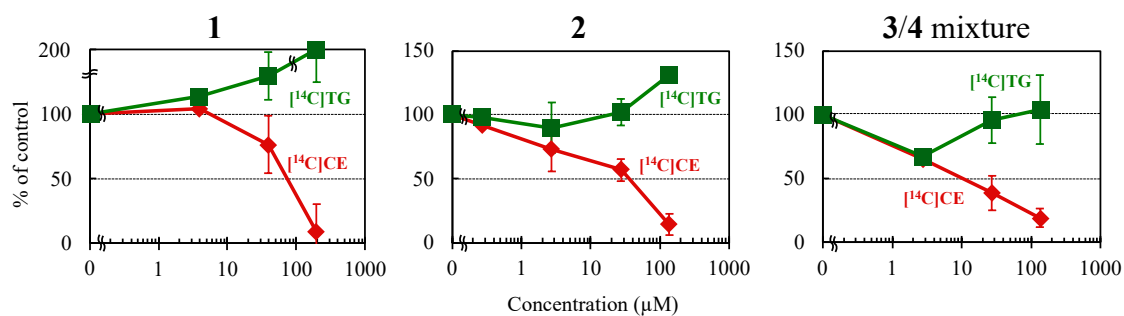


Supplemental Figure 1-8. ^{13}C -NMR spectrum of **3/4** mixture (225 MHz in CDCl_3)

Supplemental Table 1-3. ¹H- and ¹³C-NMR chemical shift of **3/4** mixture in CDCl₃.

Position	δ _C ^a , type	δ _H ^b (multi, <i>J</i> Hz)
1	62.7, CH ₂	4.26 (d, 5.5)
2	145.3, CH	6.41 (dt, 5.5, 18.0)
3	108.9, CH	5.86 (br.d, 18.0)
4	80.9, C	-
5	74.5, C	-
6	70.2, C	-
7	80.5, C	-
8	111.4, CH	5.69 (br. dd, 3.8, 17.4)
9	143.3, CH	6.65 (dd, 12.3, 17.4)
10	131.4, CH	6.30 (dd, 12.3, 17.1)
11	134.4, CH	5.76 (dd, 7.4, 17.1)
12	70.4, CH	5.41 (dd, 7.4)
13	33.3, CH ₂	1.98 (m)
14	60.2, CH ₂	4.10 (m)
1'	170.9, C	-
2'	20.8, CH ₃	2.04 (s)
1'' (3)	175.7, C	-
1'' (4)	172.1, C	-
2'' (3)	41.1, CH	2.38 (m)
2'' (4)	43.5, CH ₂	2.19 (m)
3'' (3)	26.7, CH ₂	1.47 (m), 1.63 (m)
3'' (4)	25.7, CH	2.08 (m)
4'' (3)	11.5, CH ₃	0.88 (m)
4'' (4)	22.3, CH ₃	0.95 (dd, 1.4, 7.6)
5'' (3)	16.5, CH ₃	1.14 (d, 7.9)
5'' (4)	22.3, CH ₃	0.95 (dd, 1.4, 7.6)

¹³C (225 MHz) and ¹H (900 MHz) NMR spectra were taken on an NMR 900 MHz spectrometer (Bruker). Chemical shifts are shown with reference to ^aCDCl₃ as δ 77.0, ^bCDCl₃ as δ 7.26. Multiplicity of signals as follows: s = singlet, d = doublets, dd = double doublets, dt = double triplets, m = multi. Coupling constants (Hz) were determined by the ¹H-¹H decoupling experiments.



Supplemental Figure 1-9. Effect of **1–4** on CE and TG synthesis in CHO-K1 cells
 CHO-K1 cells were incubated with [¹⁴C]oleic acid and compounds **1–4** at various concentrations for 6 hours. Cells were then lysed and cellular [¹⁴C]CE (♦) and [¹⁴C]TG (■) were separated on TLC then quantified using an image analyzer. The results obtained were plotted as % of control (without drugs). Values represent means ± SD (n = 3).

Chapter II

Terpendole congeners from *Volutella citrinella* BF-0440

This chapter described the fungus BF-0440 strain which was hit in our screening system of SOAT2 selective inhibitor. This strain was isolated from soil collected from Shizuoka-shi, Shizuoka, Japan and identified as *Volutella citrinella*. From the culture broth, new indoline-diterpene-containing compounds, termed voluhemins A (**8**) and B (**9**), and NK12838 (**10**) [95] were discovered [96]. Notably, **9** was found to be a SOAT2 selective inhibitor. Furthermore, the culture broth of the fungus still contained other structurally related compounds. As a result, new terpendoles N-P (**5–7**), were isolated from the culture broth along with four known terpendole congeners (**11–15**) [97-99] presented in Figure 2-1. This study described the strain identification, fermentation, isolation, structural elucidation and SOAT inhibitory activity of these compounds and discussed the SARs of indole/indoline-diterpenes in SOAT1/SOAT2 inhibitory activity.

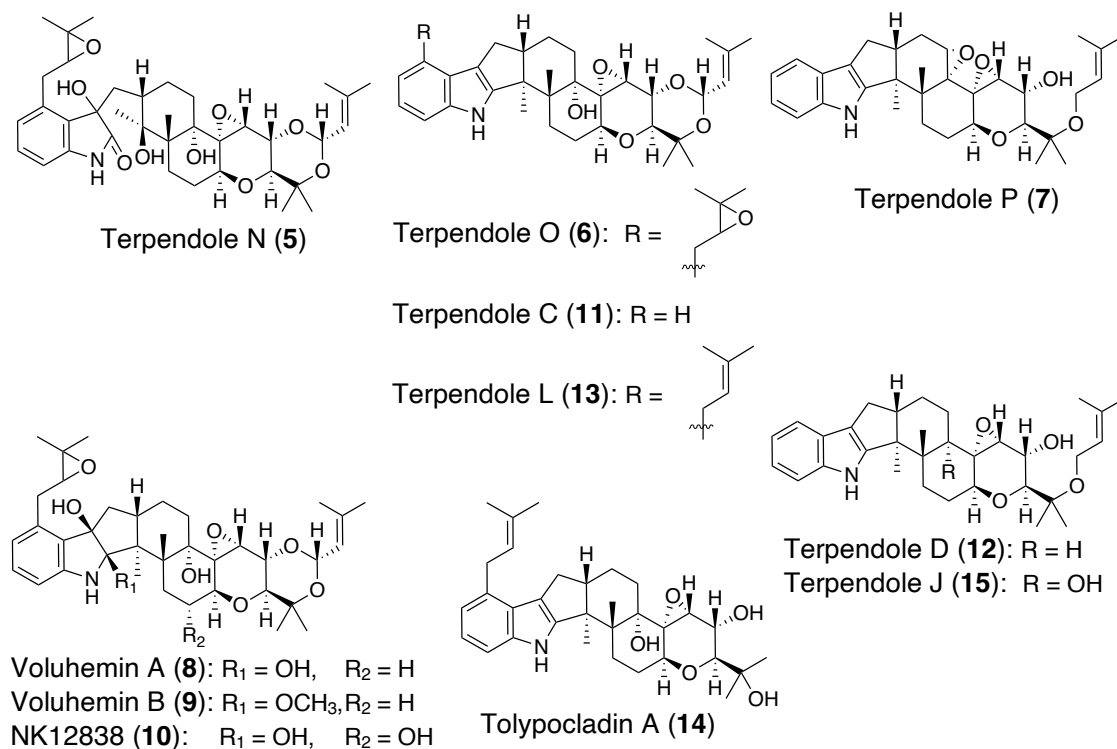


Figure 2-1. Structures of terpendole congeners **5–15** isolated from culture broth of fungus *V. citrinella* BF-0440

2-1. Fungus BF-0440 strain identification

Mycological study was commissioned to TechnoSuruga Laboratory Co., Ltd. The fungus BF-0440 strain was identified as *Volutella citrinella* from 28S rDNA-D1/D2 nucleotide sequence, internal transcribed spacer (ITS)-5.8S rDNA and morphological observation (Figure 2-2).

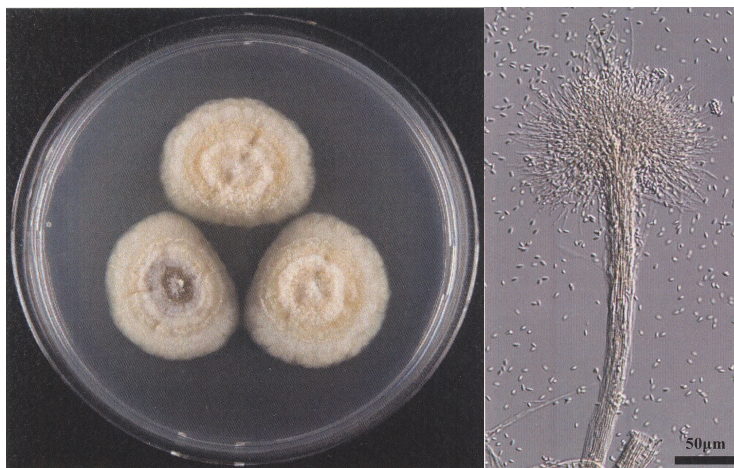


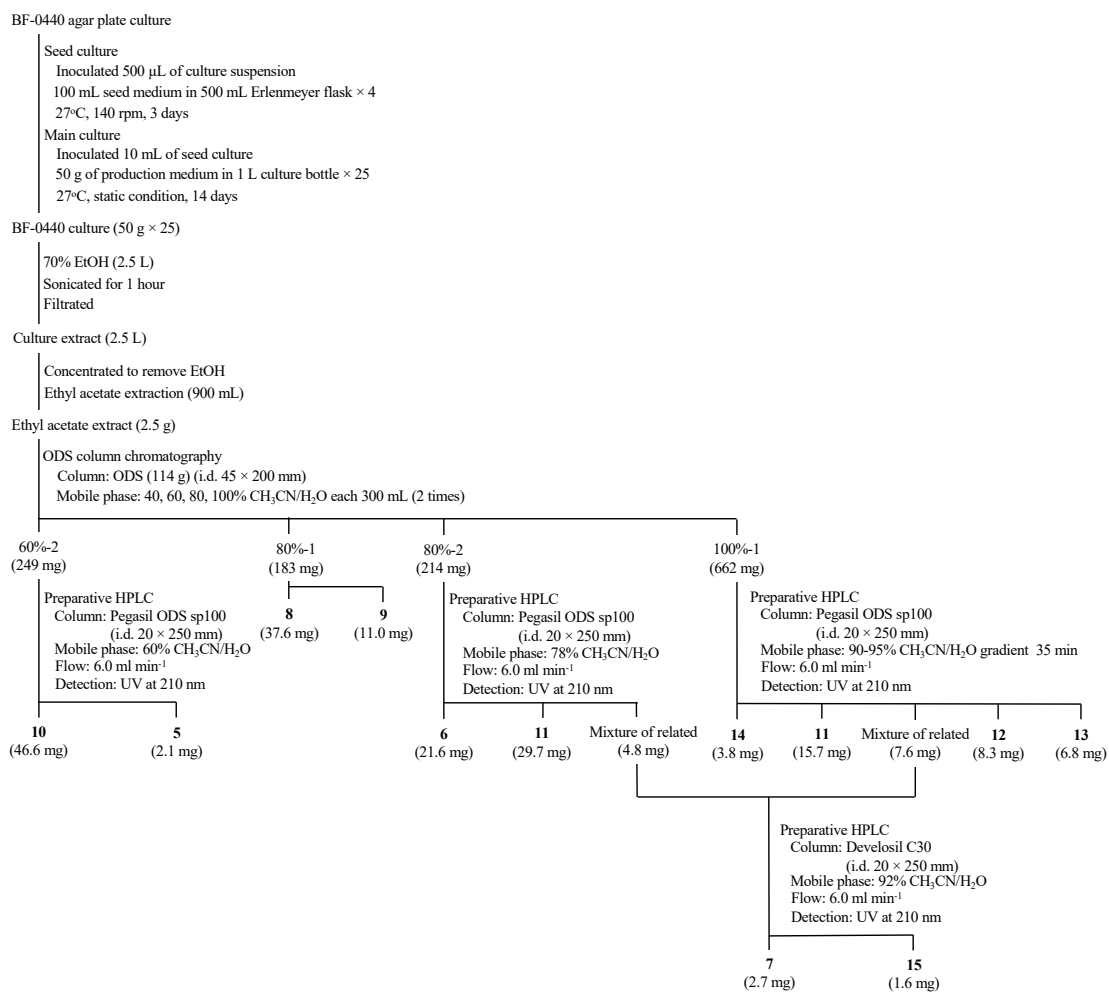
Figure 2-2. Morphological images of fungus *V. citrinella* BF-0440

2-2. *V. citrinella* BF-0440 strain fermentation and isolation of compounds

V. citrinella BF-0440 strain was isolated from soil collected in Shizuoka, Shizuoka-shi, Japan. Fermentation methods and isolation steps of compounds was shown in Scheme 2-1. A loopful of spore of BF-0440 strain grown in agar plate medium (PDA medium) was suspended in 500 μ L of sterile water. This spore suspension were then inoculated into each 100 mL of seed medium (glucose 2.0%, yeast extract 0.2%, $\text{MgSO}_4 \cdot 7\text{H}_2\text{O}$ 0.05%, polypeptone 0.5%, agar 0.1%, KH_2PO_4 0.1%, pH 6.0) in 500 mL Erlenmeyer flask (4 bottles) and incubated at 27°C, 140 rpm, for 3 days. The seed culture (10 mL) was then inoculated to each 50 g of production medium (50 g of brown rice, 5.0 mL of the following solution: PDB 2.4%, $\text{MgSO}_4 \cdot 7\text{H}_2\text{O}$ 0.5%, $\text{Mg}_3(\text{PO}_4)_2 \cdot 8\text{H}_2\text{O}$ 0.5%, K_2HPO_4 0.5%) in 1 L culture bottle (25 bottles) and incubated 27°C for 14 days in static conditions.

The 14-day-old culture (2.5 L) of BF-0440 was extracted with 70% EtOH (2.5 L). After concentration to remove EtOH, the aqueous solution was extracted with EtOAc (900 mL). The organic layer was collected and EtOAc was evaporated to give crude extract (brown material, 2.5 g). This crude extract was applied to an ODS column (114 g, i.d. 45 \times 200 mm) and eluted stepwise with 40% $\text{CH}_3\text{CN}/\text{H}_2\text{O}$, 60% $\text{CH}_3\text{CN}/\text{H}_2\text{O}$, 80% $\text{CH}_3\text{CN}/\text{H}_2\text{O}$, and 100% $\text{CH}_3\text{CN}/\text{H}_2\text{O}$ solutions (600 mL each, fractionated into two). All fractions were

concentrated *in vacuo* and the remaining water layers were extracted with EtOAc. The EtOAc layers of these fractions were collected and evaporated to dryness. Voluhemins A (**8**) and B (**9**) were purified from fraction 80%-1. Fraction 60%-2 (brown material, 249 mg) was subjected to preparative high-performance liquid chromatography (HPLC; column, Pegasil ODS SP100 i.d. 20 × 250 mm; mobile phase, 60% CH₃CN/H₂O isocratic; flow rate, 6.0 mL min⁻¹; detection, UV at 210 nm) (Figure 2-3). In these conditions, NK12838 (**10**) and terpendole N (**5**) were eluted as peaks with retention times of 27 and 29 min, respectively. Purification from fraction 80%-2 (brown material, 214 mg) by preparative HPLC (column, Pegasil ODS SP100 i.d. 20 × 250 mm; mobile phase, 78% CH₃CN/H₂O isocratic; flow rate, 6.0 mL min⁻¹; detection, UV at 210 nm) allowed isolation of three peaks, terpendole O (**6**) eluted at 23 min, terpendole C (**11**) at 24 min, and a third peak at 26 min (Figure 2-4). The third peak was, however, found to be a mixture of related compounds from proton NMR analyses. This mixture was also obtained from fraction 100%-1 along with terpendoles C (**11**), D (**12**), L (**13**), and tolypocladin A (**14**). By preparative HPLC (column, Pegasil ODS SP100 i.d. 20 × 250 mm; mobile phase, 35-min linear gradient 90–95% CH₃CN/H₂O; flow rate, 6.0 mL min⁻¹; detection, UV at 210 nm), **14**, **11**, the mixture, **12**, and **13** were eluted at 16, 18, 22, 31, and 35 min, respectively (Figure 2-5). The mixture was finally separated in different HPLC conditions (column, Develosil C30 i.d. 20 × 250 mm; mobile phase, 92% CH₃CN/H₂O isocratic; flow rate, 6.0 mL min⁻¹; detection, UV at 210 nm) to yield a new terpendole P (**7**) and a known terpendole J (**15**) eluted as peaks at 22 and 23 min, respectively (Figure 2-6). All of these peaks were collected and concentrated to dryness to give **5** (2.1 mg), **6** (21.6 mg), **7** (2.7 mg), **10** (46.6 mg), **11** (29.7 mg and 15.7 mg from 80%-2 and 100%-1, respectively), **12** (8.3 mg), **13** (6.8 mg), **14** (3.8 mg) and **15** (1.6 mg) as white powders.



Scheme 2-1. Fermentation methods and isolation steps of compounds from
V. citrinella BF-0440

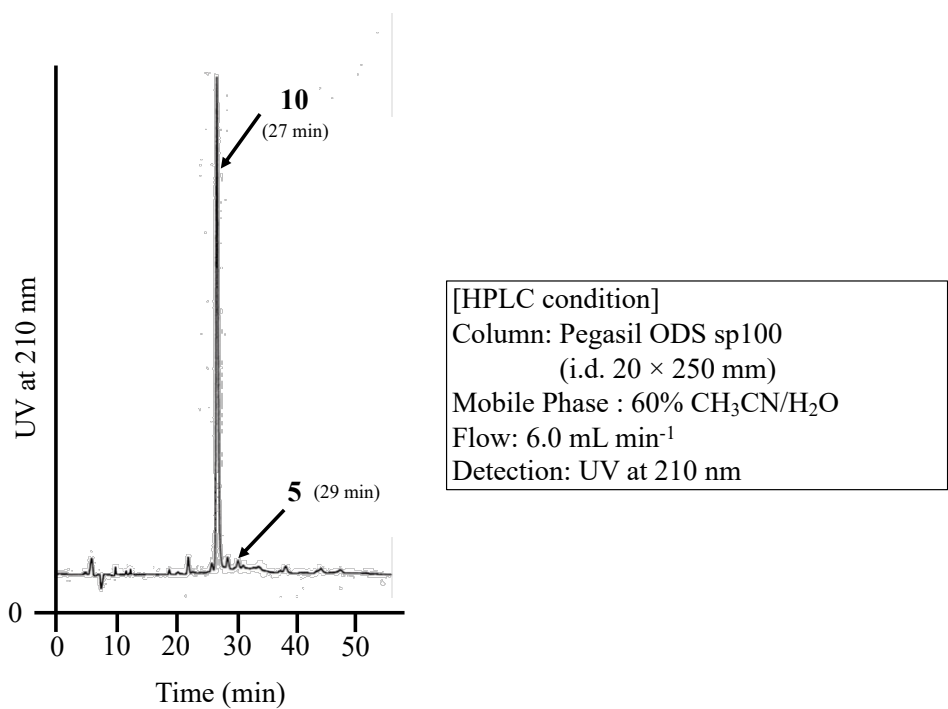


Figure 2-3. Preparative HPLC chromatogram of 60%-2 CH₃CN/H₂O fraction

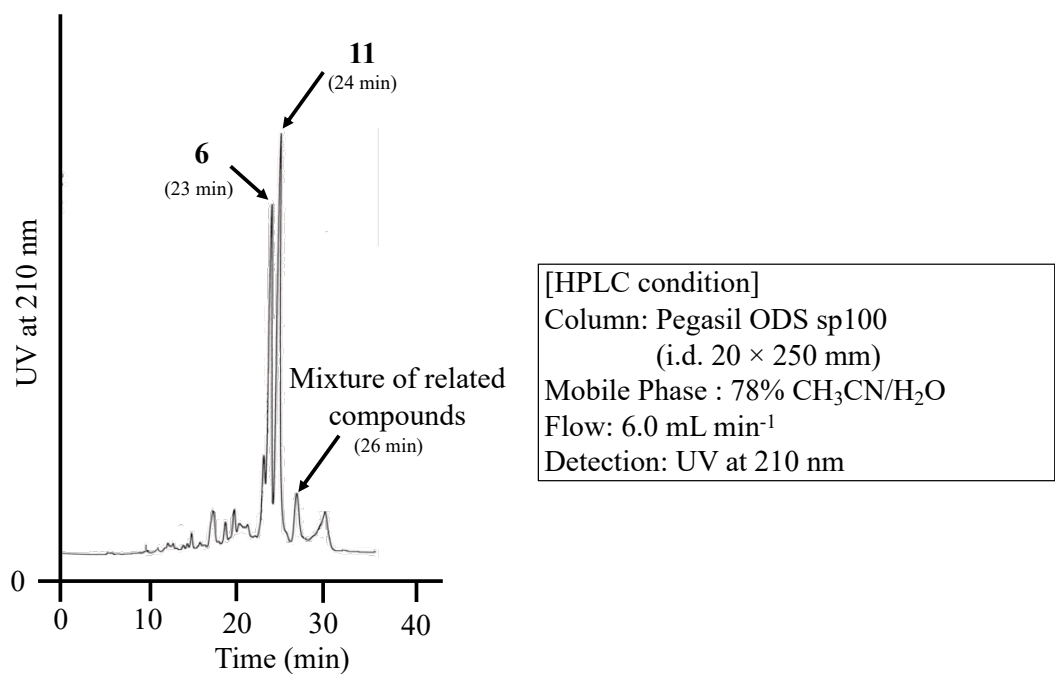


Figure 2-4. Preparative HPLC chromatogram of 80%-2 CH₃CN/H₂O fraction

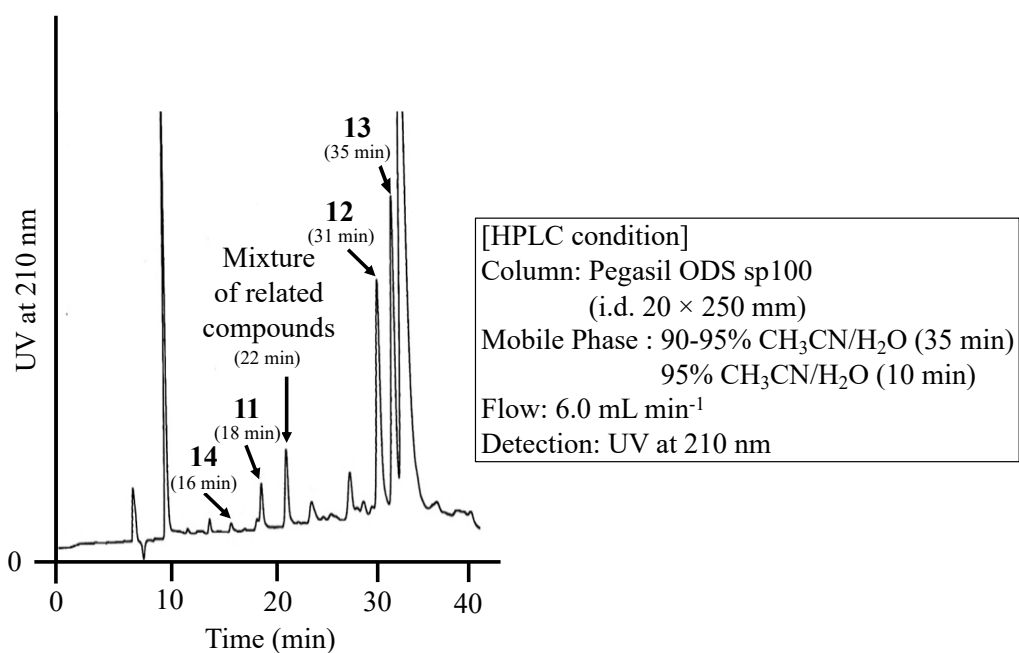


Figure 2-5. Preparative HPLC chromatogram of 100%-1 CH₃CN/H₂O fraction

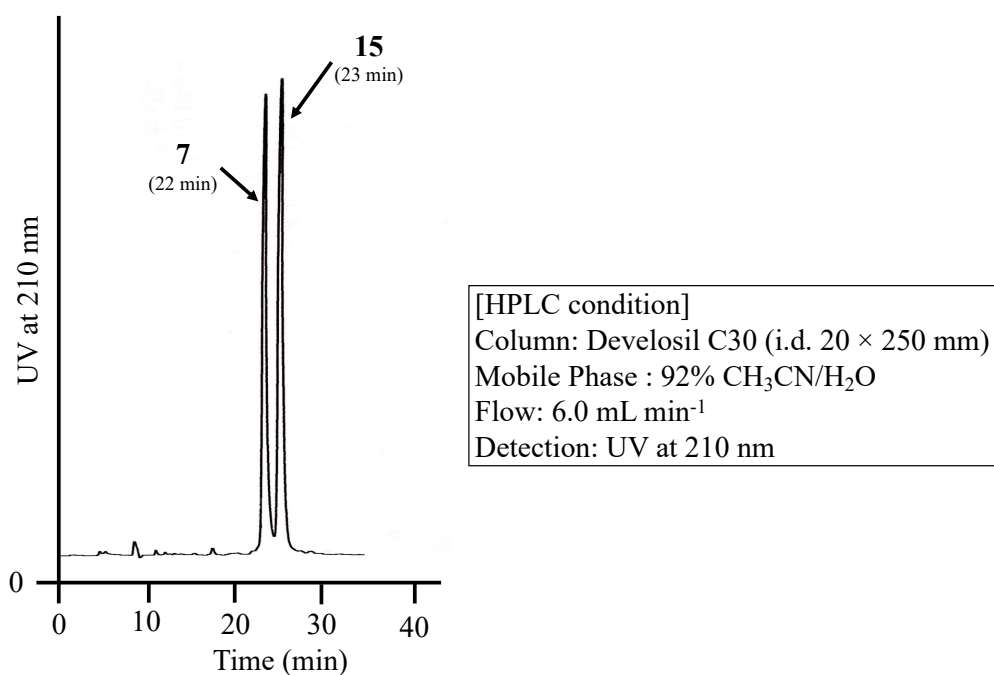


Figure 2-6. Preparative HPLC chromatogram of the mixture of related compounds

Structure determination of new terpendole N-P (**5–7**) was performed by physicochemical analyses and several NMR experiments. First, the structure elucidation of compound **6** was carried out because of its higher amount compared to others. The structures of compounds **5** and **7** were then determined by comparing their physicochemical data and NMR spectrums with **6** and other related known compounds isolated from *V. citrinella* BF-0440.

2-3. Structure elucidation of new terpendole O

The physicochemical properties of terpendole O (**6**) were summarized in Table 2-1. Compound **6** was obtained as white powder. From high resolution ESI-MS, molecular weight of **6** was 603 and its molecular formula was C₃₇H₄₉NO₆ (Supplemental Figure 2-1) indicating 14 degrees of unsaturation. Compound **6** has UV spectra (Supplemental Figure 2-2) with absorption maxima at 230 and 283 nm. The IR absorption (Supplemental Figure 2-3) at 3449 cm⁻¹ indicated the presence of hydroxyl group or amine group.

Table 2-1. Physicochemical properties of **6**

	Terpendole O (6)
Appearance	White powder
Molecular weight	603
Molecular formula	C ₃₇ H ₄₉ NO ₆
HR-ESI-MS (<i>m/z</i>)	
Calcd	604.3625 [M+H] ⁺
Found	604.3638 [M+H] ⁺
UV _{λ_{max}} ^{CH₃OH} nm (log ε)	230 (3.5), 283 (3.0)
IR _{max} ^{KBr} cm ⁻¹	3449, 2979, 2930, 1458
[α] _D ^t (c = 0.1 CH ₃ OH)	-4.0 (t=23)

¹H-NMR and ¹³C-NMR signals of **6** were first taken in DMSO-*d*₆ (Supplemental Figures 2-4 and 2-5) as shown in Table 2-2. However, the assignment of methylene protons of **6** was difficult in DMSO-*d*₆. Therefore, NMR experiments by using CDCl₃ solvent were necessary to determine the structure of **6**. ¹H-NMR and ¹³C-NMR of **6** taken in CDCl₃ (Supplemental Figures 2-6 and 2-7) were shown in Table 2-3. The ¹³C-NMR data revealed the presence of 37 carbon signals classified into 8 methyl carbons, 6 methylene carbons, four *sp*² methine carbons, 7 *sp*³ methine carbons, 6 *sp*² quaternary

carbons, and 6 sp^3 quaternary carbons using an analysis of HSQC data. The ^1H -NMR spectrum showed 49 proton signals including one amine, one hydroxy, 8 methyl protons, 6 methylene protons, four sp^2 , and 7 sp^3 methine protons. The tables below (Tables 2-2 and 2-3) summarized the correlation between protons and carbons found by analyzing the HSQC spectrum taken in $\text{DMSO-}d_6$ (Supplemental Figure 2-8) and CDCl_3 (Supplemental Figure 2-9). Furthermore, ^1H - ^1H COSY spectrum taken in $\text{DMSO-}d_6$ (Supplemental Figure 2-10) and CDCl_3 (Supplemental Figure 2-11) were used to analyze the correlation between protons and HMBC spectrum taken in $\text{DMSO-}d_6$ (Supplemental Figure 2-12) and CDCl_3 (Supplemental Figure 2-13) were used to confirm the correlation between protons and carbons of **6**.

Table 2-2. ^1H , ^{13}C NMR chemical shifts and HMBC signals taken in $\text{DMSO-}d_6$ of **6**

Terpendole O (6) ^a							
Position	δ_{C} ^b , type	δ_{H} ^c (multi, J Hz)	HMBC	Position	δ_{C} ^b , type	δ_{H} ^c (multi, J Hz)	HMBC
1-NH	-	10.69 (s)	2, 18, 19, 24	18	114.3, C	-	-
2	152.3, C	-	-	19	124.1, C	-	-
3	49.9, C	-	-	20	128.0, C	-	-
4	42.1, C	-	-	21	118.2, CH	6.71 (d, 7.2)	19, 23
5	25.5, CH ₂	1.67 (br d, 6.4) 2.42 (br d, 6.4)	26	22	119.5, CH	6.86 (t, 7.6)	20, 24
6	28.53, CH ₂	2.12 (br m)	-	23	110.1, CH	7.12 (d, 8.0)	19, 21
7	70.6, CH	4.26 (t, 8.8)	9, 11	24	139.7, C	-	-
9	71.0, CH	3.40 (d, 9.6)	7, 27, 28, 29	25	16, CH ₃	1.16 (s)	2, 3, 4
10	70.1, CH	4.04 (d, 9.6)	27	26	18, CH ₃	1.02 (s)	3, 4, 5, 13
11	58.9, CH	3.50 (br. s)	7, 9, 12	27	74.1, C	-	-
12	67.0, C	-	-	28	16.7, CH ₃	1.22 (s)	9, 27, 29
13	76.5, C	-	-	29	28.2, CH ₃	1.12 (s)	9, 27, 28
13-OH	-	4.50 (s)	4	31	91.9, CH	5.50 (d, 6.4)	10, 27, 34
14	28.38, CH ₂	1.46 (br m) 1.52 (br s)	-	33	122.5, CH	5.10 (d, 6.4)	35, 36
15	20.3, CH ₂	1.46 (br m) 1.80 (br m)	-	34	137.4, C	-	-
16	49.6, CH	2.71 (br m) 2.45 (br s)	-	35	18.3, CH ₃	1.63 (d, 0.8)	33, 34, 36
17	28.58, CH ₂	2.71 (br m)	2, 3, 18	36	25.0, CH ₃	1.64 (s) 2.93 (m)	33, 34, 35
				37	32.3, CH ₂	3.01 (dd, 16.0, 8.4)	21
				38	63.4, CH	2.93 (m)	20, 21
				39	57.9, C	-	-
				40	18.7, CH ₃	1.32 (s)	38, 39, 41
				41	24.6, CH ₃	1.23 (s)	38, 39, 40

^a ^{13}C (100 MHz) and ^1H (400 MHz) NMR spectra were taken on an NMR 400 MHz spectrometer (Agilent). Chemical shifts are shown with reference to ^b $\text{DMSO-}d_6$ as δ 39.5, ^c $\text{DMSO-}d_6$ as δ 2.48. Multiplicity of signals as follows: s = singlet, d = doublets, dd = double doublets, t = triplet, m = multi. Coupling constants (Hz) were determined by the ^1H - ^1H decoupling experiments.

Table 2-3. ^1H , ^{13}C NMR chemical shifts and HMBC signals taken in CDCl_3 of **6**

Terpendole O (6) ^a							
Position	$\delta_{\text{C}}^{\text{b}}$, type	$\delta_{\text{H}}^{\text{c}}$ (multi, J Hz)	HMBC	Position	$\delta_{\text{C}}^{\text{b}}$, type	$\delta_{\text{H}}^{\text{c}}$ (multi, J Hz)	HMBC
1-NH	-	7.90 (s)	2, 18, 19, 24	18	116.7, C	-	-
2	151.5, C	-	-	19	124.7, C	-	-
3	50.3, C	-	-	20	129.0, C	-	-
4	42.3, C	-	-	21	119.3, CH	6.86 (d, 6.8)	19, 23
		1.34 (m)		22	120.9, CH	7.02 (t, 7.6)	20, 24
5	27.4, CH_2	2.70 (br td, 13.4, 5.6)	13, 26	23	109.9, CH	7.19 (d, 7.6)	19, 21
		2.28 (br m)		24	139.6, C	-	-
6	28.0, CH_2	1.78 (br m)	4	25	15.9, CH_3	1.27 (s)	2, 4, 16
				26	18.8, CH_3	1.14 (s)	3, 4, 5, 14, 16
7	71.5, CH	4.38 (dd, 8.0, 10.0)	9, 11, 12	27	74.7, C	-	-
				28	16.6, CH_3	1.29 (d, 2.8)	9, 27, 29
9	71.18, CH	3.57 (d, 9.6)	7, 27, 28, 29	29	28.2, CH_3	1.29 (d, 2.8)	9, 27, 28
10	71.12, CH	3.91 (d, 9.6)	27	31	92.6, CH	5.53 (d, 6.8)	10, 27, 34
11	61.1, CH	3.61 (s)	7	33	121.9, CH	5.30 (d, 6.8)	35, 36
12	67.8, C	-	-	34	139.6, C	-	-
13	78.0, C	-	-	35	18.6, CH_3	1.74 (d, 0.8)	33, 34, 36
13-OH	-	-	-	36	25.6, CH_3	1.73 (d, 1.2)	33, 34, 35
		1.43 (br m)				2.98 (m)	
14	30.2, CH_2	1.56 (br s)	-	37	32.7, CH_2	3.29 (dd, 14.0, 5.2)	21, 39
		1.60 (br m)		38	64.3, CH	3.09 (dd, 5.2)	19, 20
15	20.5, CH_2	1.90 (br m)	-	39	58.7, C	-	-
16	50.2, CH	2.80 (br m)	-	40	18.9, CH_3	1.42 (s)	38, 39, 41
		2.60 (br t, 11.2)					
17	29.0, CH_2	2.83 (m)	2, 18	41	24.9, CH_3	1.34 (s)	38, 39, 40

^a ^{13}C (100 MHz) and ^1H (400 MHz) NMR spectra were taken on an NMR 400 MHz spectrometer (Agilent). Chemical shifts are shown with reference to ^b CDCl_3 as δ 77.0, ^c CDCl_3 as δ 7.26. Multiplicity of signals as follows: s = singlet, d = doublets, dd = double doublets, t = triplet, td = triplet doublets, m = multi, q = quartet. Coupling constants (Hz) were determined by the ^1H - ^1H decoupling experiments.

Analysis of the ^1H - ^1H correlation spectroscopy (COSY) spectrum gave 6 partial structures I to VI (Figure 2-7); (I) 5- H_2 (δ 1.67, 2.42), 6- H_2 (δ 2.12) and 7-H (δ 4.26), (II) 9-H (δ 3.40), 10-H (δ 4.04) and 11-H (δ 3.50), (III) 14- H_2 (δ 1.46, 1.52), 15- H_2 (δ 1.46, 1.80), 16-H (δ 2.71) and 17- H_2 (δ 2.45, 2.71), (IV) 21-H (δ 6.71), 22-H (δ 6.86) and 23-H (δ 7.12), (V) 31-H (δ 5.50), and 33-H (δ 5.10), and (VI) 37- H_2 (δ 2.93, 3.01), and 38-H (δ 2.93). The COSY correlations of 14- H_2 (δ 1.43, 1.56) and 15- H_2 (δ 1.60, 1.90), and 37- H_2 (δ 2.98, 3.29) and 38-H (δ 3.09) were more clearly observed in CDCl_3 .

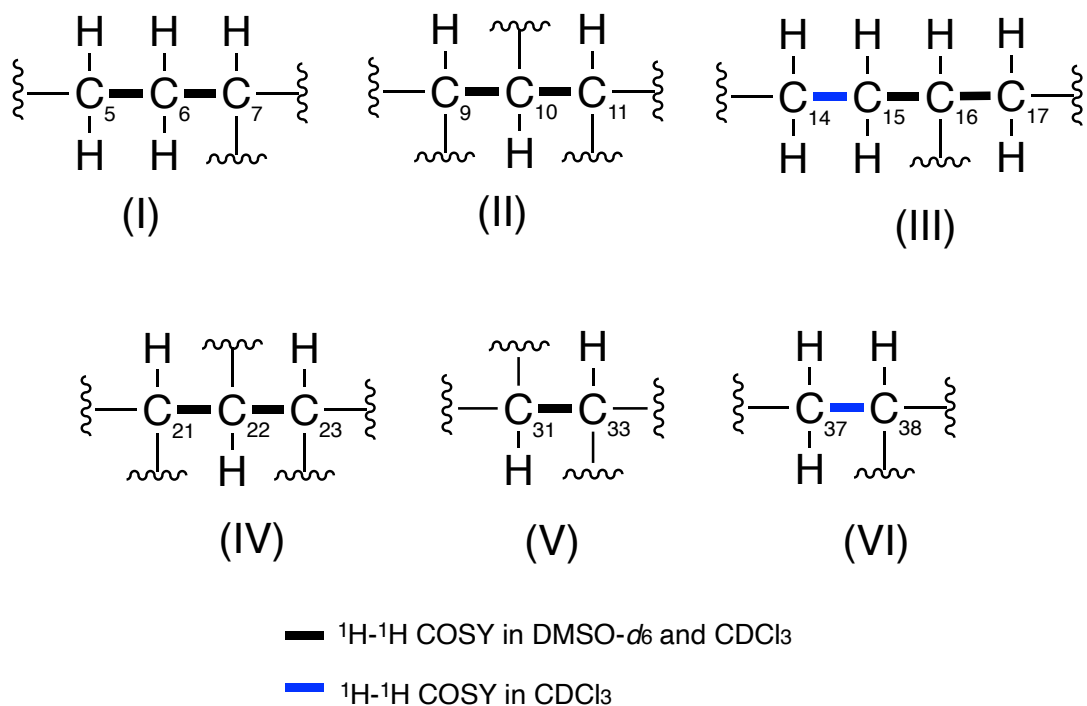


Figure 2-7. Six partial structures of **6** from ^1H - ^1H COSY spectrum analyses

Furthermore, the following linkages including partial structures I to VI were elucidated using ^{13}C - ^1H long range couplings of 2J and 3J in the HMBC spectrum. The cross peaks from 21-H and 23-H to C-19 (δ 124.1) and from 22-H to C-20 (δ 128.0) and C-24 (δ 139.7) indicated the presence of a trisubstituted benzene ring containing partial structure IV. The cross peaks from 1-NH (δ 10.69) to C-2 (δ 152.3), C-18 (δ 114.3), C-19, and C-24 indicated that a pyrrole ring is directly attached to the benzene, showing the presence of an indole moiety. The cross peaks from 37- H_2 (δ 2.93, 3.01) to C-39 (δ 57.9), from 40- H_3 (δ 1.32) to C-38 (δ 63.4), C-39, and C-41 (δ 24.6) and from 41- H_3 (δ 1.23) to C-38, C-39, and C-40 suggested the presence of an isopentanyl unit containing partial structure VI. Taking the chemical shifts of C-38 and C-39 into consideration, these carbons were involved in the formation of an epoxide moiety. The cross peaks from 21-H to C-37 (δ 32.3) and from 38-H to C-20 supported that an epoxy-isopentanyl unit is connected to C-20 of the indole moiety (Figure 2-8).

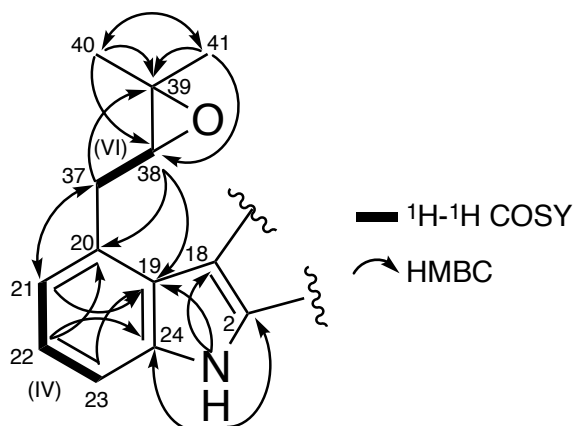


Figure 2-8. Epoxyprenyld indole moiety of **6** by ^1H - ^1H COSY and HMBC analyses

The cross peaks from 17- H_2 (δ 2.45, 2.71) to C-2, C-3 (δ 49.9), and C-18 suggested that a cyclopentene ring (ring A) is attached to the indole ring. The cross peaks from 25- H_3 (δ 1.16) to C-3 and C-4 (δ 42.1) and from 26- H_3 (δ 1.02) to C-3, C-4, C-5 (δ 25.5), and C-13 (δ 76.5) and the clear cross peaks from 5- H_2 (δ 1.34, 2.70) to C-13 (δ 78.0), 6- H_2 (δ 2.28, 1.78) to C-4 (δ 42.3), and 7- H (δ 4.38) to C-12 (δ 67.8) in CDCl_3 supported that two cyclohexane rings (rings B and C) are attached to ring A, covering partial structure I and III. The cross peak from 13-OH (δ 4.50) to C-4 indicated the presence of a hydroxy group at quaternary C-13 (Figure 2-9).

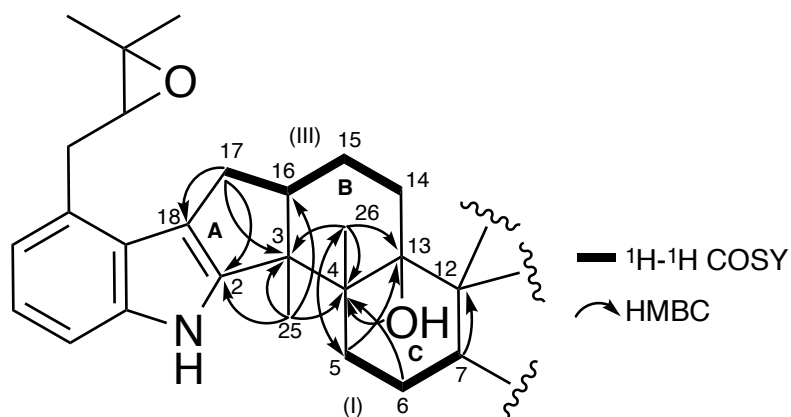


Figure 2-9. Rings A-C of **6** by ^1H - ^1H COSY and HMBC analyses

The cross peaks from 7-H to C-9 (δ 71.0) and C-11 (δ 58.9), from 11-H to C-7 (δ 70.6) and C-12 (δ 67.0), from 9-H to C-27 (δ 74.1), C-28 (δ 16.7), and C-29 (δ 28.2), from 10-H to C-27, from 28-H₃ (δ 1.22) to C-9, C-27, and C-29, from 29-H₃ (δ 1.12) to C-9, C-27, and C-28, and from 31-H to C-10 (δ 70.1) and C-27 showed the presence of a tetrahydropyran ring (ring D) and 1,3-dioxane ring (ring E), which includes a partial structure II. In addition, the cross peaks from 31-H to C-34 (δ 137.4), from 33-H to C-35 (δ 18.3) and C-36 (δ 25.0), from 35-H₃ (δ 1.63) to C-33 (δ 122.5), C-34, and C-36, and from 36-H₃ (δ 1.64) to C-33, C-34, and C-35 suggested that a 2-methyl-2-butene with partial structure V is bound to C-31 of ring E (Figure 2-10).

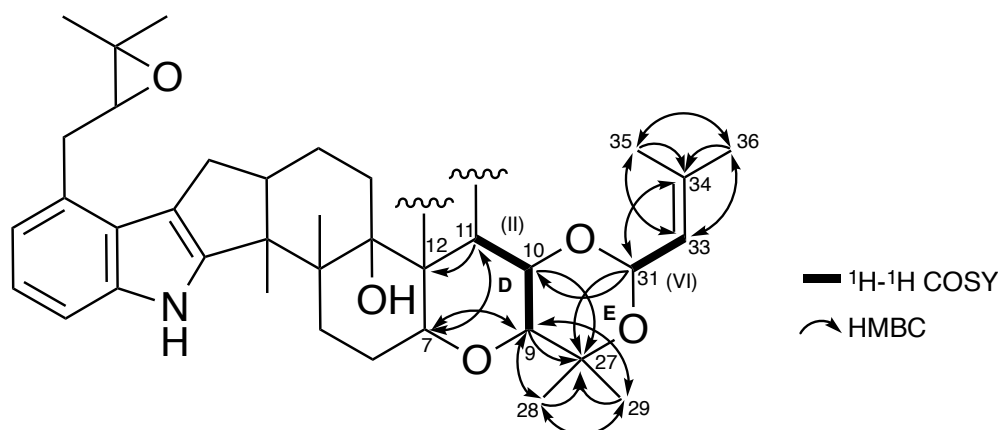


Figure 2-10. Ring D, E and 2-methyl-2-butene moiety of **6** by ¹H-¹H COSY and HMBC analyses

Taking the molecular formula, the carbon chemical shifts and the degrees of unsaturation into consideration, an oxygen atom should build epoxy group between C-11 and C-12. Taken together, the planar structure of **6** was elucidated as shown in Figure 2-11.

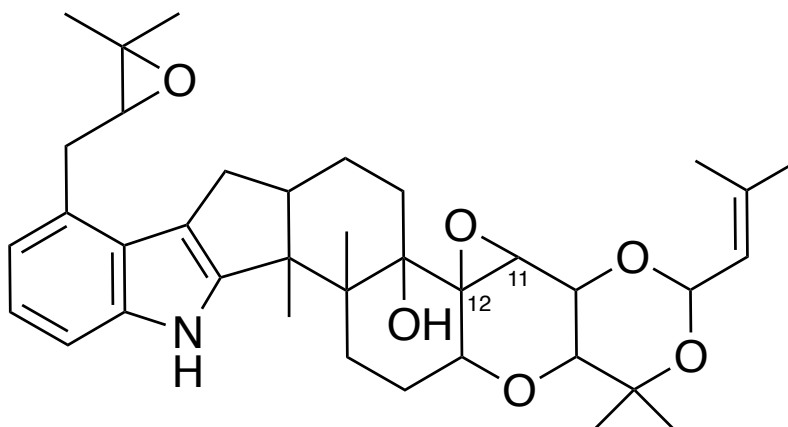


Figure 2-11. Planar structure of **6**

To elucidate the relative stereochemistry of 11 chiral carbons in **6**, ^1H - ^1H coupling constants and nuclear Overhauser effect spectroscopy (NOESY) experiments in $\text{DMSO-}d_6$ and CDCl_3 were analyzed (Supplemental Figures 2-14 and 2-15). The large coupling constant (9.6 Hz) between 9-H and 10-H indicated that they are in an axial position. In $\text{DMSO-}d_6$, nuclear Overhauser effect (NOE) correlations were observed between 25- H_3 and 5- H_a (δ 2.42) and 13-OH and 7-H. In CDCl_3 , additional NOEs were observed between 25- H_3 (δ 1.27) and 15- H_a (δ 1.90), 25- H_3 and 17- H_a (δ 2.60), 5- H_a (δ 2.70) and 6- H_a (δ 2.28), 6- H_a and 7-H (δ 4.38), and 7-H and 9-H (δ 3.57). These data indicated that these protons were oriented in the same side of the plane of the consecutive ring system. In contrast, NOEs were observed between 16-H and 26- H_3 , 10-H and 26- H_3 , and among 10-H, 31-H, and 28- H_3 in $\text{DMSO-}d_6$, and between 16-H (δ 2.80) and 17- H_b (δ 2.83), 6- H_b (δ 1.78) and 26- H_3 (δ 1.14) in CDCl_3 . The data indicated that these protons were present on the opposite side. Furthermore, NOE was observed between 11-H (δ 3.61) and 14- H_a (δ 1.43) in CDCl_3 , suggesting that 11-H was in the equatorial position (Figure 2-12), that was supported with no J coupling between 10-H and 11-H. Taken together, the relative stereochemistry of **2** except for C-38 was elucidated to be $3S^*$, $4R^*$, $7S^*$, $9S^*$, $10R^*$, $11R^*$, $12S^*$, $13S^*$, $16S^*$, and $31S^*$.

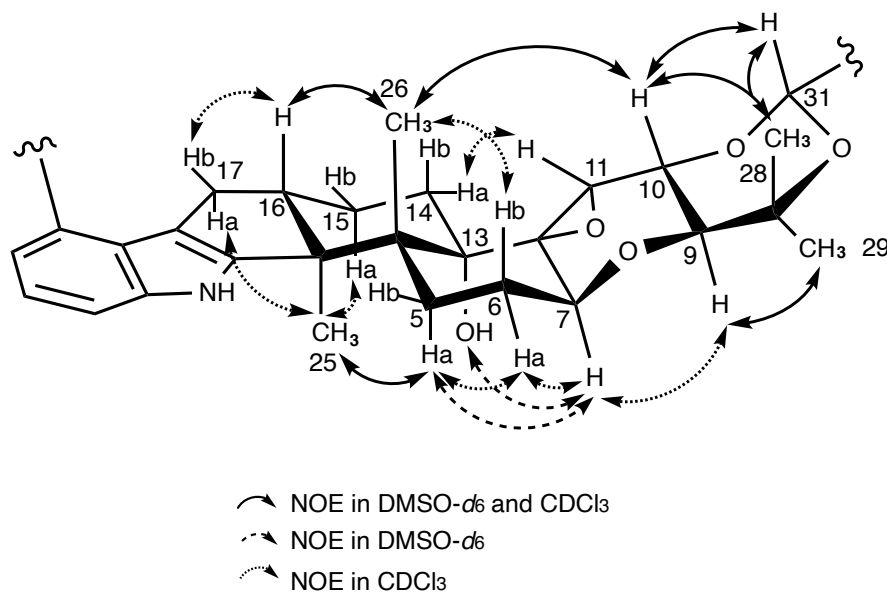


Figure 2-12. NOESY experiment of **6**

2-4. Structure elucidation of new terpendole N

The physicochemical properties of terpendole N (**5**) were summarized in Table 2-4. Compound **5** was obtained as white powder. From high resolution ESI-MS, molecular weight of **5** was 653 and its molecular formula was C₃₇H₅₁NO₉ (Supplemental Figure 2-16) indicating 13 degrees of unsaturation. Compound **5** has UV spectra (Supplemental Figure 2-17) with absorption maxima at 213, 248 and 290 nm. The IR absorptions (Supplemental Figure 2-18) at 3413, 2977, 2930 and 1718 cm⁻¹ were similar to those of reported terpendoles.

Table 2-4. Physicochemical properties of **5**

Terpendole N (5)	
Appearance	White powder
Molecular weight	653
Molecular formula	C ₃₇ H ₅₁ NO ₉
HR-ESI-MS (<i>m/z</i>)	
Calcd	654.3642 [M+H] ⁺
Found	654.3637 [M+H] ⁺
UV _{λ_{max}} ^{CH₃OH} nm (log ε)	213 (4.2), 248 (4.3), 290 (3.7)
IR _{max} ^{KBr} cm ⁻¹	3413, 2977, 2930, 1718
[α] _D ^t (c = 0.1 CH ₃ OH)	-16.6 (t=25)

¹H-NMR (Supplemental Figure 2-19) and ¹³C-NMR (Supplemental Figure 2-20) signals of **5** taken in DMSO-*d*₆ were shown in Table 2-5. The ¹³C-NMR data revealed the presence of 37 carbon signals classified into 8 methyl carbons, 6 methylene carbons, four *sp*² methine carbons, 7 *sp*³ methine carbons, 5 *sp*² quaternary carbons, and 7 *sp*³ quaternary carbons by an analysis of HSQC data. The ¹H-NMR spectrum of **5** showed 51 proton signals, which were classified into 8 methyl protons, 6 methylene protons, four *sp*² and 7 *sp*³ methine protons, one amine proton, and three hydroxy protons. The table below (Table 2-5) summarized the correlation between protons and carbons found by analyzing the HSQC spectrum (Supplemental Figure 2-21). Furthermore, ¹H-¹H COSY spectrum (Supplemental Figure 2-22) was used to analyze the correlation between protons and HMBC spectrum (Supplemental Figure 2-23) was used to confirm the correlation between protons and carbon of **5**.

Table 2-5. ¹H and ¹³C NMR chemical shifts and HMBC signals of **5**

Terpendole N (5) ^a							
Position	δ _C ^b , type	δ _H ^c (multi, <i>J</i> Hz)	HMBC	Position	δ _C ^b , type	δ _H ^c (multi, <i>J</i> Hz)	HMBC
1-NH	-	10.08 (s)	2, 18, 19, 24	18	76.8, C	-	-
2	180.2, C	-	-	18-OH	-	5.72 (s)	18, 19
3	74.6, C	-	-	19	128.9, C	-	-
3-OH	-	3.74 (s)	3, 16, 25	20	136.7, C	-	-
4	44.9, C	-	-	21	121.9, CH	6.81 (d, 7.6)	19, 23
5	23.2, CH ₂	1.15-1.21 (m)	4	22	128.8, CH	7.11 (t, 7.6)	20, 24
		1.92 (m)		23	107.5, CH	6.63 (d, 7.6)	19, 21
6	28.1, CH ₂	1.32 (m)	4, 7, 12	24	141.7, C	-	-
		1.88 (m)		25	19.5, CH ₃	1.08 (s)	3, 16
7	70.5, CH	4.02 (dd, 10.2, 7.4)	6, 11, 12	26	16.7, CH ₃	0.59 (s)	4, 5, 13
				27	74, C	-	-
9	70.9, CH	3.34 (d, 9.6)	27, 28, 29	28	16.7, CH ₃	1.14 (s)	9, 27, 29
10	70.1, CH	3.92 (d, 9.6)	-	29	28.3, CH ₃	1.073 (s)	9, 27, 28
11	59.1, CH	3.33 (br s)	7, 9, 12	31	92, CH	5.42 (d, 6.4)	10, 27, 34
12	66.8, C	-	-	33	122.5, CH	5.05 (br d, 6.4)	35, 36
13	75.9, C	-	-	34	137.5, C	-	-
13-OH	-	4.18 (s)	4, 13, 14	35	18.4, CH ₃	1.61 (d, 1.2)	34, 36
		0.81-0.90 (m)		36	25, CH ₃	1.63 (s)	34, 35
14	25.5, CH ₂	1.04-1.08 (m)	4	37	29.7, CH ₂	2.87 (m)	19, 20, 21,
						3.03 (m)	39
15	23.7, CH ₂	1.10 (d, 4.8)	17	38	62.9, CH	3.02 (m)	20
		1.27 (s)		39	57.8, C	-	-
16	37.5, CH	1.27-1.34 (m)	-	40	18.9, CH ₃	1.27 (s)	41
		1.68 (dd, 12.6,					
17	37.1, CH ₂	10.6)	2, 3, 15, 18	41	24.7, CH ₃	1.23 (s)	38, 39, 40
		2.29 (d, 12.6)					

^a ¹³C (100 MHz) and ¹H (400 MHz) NMR spectra were taken on an NMR 400 MHz spectrometer (Agilent). Chemical shifts are shown with reference to ^b DMSO-*d*₆ as δ 39.5, ^c DMSO- *d*₆ as δ 2.48. Multiplicity of signals as follows: s = singlet, d = doublets, dd = double doublets, t = triplet, m = multi. Coupling constants (Hz) were determined by the ¹H-¹H decoupling experiments.

Compared with the ^{13}C -NMR spectra of **6**, the chemical shift values of **5** at C-2, C-3, and C-18 were remarkably shifted, suggesting that **5** has one additional sp^2 and two additional sp^3 oxygenated carbons. From the ^{13}C - ^1H long range couplings of 2J and 3J in the HMBC spectrum, the cross peaks from 18-OH (δ 5.72) to oxygenated C-18 (δ 76.8) and aromatic C-19 (δ 128.9) (Figure 12-13 (a)), and from 3-OH (δ 3.74) to oxygenated C-3 (δ 74.6), C-16 (δ 37.5), and C-25 (δ 19.5) (Figure 12-13 (b)) indicated that a hydroxy moiety was directly bound to C-18 and C-3. Furthermore, the chemical shift value at C-2 (δ 180.2) supported the presence of an amide group, which implied that **5** contains an indolinone moiety (Figure 12-13 (a)). Taken together, the planar structure of **5** was proposed as shown in Figure 12-14, which fulfilled the molecular formula and degrees of unsaturation.

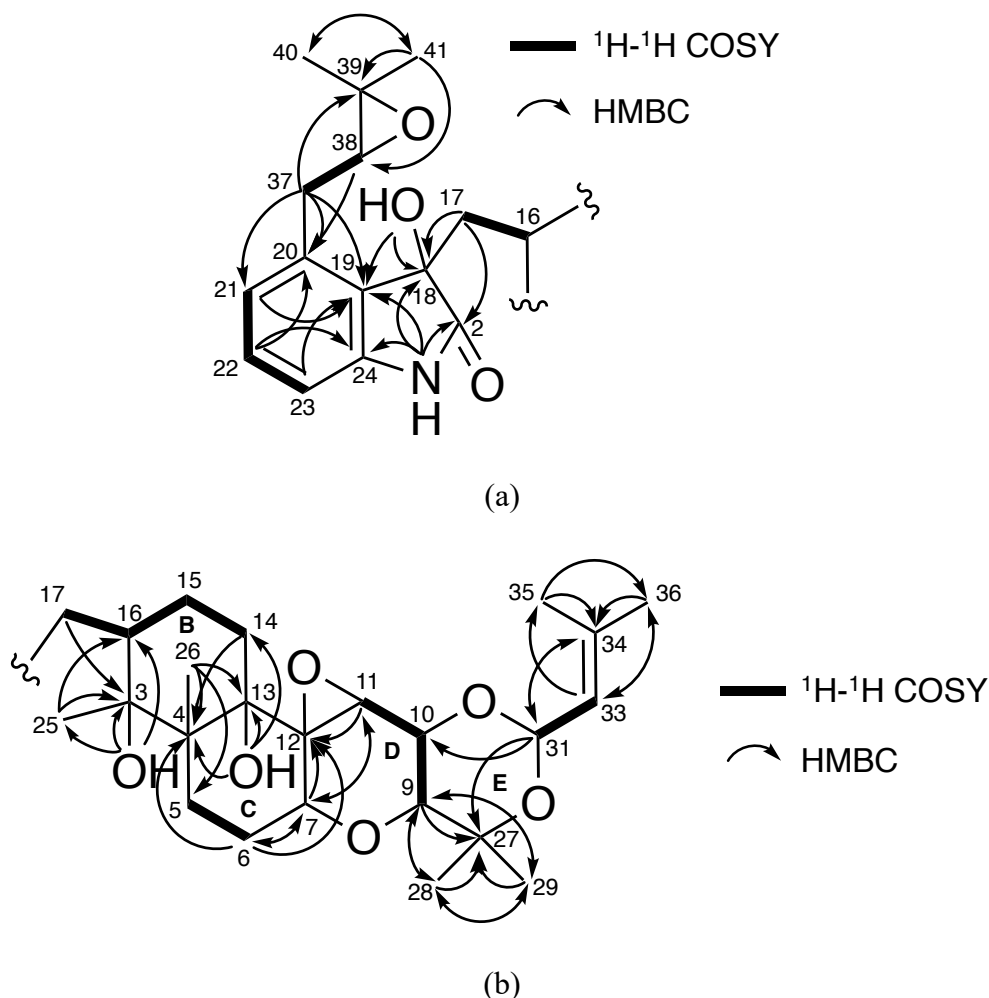


Figure 2-13. Partial structures (a) and (b) of **5** by ^1H - ^1H COSY and HMBC spectrum

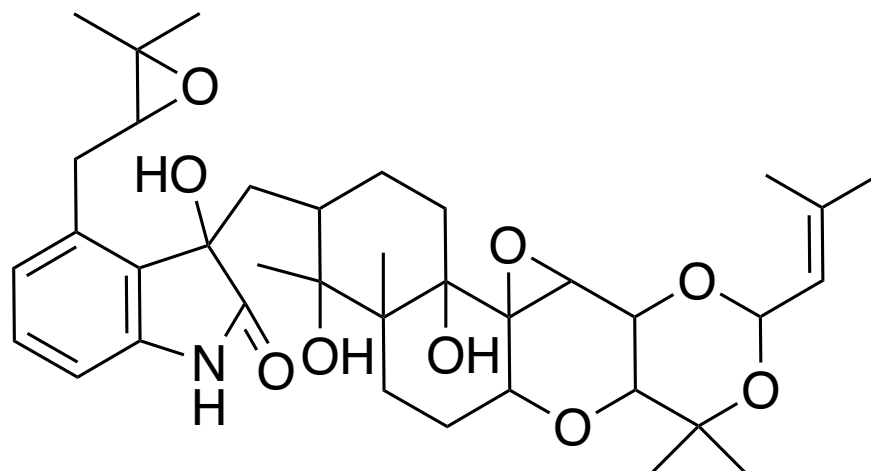


Figure 2-14. Planar structure of **5**

Relative stereochemistry of **5** was elucidated by analyses of ^1H - ^1H coupling constants and ROESY experiments (Supplemental Figure 2-24). As shown in Figure 2-15, the NOE correlations of **5** were very similar to those of **6**. Consequently, the relative stereochemistry of 12 chiral carbons except for C-18 and C-38 of **1** was determined to be $3S^*$, $4R^*$, $7S^*$, $9S^*$, $10R^*$, $11R^*$, $12S^*$, $13S^*$, $16S^*$ and $31S^*$.

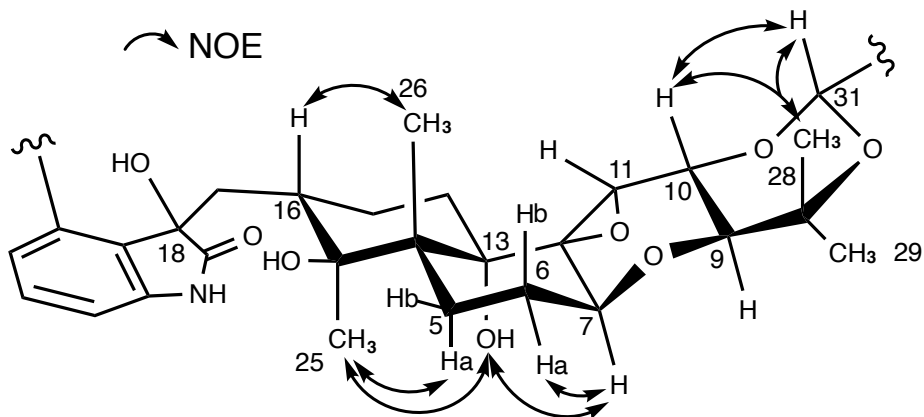


Figure 2-15. ROESY experiment of **5**

2-5. Structure elucidation of new terpendole P

The physicochemical properties of terpendole P (**7**) were summarized in Table 2-6. Compound **7** was obtained as white powder. From high resolution ESI-MS, molecular weight of **7** was 519 and its molecular formula was C₃₂H₄₁NO₅ (Supplemental Figure 2-25) indicating 13 degrees of unsaturation. Compound **7** has UV spectra (Supplemental Figure 2-26) with absorption maxima at 227 and 280 nm. The IR absorption (Supplemental Figure 2-27) at 3380, 3004, 2931, and 1681 cm⁻¹ were similar with reported terpendoles.

Table 2-6. Physicochemical properties of 7	
	Terpendole P (7)
Appearance	White powder
Molecular weight	519
Molecular formula	C ₃₂ H ₄₁ NO ₅
HR-ESI-MS (<i>m/z</i>)	
Calcd	520.3067 [M+H] ⁺
Found	520.3063 [M+H] ⁺
UV _{λ_{max}} ^{CH₃OH} nm (log ε)	227 (4.4), 280 (3.7)
IR _{max} ^{KBr} cm ⁻¹	3380, 3004, 2931, 1681
[α] _D ^t (c = 0.1 CH ₃ OH)	-27.8 (t=25)

¹H-NMR (Supplemental Figure 2-28) and ¹³C-NMR (Supplemental Figure 2-29) signals of **7** taken in DMSO-*d*₆ were shown in Table 2-7. The presence of 32 carbon signals classified into 6 methyl carbons, 5 methylene carbons, 5 *sp*² methine carbons, 6 *sp*³ methine carbons, 5 *sp*² quaternary carbons and 5 *sp*³ quaternary carbons using HSQC experiments. The ¹H-NMR spectrum showed one amine, one hydroxy and 39 proton signals which were classified into 6 methyl protons, 5 methylene protons, 5 *sp*² and 6 *sp*³ methine protons compatible with the molecular formula. The table below (Table 2-7) summarized the correlation between protons and carbons found by analyzing the HSQC spectrum (Supplemental Figure 2-30). Furthermore, ¹H-¹H COSY spectrum (Supplemental Figure 2-31) was used to analyze the correlation between protons and HMBC spectrum (Supplemental Figure 2-32) was used to confirm the correlation between protons and carbon of compound **7**.

Table 2-7. ¹H and ¹³C NMR chemical shifts and HMBC signals of **7**

Terpendole P (7) ^a							
Position	δ _C ^b , type	δ _H ^c (multi, J Hz)	HMBC	Position	δ _C ^b , type	δ _H ^c (multi, J Hz)	HMBC
1-NH	-	10.81 (s)	2, 18, 19, 24	18	114.7, C	-	-
2	150.6, C	-	-	19	124.1, C	-	-
3	38.3, C	-	-	20	117.8, CH	7.26 (d, 7.8)	18, 22
4	48.3, C	-	-	21	118.4, CH	6.88 (td, 7.8, 1.2)	19, 23
5	27.9, CH ₂	2.05 (m)	3, 4, 7, 13	22	119.5, CH	6.93 (td, 7.8, 1.2)	20, 24
6	28.2, CH ₂	1.75 (m) 2.30 (m)	-	23	111.7, CH	7.24 (d, 7.8)	19, 21
7	70.6, CH	3.86 (m)	9, 12	24	140.1, C	-	-
9	75.5, CH	3.25 (d, 9.0)	7, 11, 27, 28, 29	25	16.2, CH ₃	0.99 (s)	2, 3, 4, 16
10	65.5, CH	3.89 (m)	-	26	18, CH ₃	1.12 (s)	3, 4, 5, 13
10-OH	-	4.78 (d, 4.2)	9, 10, 11	27	76.9, C	-	-
11	63.1, CH	3.32 (s)	9, 10, 12	28	21.4, CH ₃	1.17 (s)	9, 27, 29
12	62.9, C	-	-	29	23.9, CH ₃	1.16 (s)	9, 27, 28
13	66.9, C	-	-	31	58.1, CH ₂	3.87 (m) 3.91 (m)	10, 27, 34
14	54.7, CH	3.19 (d, 5.4)	12, 13	33	122.1, CH	5.18 (dd, 7.0, 1.2)	35, 36
15	24.5, CH ₂	2.02 (m) 1.85 (m)	13, 17	34	134.5, C	-	-
16	45, CH	2.63 (m)	2, 3, 4, 18	35	17.7, CH ₃	1.58 (s)	34, 36
17	26.7, CH ₂	2.17 (m) 2.62 (m)	2, 3, 15, 18	36	25.3, CH ₃	1.65 (s)	33, 34, 35

^a ¹³C (150 MHz) and ¹H (600 MHz) NMR spectra were taken on an NMR 600 MHz spectrometer (Agilent). Chemical shifts are shown with reference to ^b DMSO-*d*₆ as δ 39.5, ^c DMSO-*d*₆ as δ 2.48. Multiplicity of signals as follows: s = singlet, d = doublets, dd = double doublets, td = triplet doublets, m = multi. Coupling constants (Hz) were determined by the ¹H-¹H decoupling experiments.

COSY correlations between aromatic protons 20-H (δ 7.26), 21-H (δ 6.88), 22-H (δ 6.93), and 23-H (δ 7.24) and HMBC correlations from 22-H to C-24 (δ 140.1) and from 23-H to C-19 (δ 124.1) indicated the presence of disubstituted benzene ring. Thus, **7** does not having epoxyprenyl moiety like **5** and **6**. Unlike **5** and **6**, the ether bond between O-10 and C-31 was hydroxylated because of the observed ¹H-¹H COSY couplings between oxymethylene proton of 31-H₂ (δ 3.87, 3.91) and *sp*² methine proton of 33-H (δ 5.18). An isoprenyl moiety were also observed by HMBC correlations from 31-H₂ to C-34 (δ 134.5), 33-H to C-35 (δ 17.7) and C-36 (δ 25.3). This isoprenyl moiety was connected to ring D by long-range correlation from 31-H₂ to C-10 (δ 65.5), C-27 (δ 76.9) (Figure 2-16). Taking together, **7** is having a very similar structure to reported terpendole J (**15**). The ¹³C chemical shifts of **7** were similar to these of **15** [98] (C₃₂H₄₃NO₅) except for C-14 (δ 54.7). Considering the different molecular formula between **7** and **15**, the presence of an epoxide moiety was suggested between C-13 and C-14. Therefore, the structure of **7** was elucidated as shown in Figure 2-17, which fulfilled the molecular formula and degrees of unsaturation. The relative stereochemistry of 10 chiral carbons of **7** was determined to be

3*S**, 4*R**, 7*S**, 9*S**, 10*R**, 11*R**, 12*S**, 13*R**, 14*S**, and 16*R** by NOE experiments in a similar way for **5** and **6** (Figure 2-18 and Supplemental Figure 2-33).

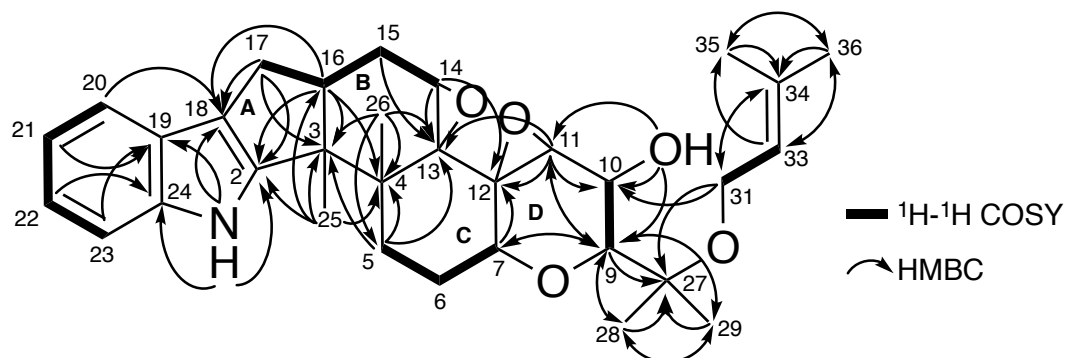


Figure 2-16. ^1H - ^1H COSY and HMBC analyses of **7**

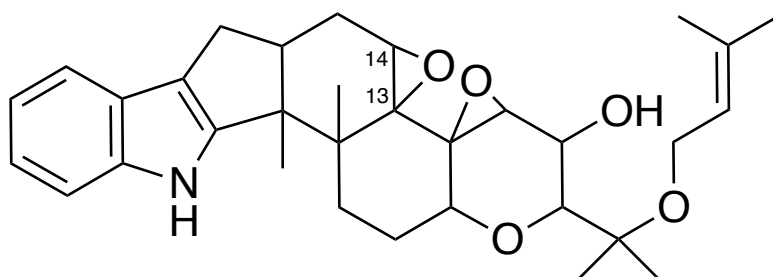


Figure 2-17. Planar structure of **7**

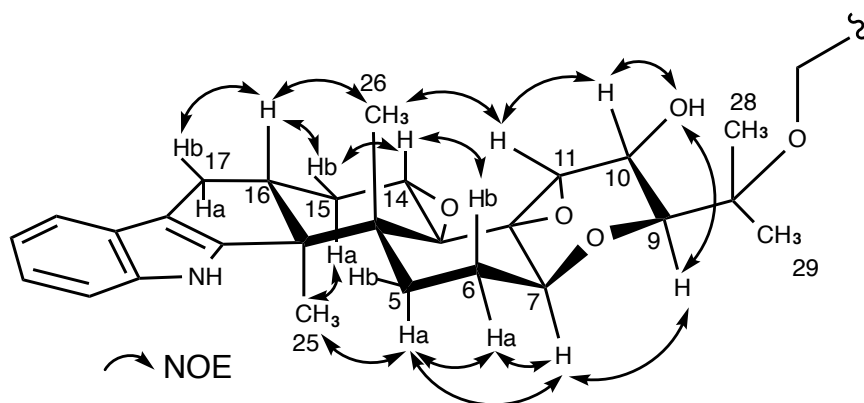


Figure 2-18. ROESY experiment of **7**

2-6. Other terpendole congeners identification

Based on spectral data including ^1H -NMR, ^{13}C -NMR, and MS (Supplemental Figures 2-34~2-54), and the search results of SciFinder Scholar, the structures of **8–15** were identified as the known NK-12838 (**10**), terpendoles C (**11**), D (**12**), L (**13**), and J (**15**), and tolypocladin A (**14**) [95, 97-99] (Figure 2-1).

2-7. Inhibition of SOAT isozymes using SOAT1- and SOAT2-CHO cells

The obtained new compounds were evaluated for CE synthesis inhibitory activity at a cellular level (Figure 2-19). The activities were evaluated in accordance with our established method using hSOAT1-CHO cells and hSOAT2-CHO cells [67, 68]. The human SOAT inhibitory activities of terpendole congeners (**5–15**) were summarized in Table 2-8.

Terpendoles O and P (**6** and **7**) which contain an indole moiety inhibited both SOAT1 and SOAT2 activity to a similar extent (IC_{50} values ranging from 2.4 to 6.9 μM), giving selectivity index (SI; $\log(\text{IC}_{50} \text{ for SOAT1}/\text{IC}_{50} \text{ for SOAT2})$) values of +0.06 and -0.06, respectively. Thus, we defined that **6** and **7** are dual-type SOAT inhibitors [96]. On the other hand, **5** containing an indolinone moiety showed no inhibitory activity against both SOAT isozymes ($\text{IC}_{50\text{S}}, >14 \mu\text{M}$). In addition, no morphological abnormality of cells was observed under the microscope at the added concentrations of any compounds.

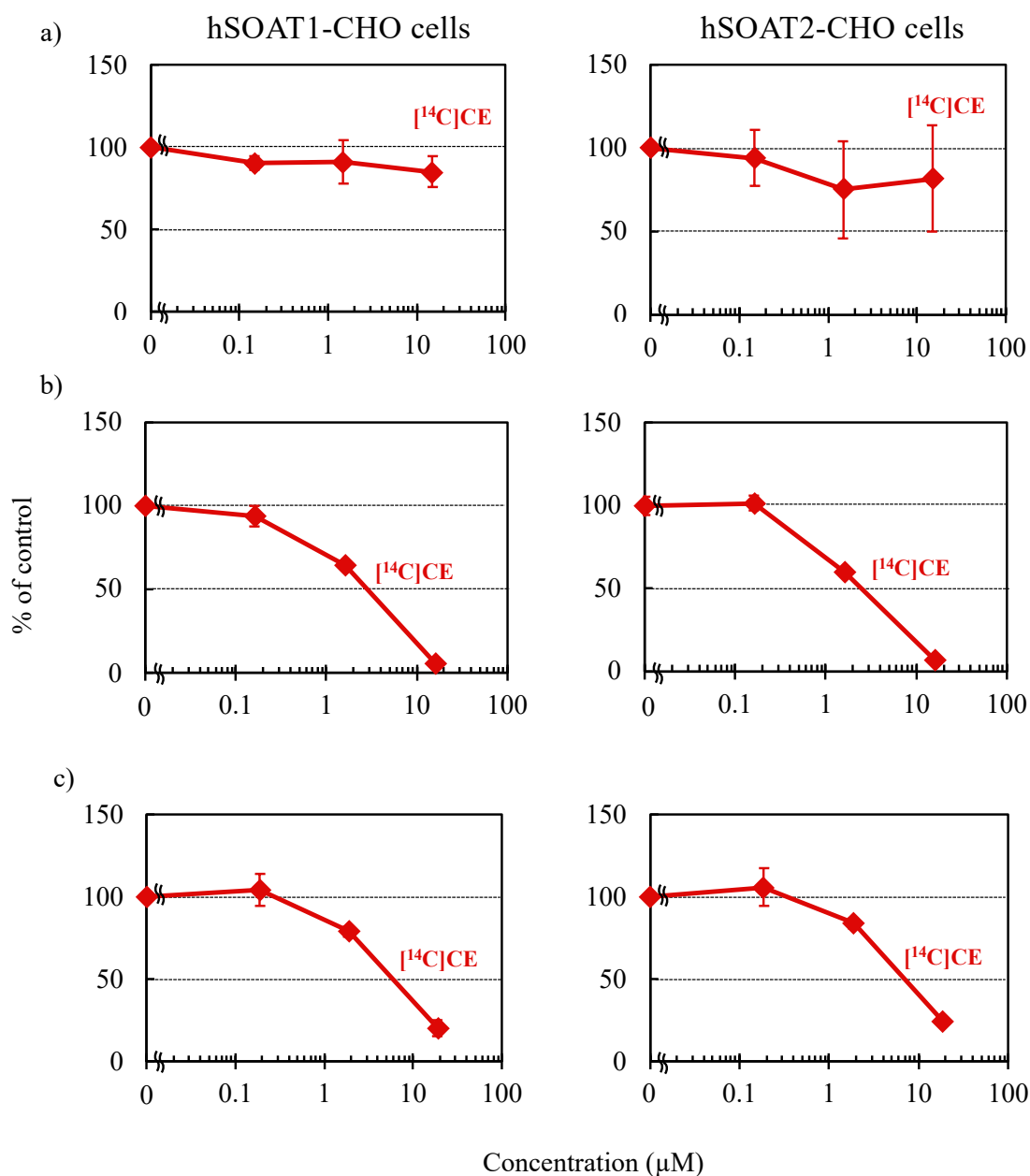


Figure 2-19. Effect of new terpendoles N-P (5–7) on CE synthesis in human SOAT1- and SOAT2-CHO cells

hSOAT1-/ hSOAT2-CHO cells were incubated with [^{14}C]oleic acid and a) terpendole N (5), b) terpendole O (6), c) terpendole P (7) at various concentrations for 6 hours. Cells were then lysed and cellular [^{14}C]CE (♦) separated on TLC then quantified using an image analyzer. The results obtained were plotted as % of control (without drugs). Values represent means \pm SD (n = 3).

Table 2-8. Inhibitory activity against SOAT1/SOAT2 of **5–15**

Compound	IC ₅₀ (μM) ^a		SI ^b (Type) ^c
	SOAT1	SOAT2	
5	>14	>14	–
6	2.8	2.4	+0.06 (dual)
7	5.9	6.9	-0.06 (dual)
8 ^d	0.67	0.24	+0.45 (dual)
9 ^d	6.12	0.073	+1.92 (SOAT2)
10 ^d	6.7	3.5	+0.27 (dual)
11	2.0	2.2	-0.04 (dual)
12	0.8	2.1	-0.42 (dual)
13	6.8	1.8	+0.57 (dual)
14	>18	>18	–
15	18.6	10.7	+0.24 (dual)
Sespendole ^e	12	6.5	+0.26 (dual)

^an ≥ 3. ^bSelectivity Index = log(IC₅₀ for SOAT1/IC₅₀ for SOAT2). ^cType of inhibitors (Dual with -1.0 < SI < +1.0, SOAT1 with SI ≤ -1.0, SOAT2 with +1.0 ≤ SI). ^dData from Ref. [96]. ^eData from Ref. [42] (African green monkey SOAT1- and SOAT2-CHO cells).

2-8. Discussion

During the screening study for SOAT inhibitors, our group have reported a series of fungal indole/indoline-containing di/sesquiterpenes; namely terpendoles produced by *Albophoma yamanashiensis* [97, 98], sespendole (Figure 2-20) produced by *Pseudobotrytis terrestris* FKA-25 [42, 100], and voluhemins by *Volutella citrinella* BF-0440 [96]. As described in the present study, a total of 11 terpendole congeners (**5–15**) were isolated from the voluhemin-producing fungus. Herein, the SOAT inhibitory activity (IC₅₀ value) and selectivity (SI value) toward SOAT1 and SOAT2 isozymes of these compounds in cell-based assays are summarized in Table 2-8. Those of sespendole are also added to Table 2-8. Additionally, these terpendole congeners were not affected PL synthesis in cell-based assay.

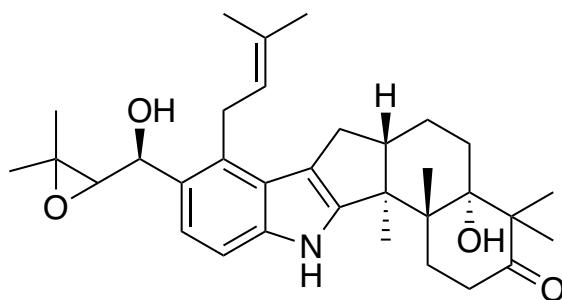


Figure 2-20. Structure of sespendole

The most common structure from these terpendole congeners and diverse moieties R1 to R7 are illustrated in Figure 2-21 to discuss the SARs. (1) Ring systems: five (sespendole), six (**7**, **12**, and **15**), and seven (**6**, **8**, **9**, **10**, **11**, and **13**) consecutive rings including an indole/indoline maintain SOAT inhibitory activity. Compound **5**, which has opened ring A, lost SOAT inhibitory activity. These data indicated that five, six and seven consecutive ring systems are important for exhibiting SOAT inhibitory activity. (2) R1 and R2; comparison among compounds **6**, **8**, **9**, **10**, **11**, and **13**; compounds **7**, **12**, and **15**; and sespendole indicated that the presence of an isoprenyl-derived moiety at R1 and R2 is not essential for SOAT inhibition. (3) R3 and R4; compounds with an indoline containing a hydroxyl group at R3 and R4 (**8** and **10**) maintained SOAT inhibitory activity, indicating that both hydroxy indoline- and indole-type compounds exhibit SOAT inhibition. (4) R5; comparison between **8** and **10** revealed that the presence of a proton at R5 enhances SOAT inhibitory activities (both SOAT1 and SOAT2) approximately 10-fold. (5) R6; comparison between **12** and **15** showed that R6 markedly prefers a proton (**12**) to a hydroxyl group (**15**) for more potent SOAT inhibition (both SOAT1 and SOAT2, approximately 20- to 5-fold). Compound **7** with an epoxy group between C-13 and C-14 partially covering R6 showed an intermediate inhibitory activity. (6) R7; comparison between compounds (**7**, **12**, and **15**) and **14** strongly suggested that the presence of a free hydroxyl group at R7 loses SOAT inhibitory activity.

Importantly, most terpendole congeners are intrinsically dual-type SOAT inhibitors, whereas only voluhemin B (**9**) exhibited SOAT2 selective inhibition. This finding indicated that the presence of a methoxy moiety at R4 is important for SOAT2 selectivity.

The structure of SOAT localized in the endoplasmic reticulum membrane had not been defined. Very recently, three research groups have just reported the structure of human-SOAT1 [62, 63, 78] and human-SOAT2 [64] using cryo-electron microscopy. As a future plan, the explanation of SAR and the selectivity of SOAT inhibitors (dual-type, SOAT1-selective or SOAT2-selective ones) toward SOAT isozymes can be explored on a molecular basis. Voluhemins (**8–9**) with hemiaminal group and terpendole N (**5**) with

indolinone and four consecutive rings system are rare and interesting discoveries. Thus, the study of biosynthetic gene cluster can lead to the possible discovery of new biosynthetic genes.

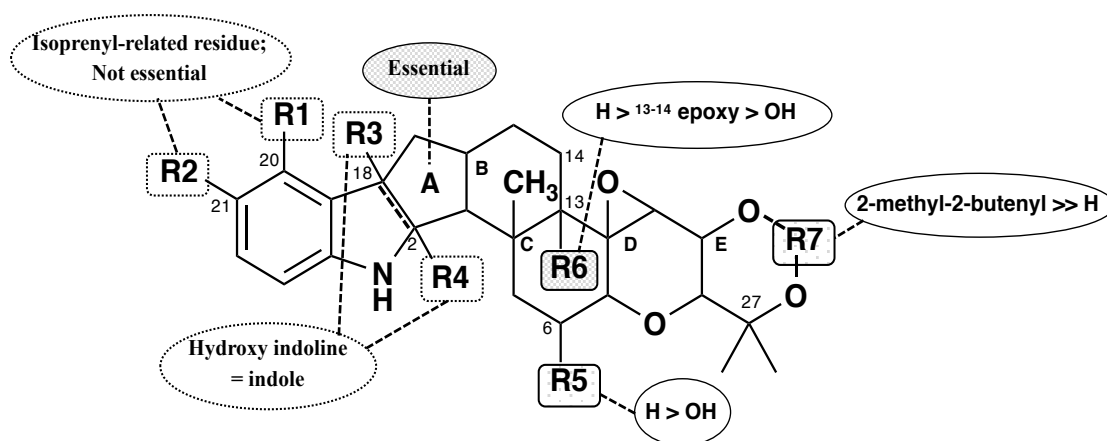
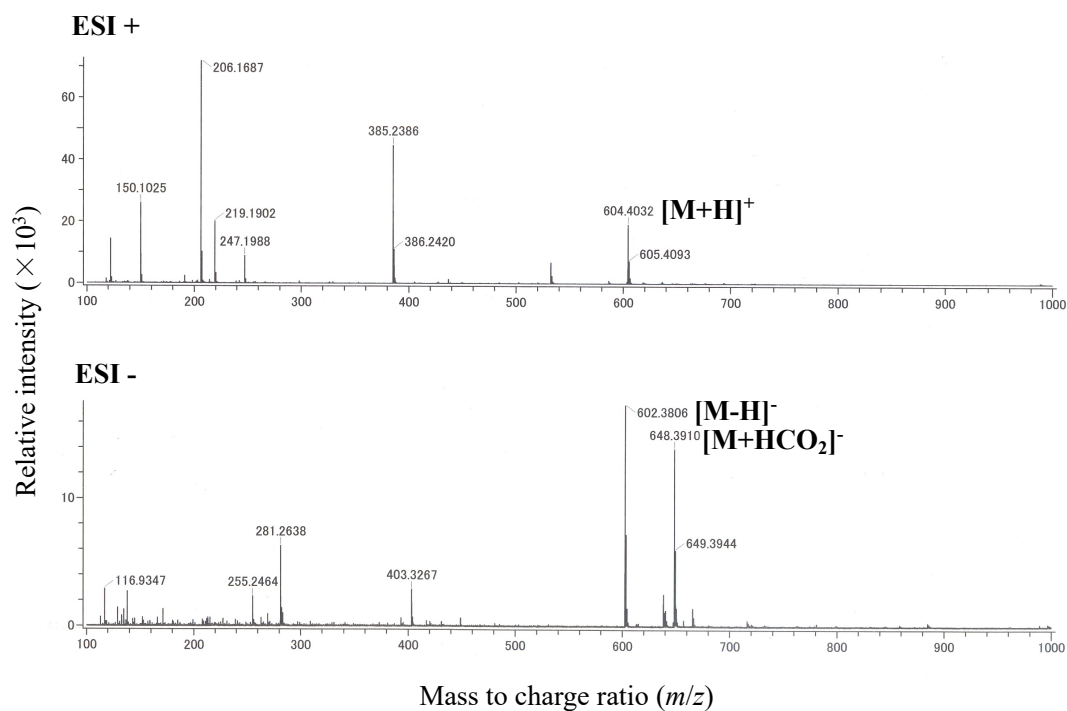
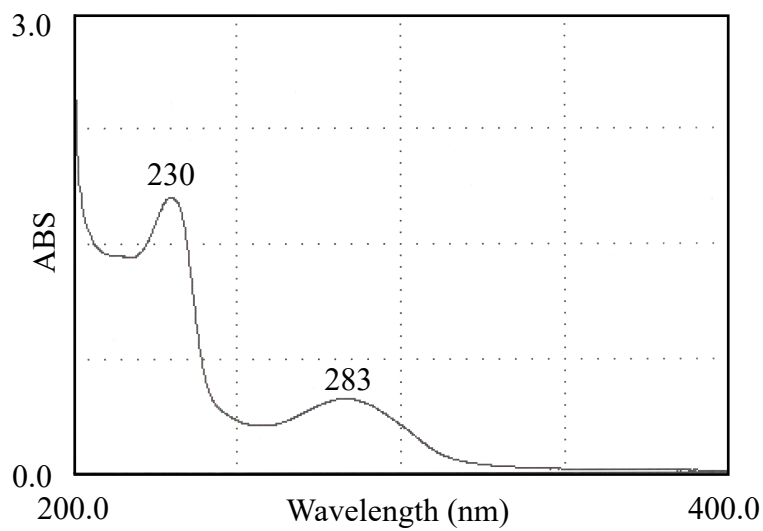


Figure 2-21. Structure activity relationship (SAR) study

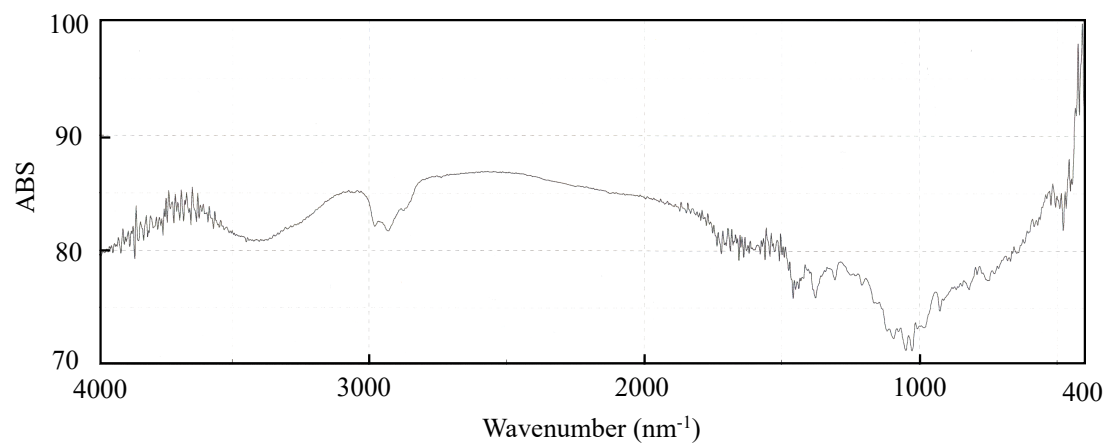
2-9. Supplemental data



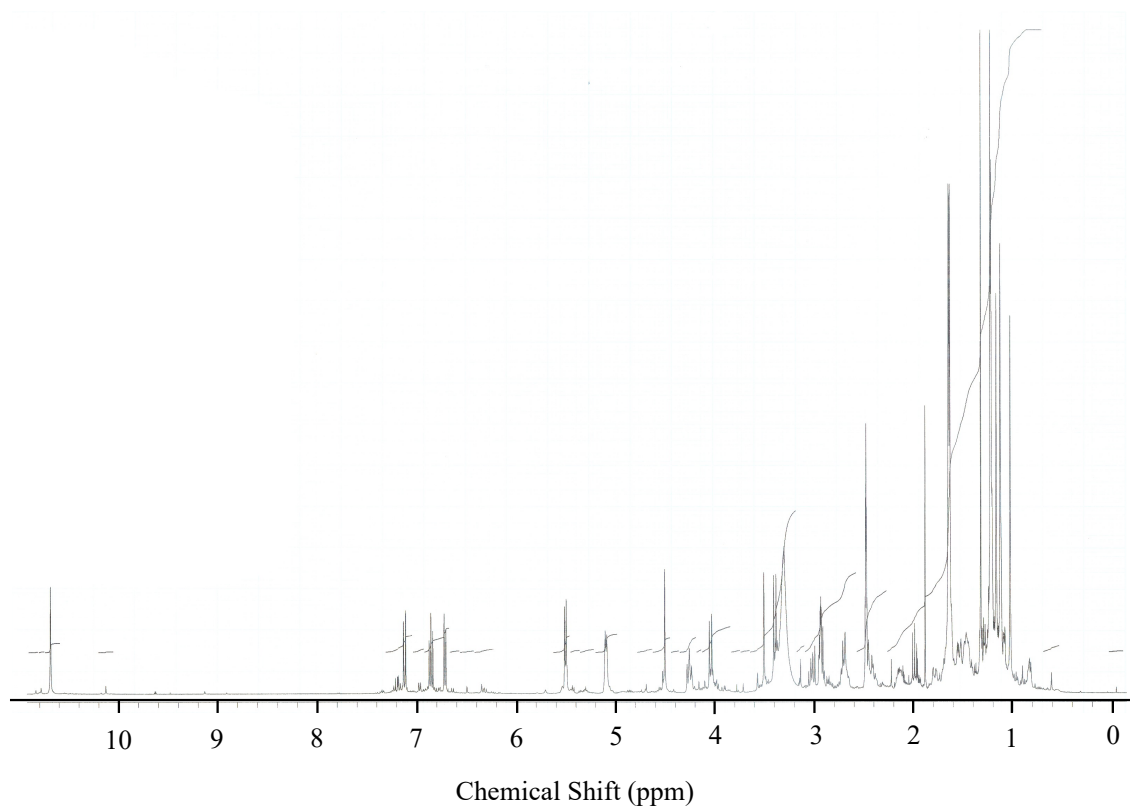
Supplemental Figure 2-1. MS spectrum of terpendole O (6)



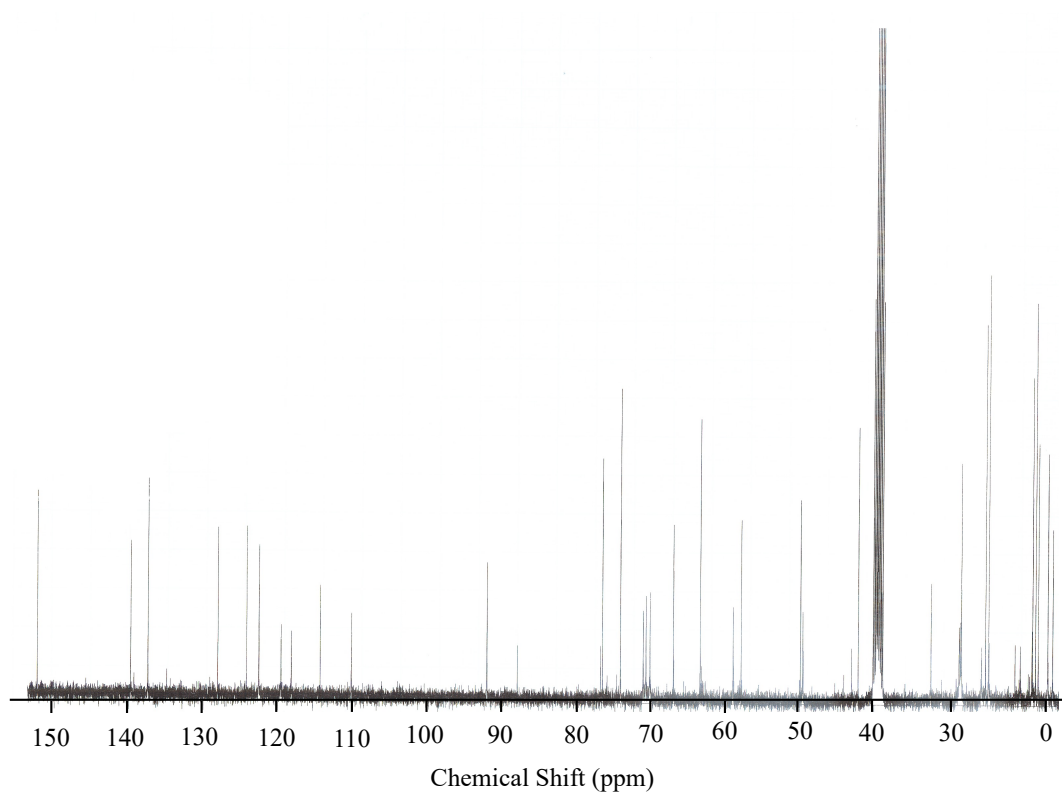
Supplemental Figure 2-2. UV spectrum of terpendole O (6)



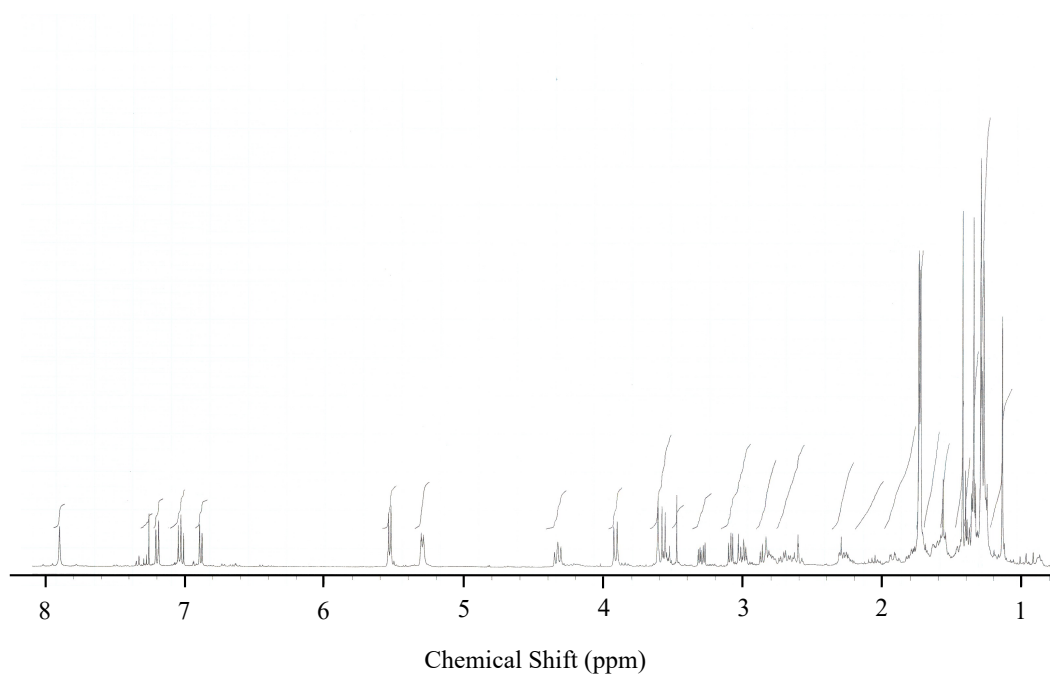
Supplemental Figure 2-3. IR spectrum of terpendole O (**6**)



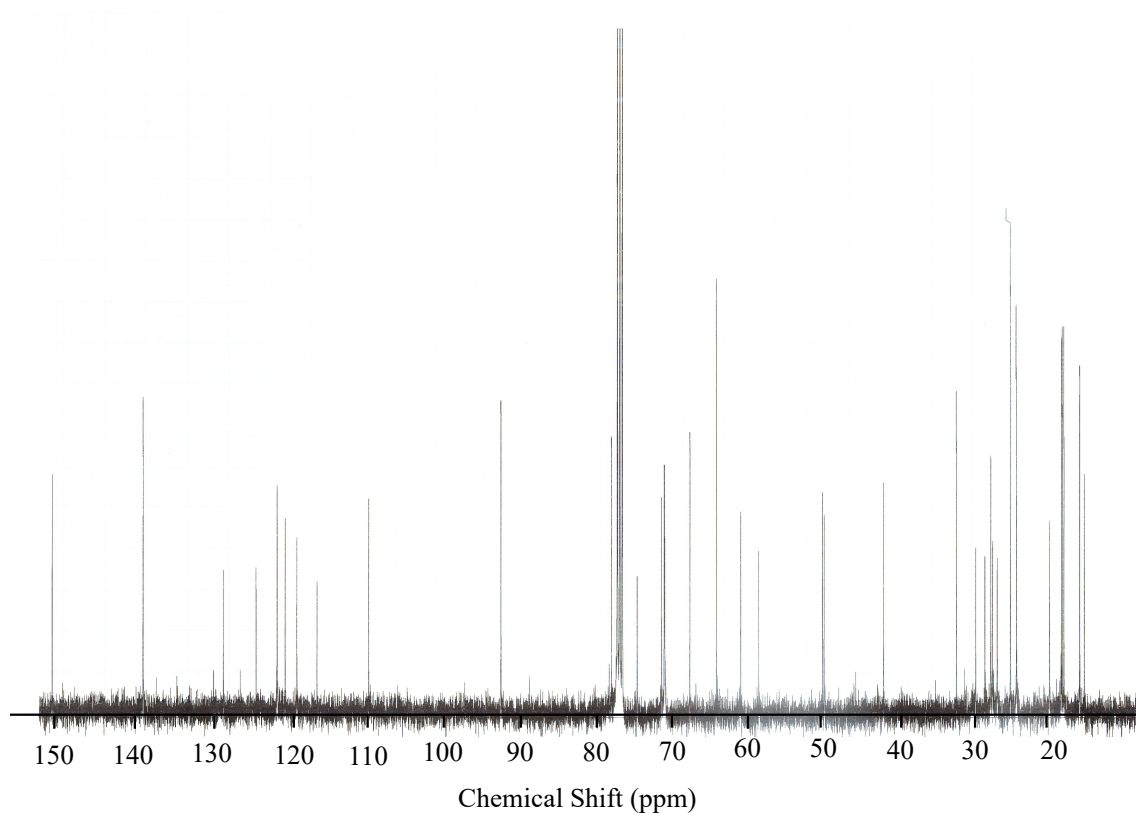
Supplemental Figure 2-4. ¹H-NMR spectrum of terpendole O (**6**)
(400 MHz in DMSO-*d*₆)



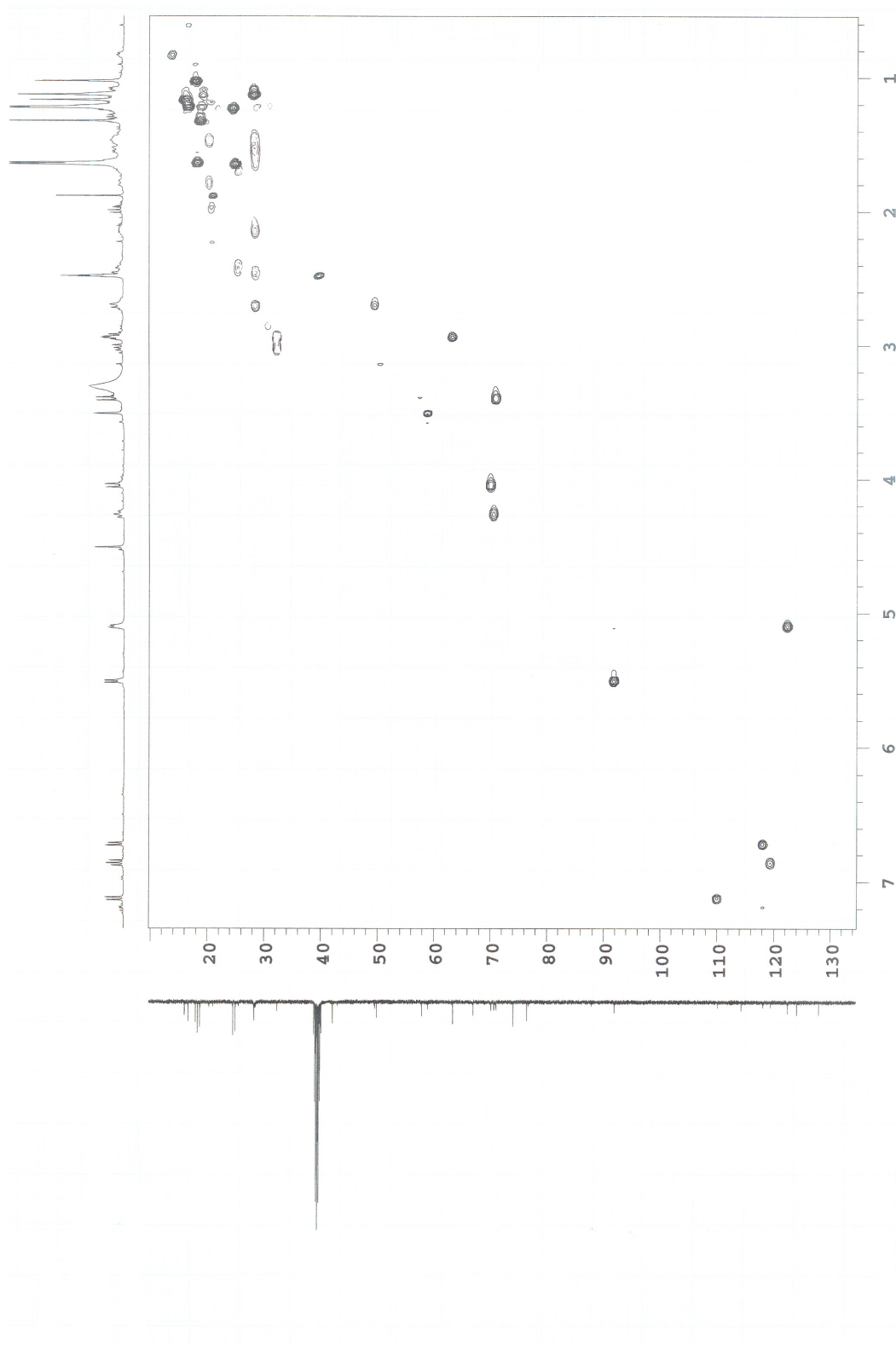
Supplemental Figure 2-5. ^{13}C -NMR spectrum of terpendole O (**6**)
(100 MHz in $\text{DMSO}-d_6$)



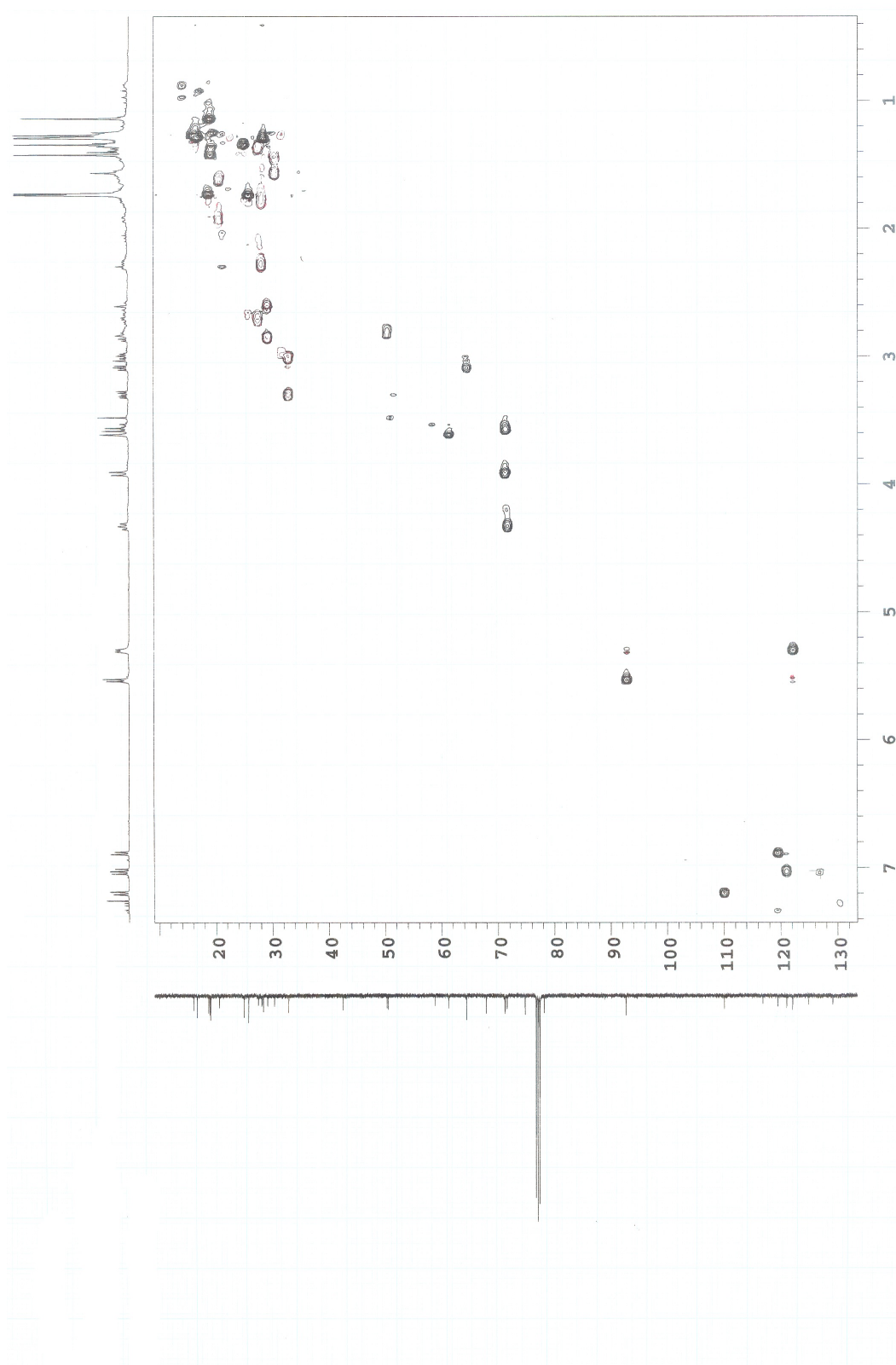
Supplemental Figure 2-6. ^1H -NMR spectrum of terpendole O (**6**)
(400 MHz in CDCl_3)



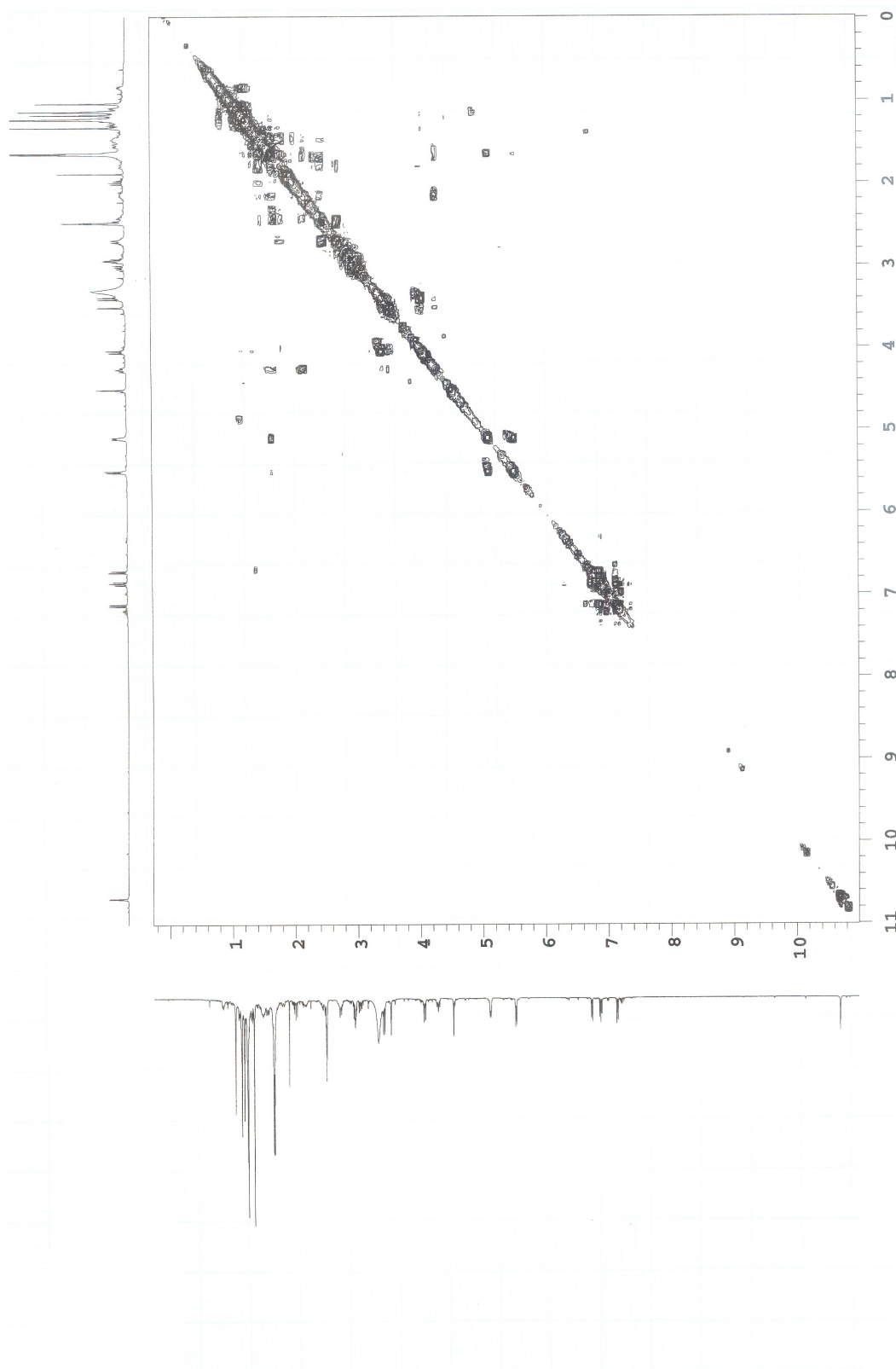
Supplemental Figure 2-7. ^{13}C -NMR spectrum of terpendole O (**6**)
(100 MHz in CDCl_3)



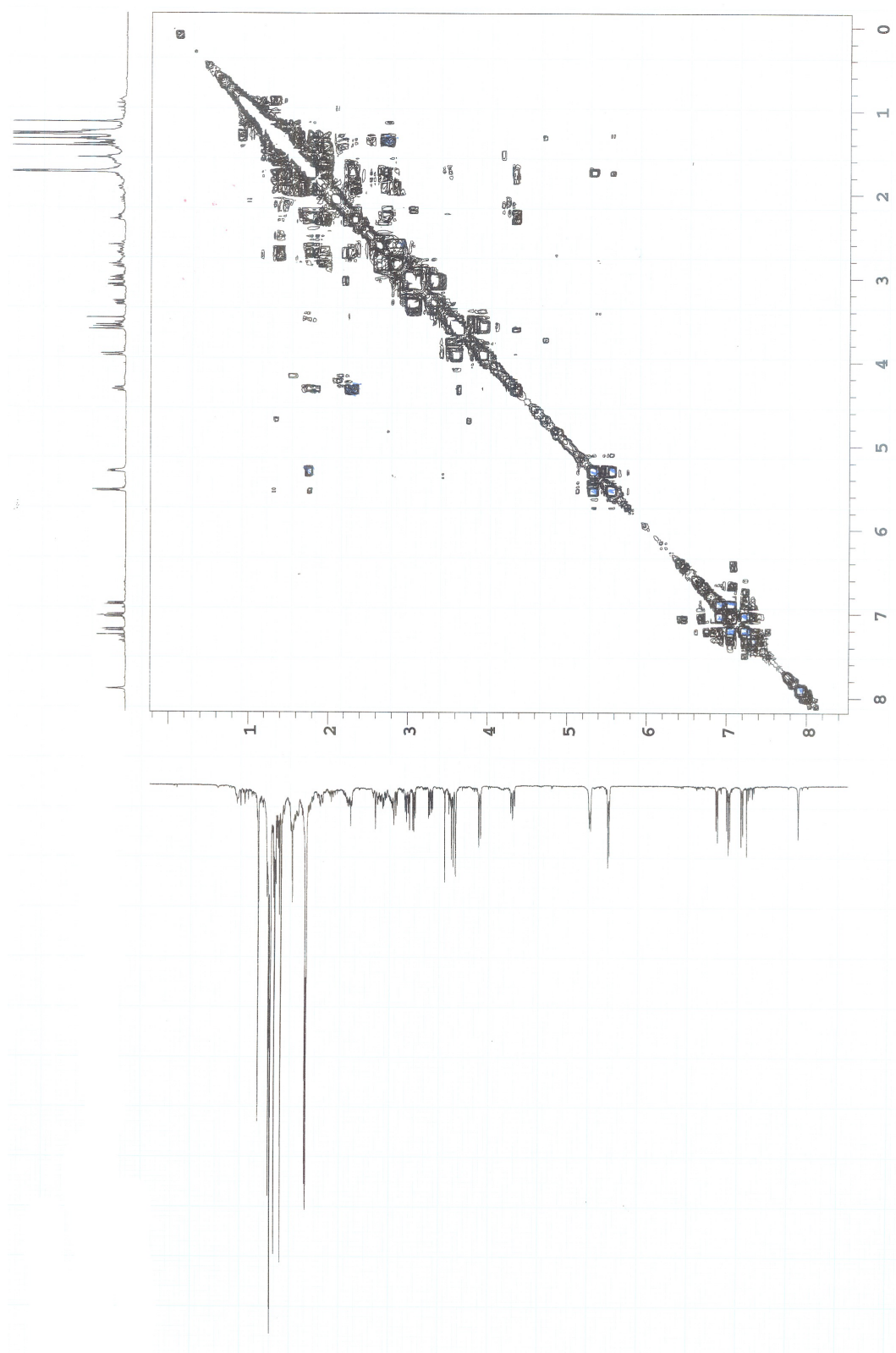
Supplemental Figure 2-8. HSQC spectrum of terpendole O (**6**) taken in DMSO- d_6



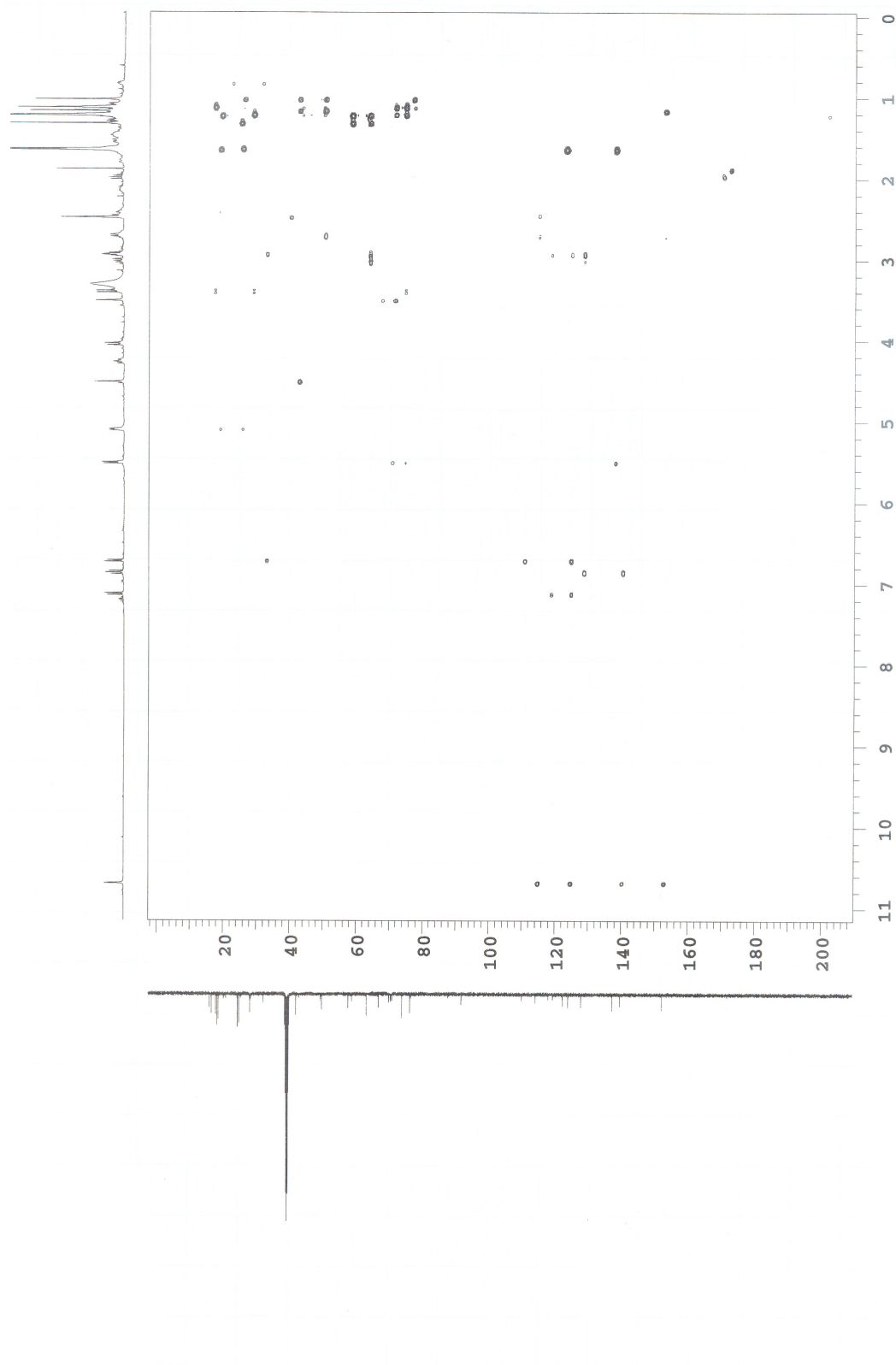
Supplemental Figure 2-9. HSQC spectrum of terpendole O (6) taken in CDCl₃

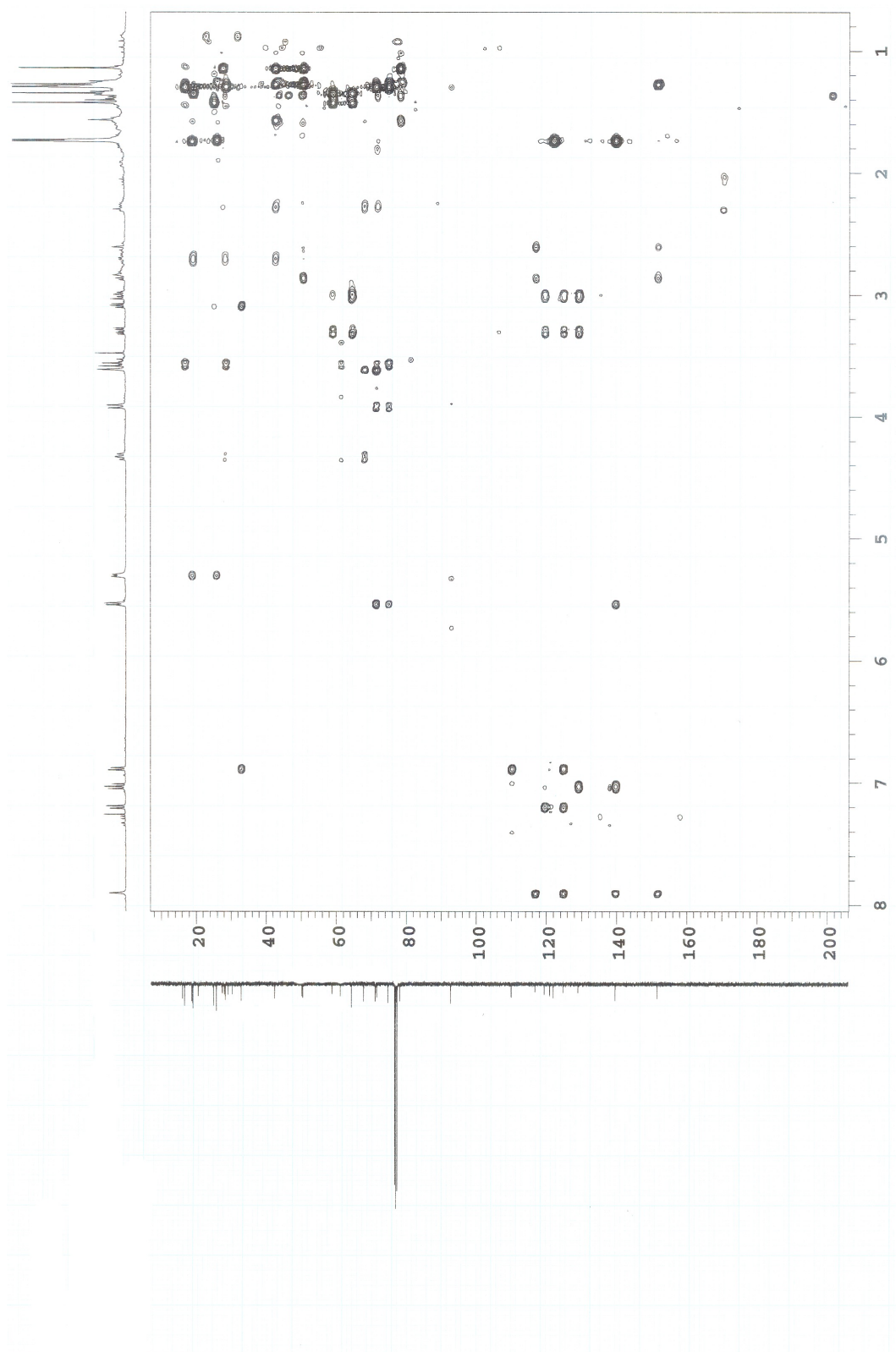


Supplemental Figure 2-10. ^1H - ^1H COSY spectrum of terpendole O (**6**) taken in $\text{DMSO}-d_6$

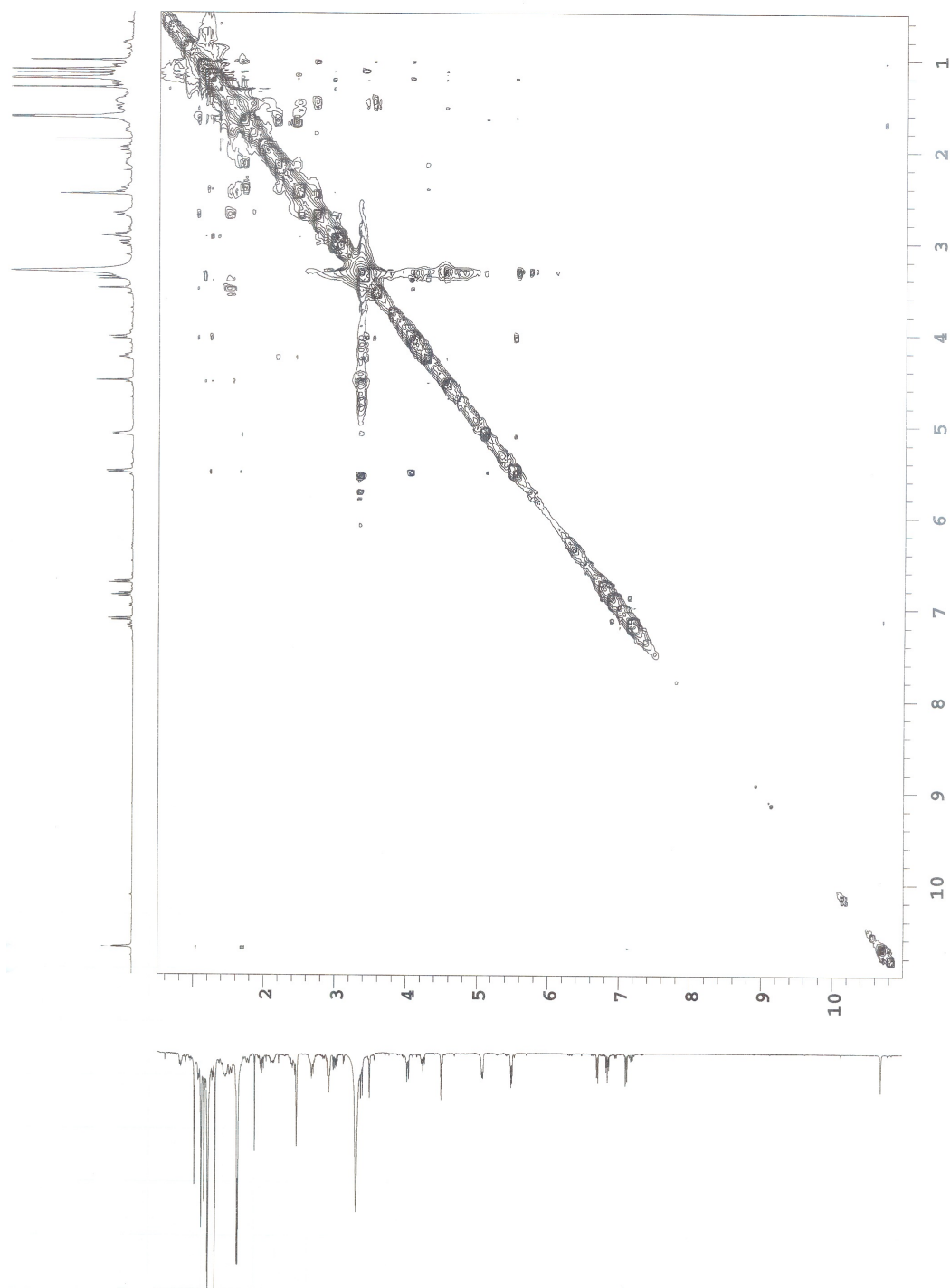


Supplemental Figure 2-11. ^1H - ^1H COSY spectrum of terpendole O (6) taken in CDCl_3

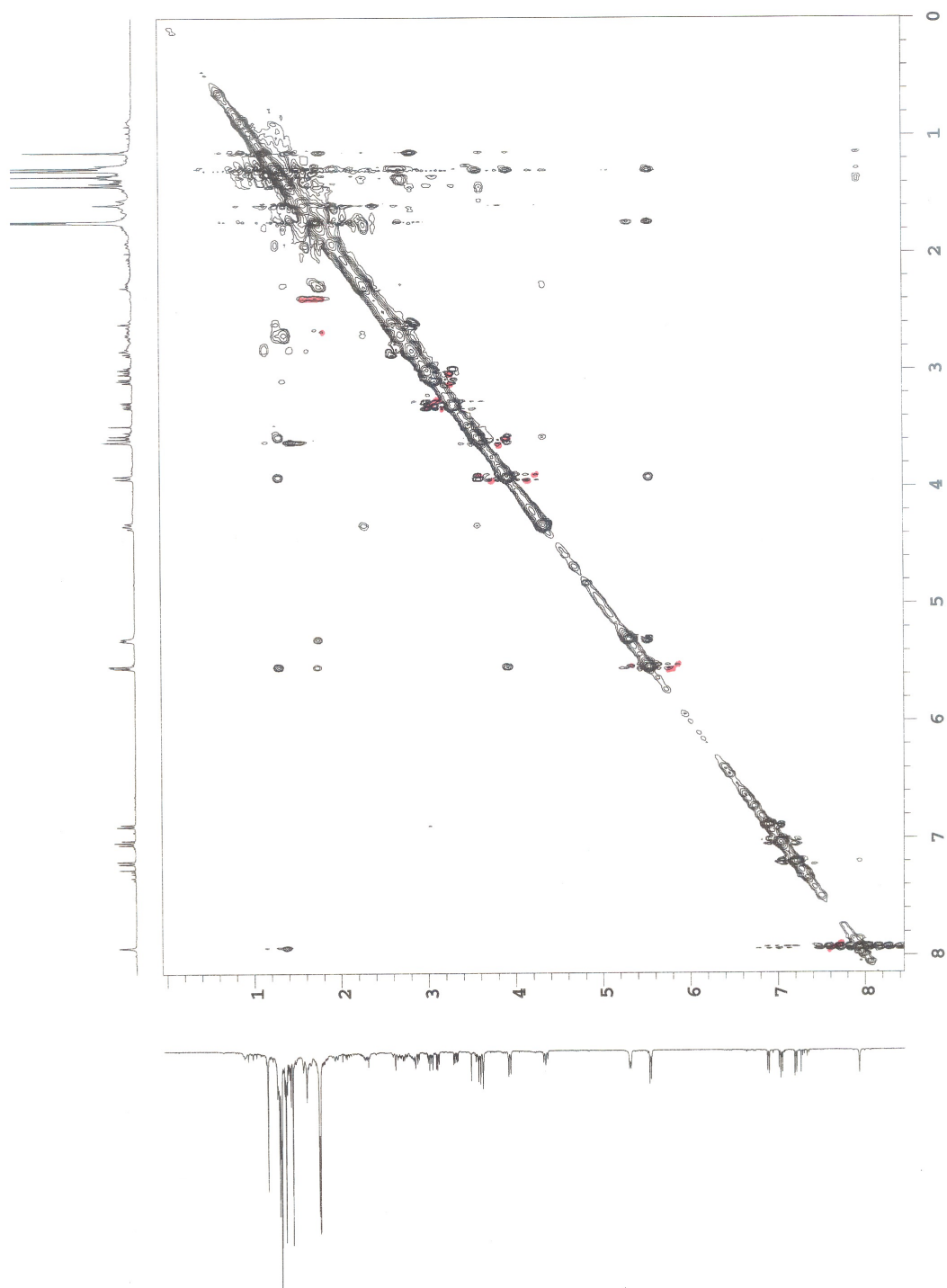




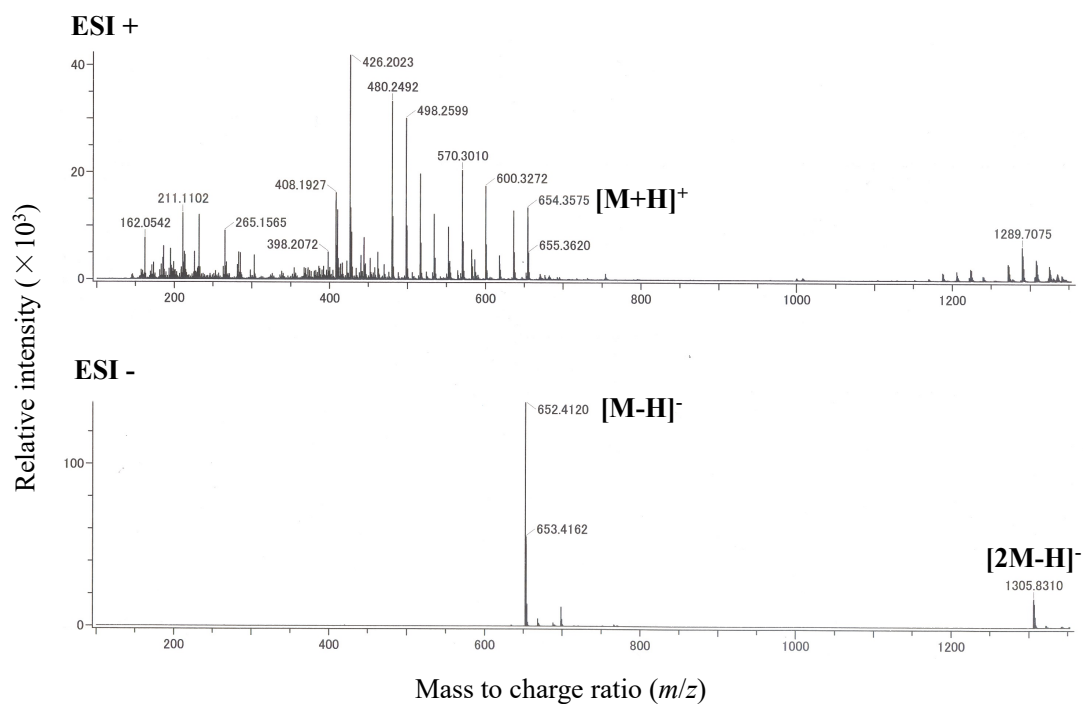
Supplemental Figure 2-13. HMBC spectrum of terpendole O (6) taken in CDCl_3



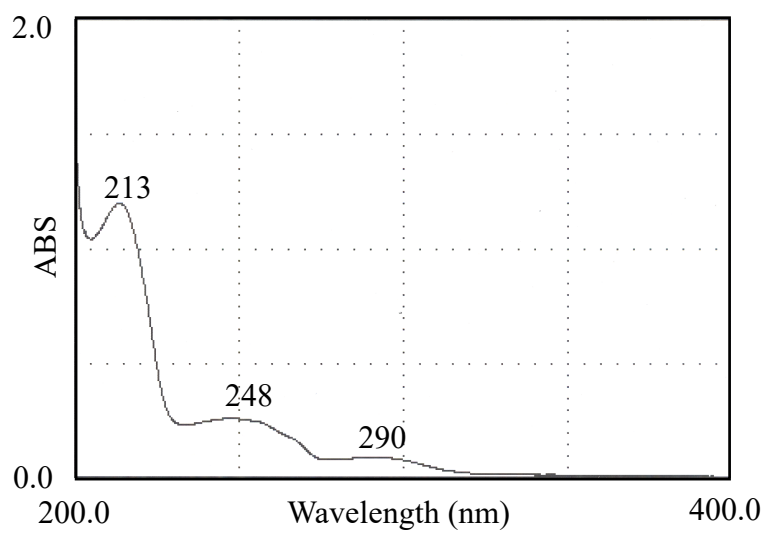
Supplemental Figure 2-14. NOESY spectrum of terpendole O (6) taken in DMSO- d_6



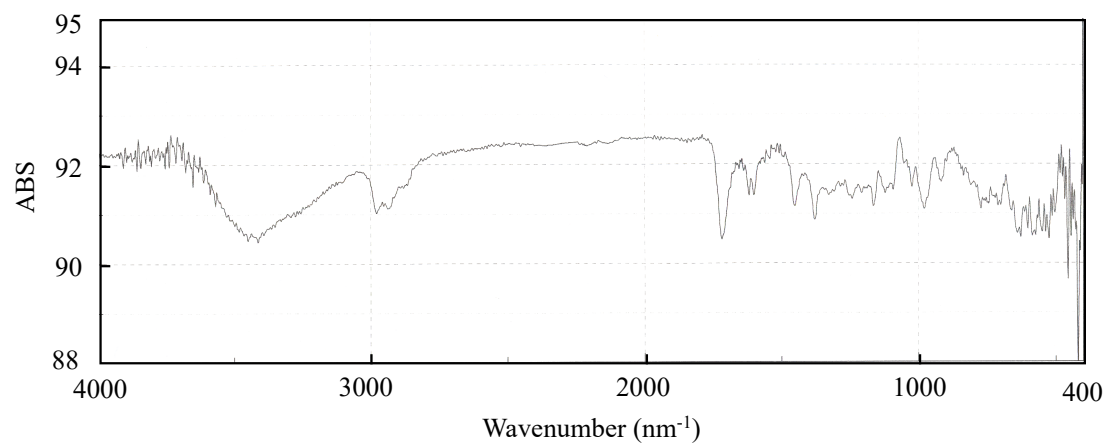
Supplemental Figure 2-15. NOESY spectrum of terpendole O (6) taken in CDCl₃



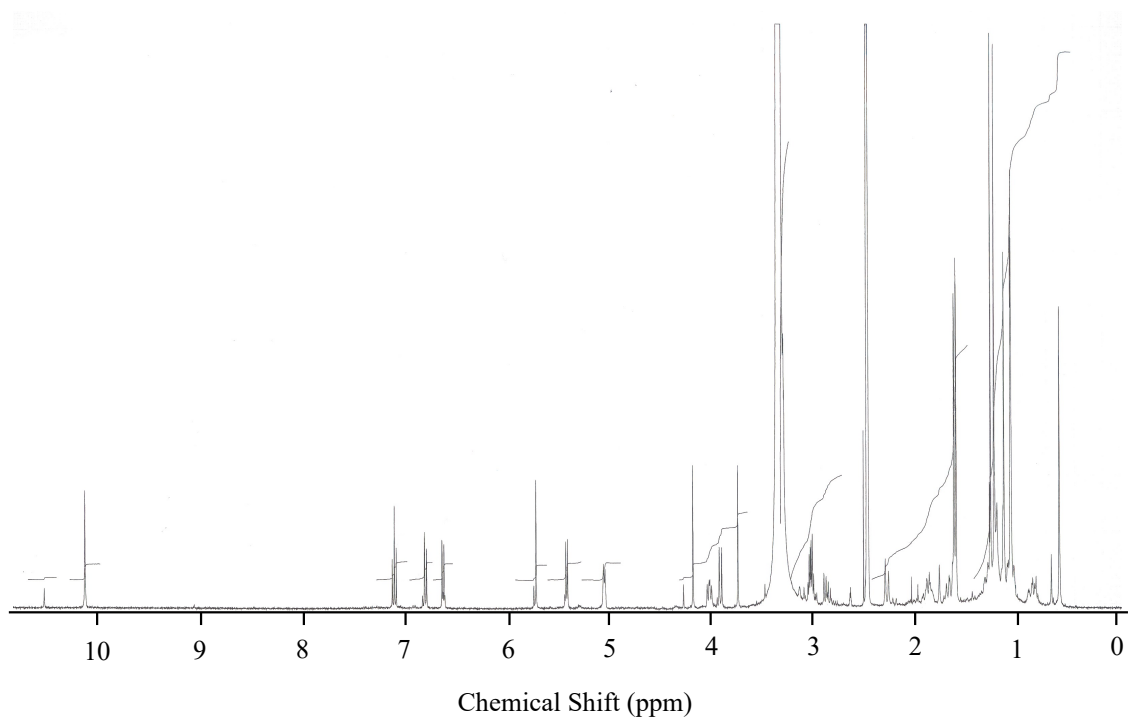
Supplemental Figure 2-16. MS spectrum of terpendole N (**5**)



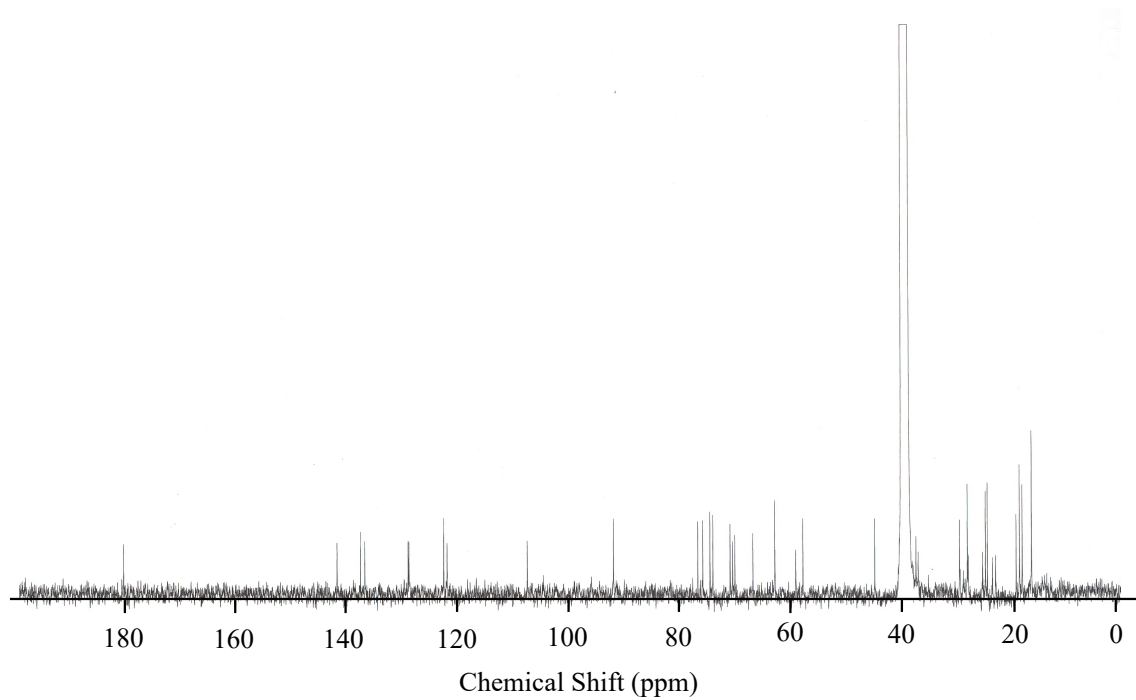
Supplemental Figure 2-17. UV spectrum of terpendole N (**5**)



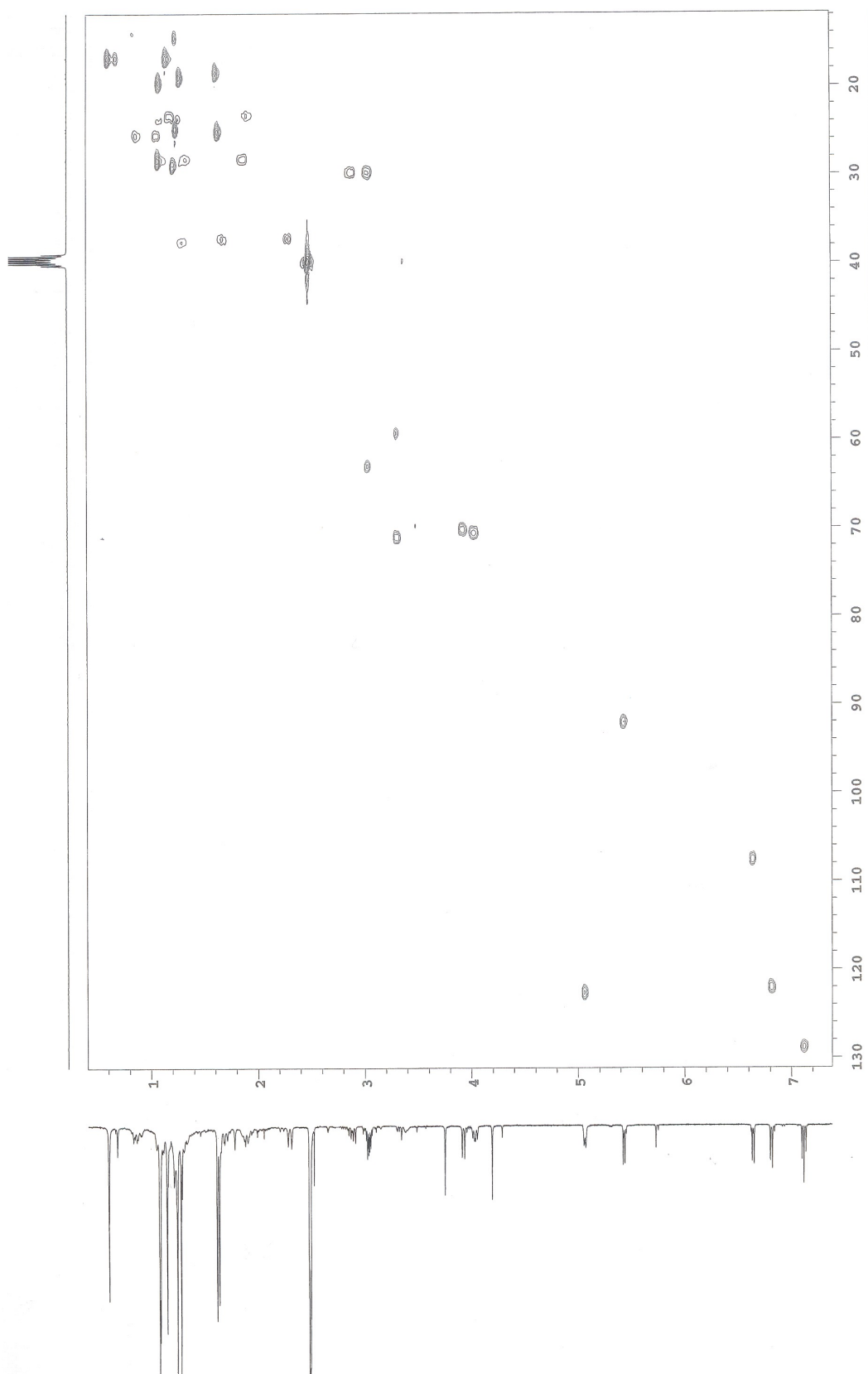
Supplemental Figure 2-18. IR spectrum of terpendole N (**5**)



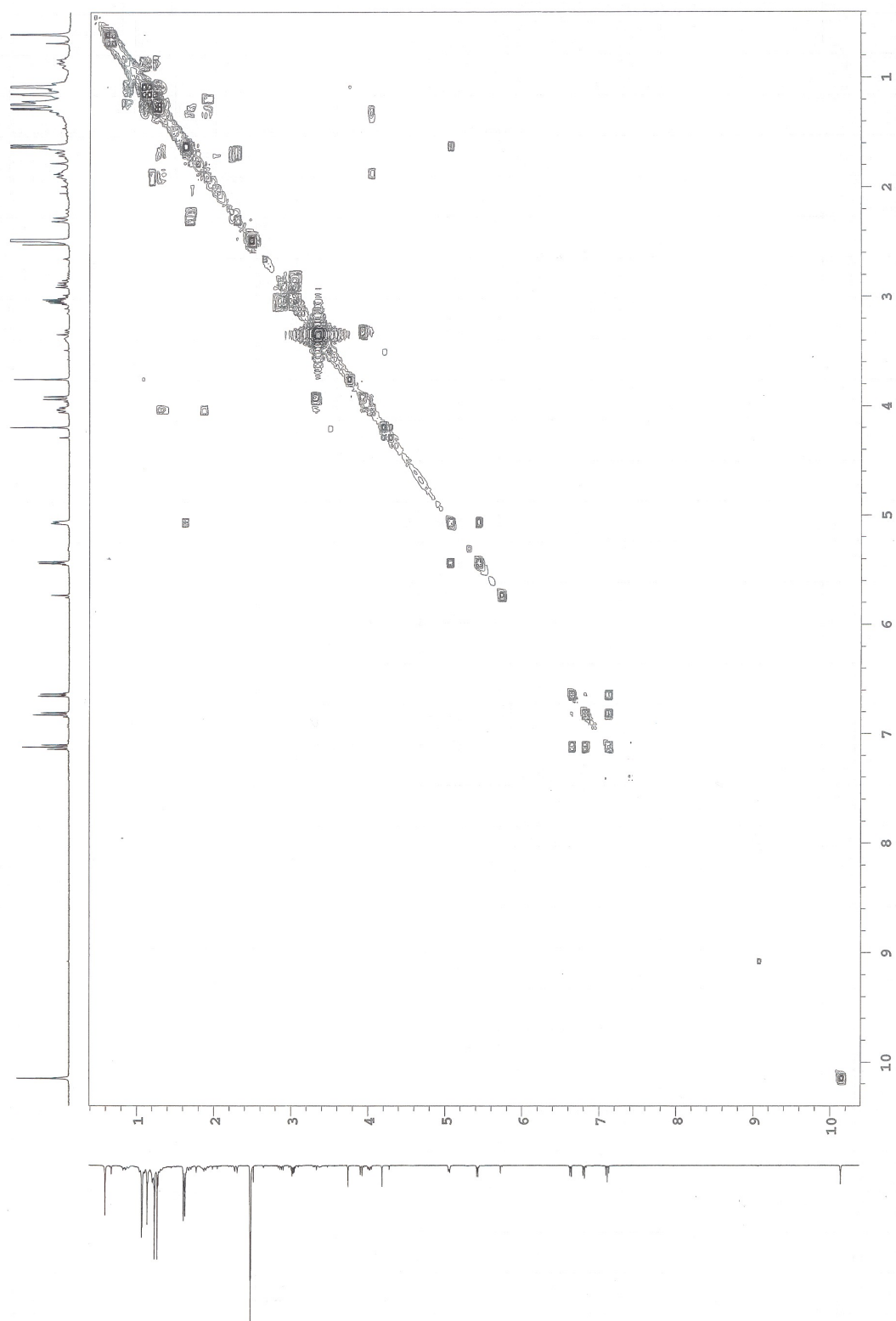
Supplemental Figure 2-19. ¹H-NMR spectrum of terpendole N (**5**)
(400 MHz in DMSO-*d*₆)



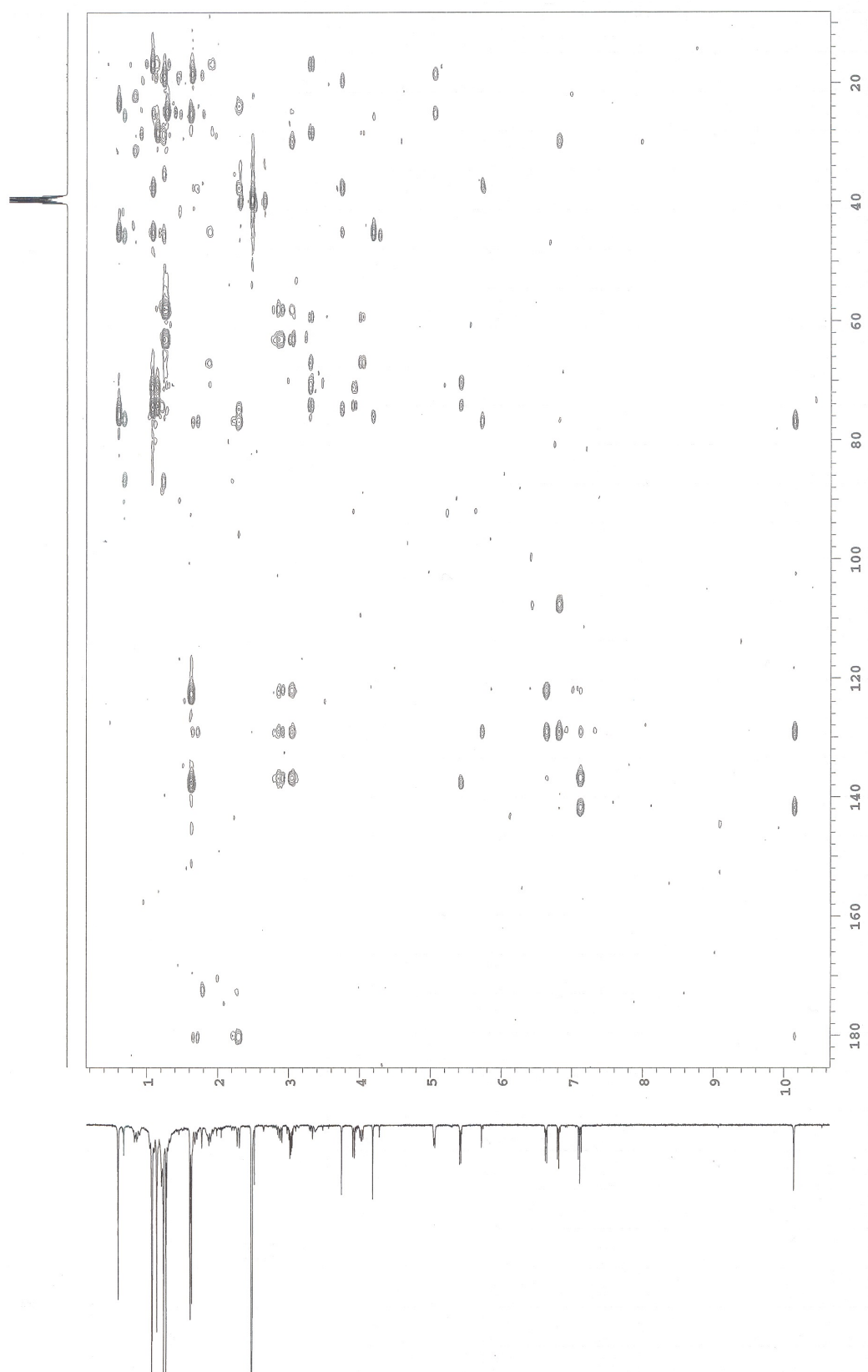
Supplemental Figure 2-20. ^{13}C -NMR spectrum of terpendole N (**5**)
(100 MHz in DMSO- d_6)



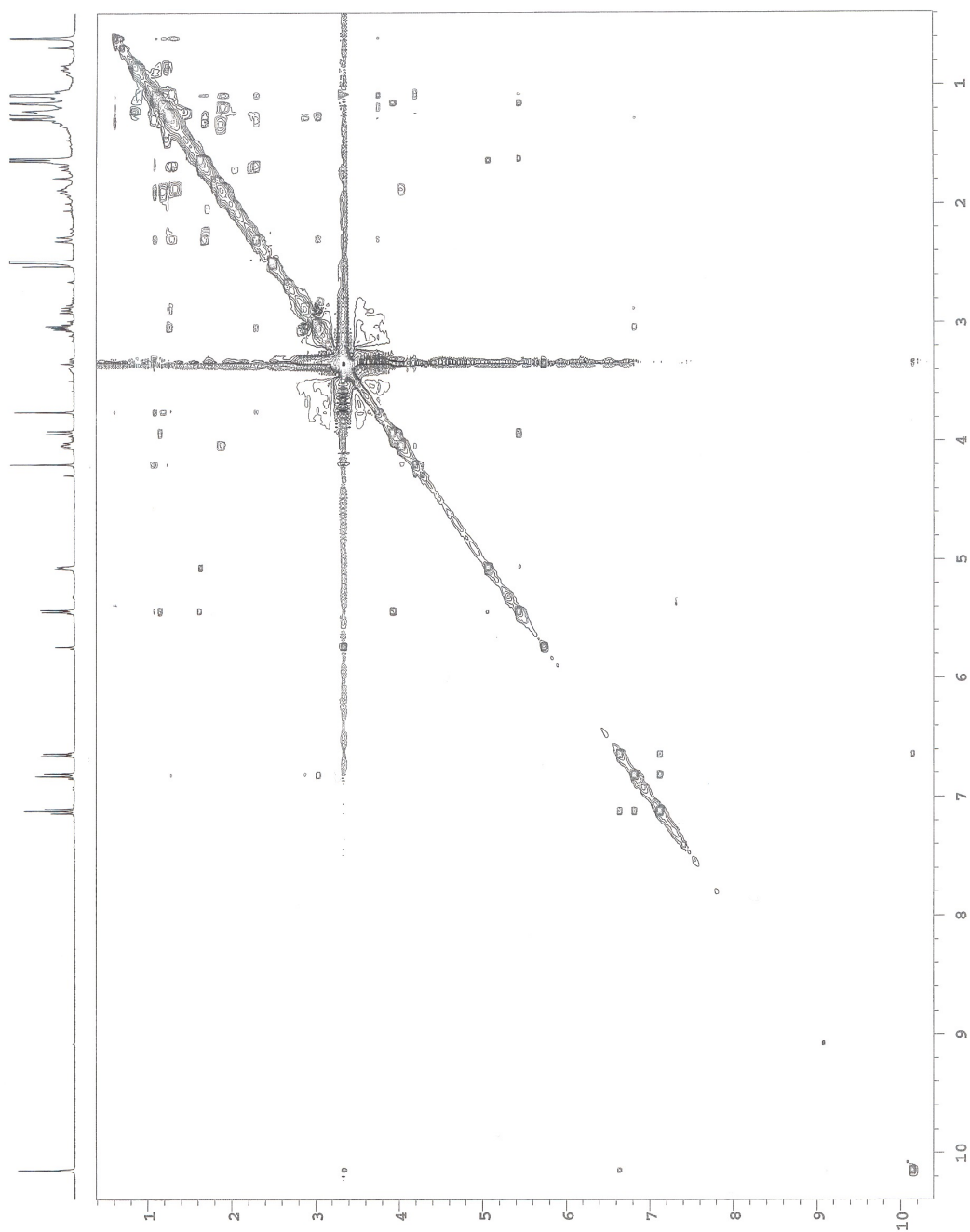
Supplemental Figure 2-21. HSQC spectrum of terpendole N (5) taken in DMSO- d_6



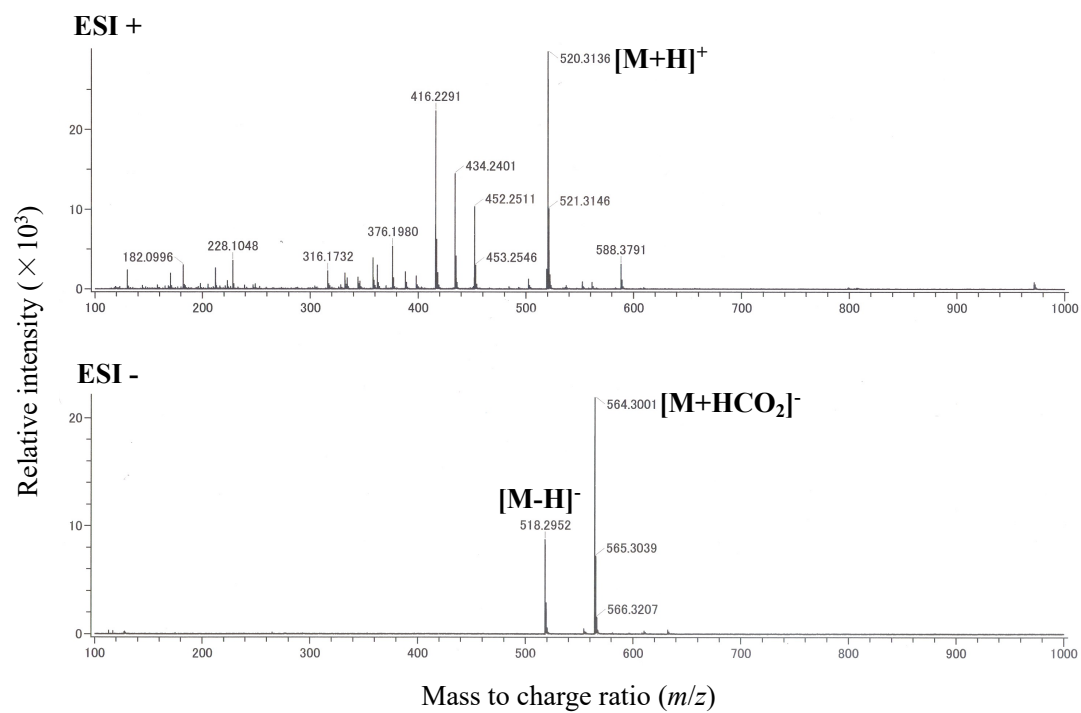
Supplemental Figure 2-22. ^1H - ^1H COSY spectrum of terpendole N (**5**) taken in $\text{DMSO}-d_6$



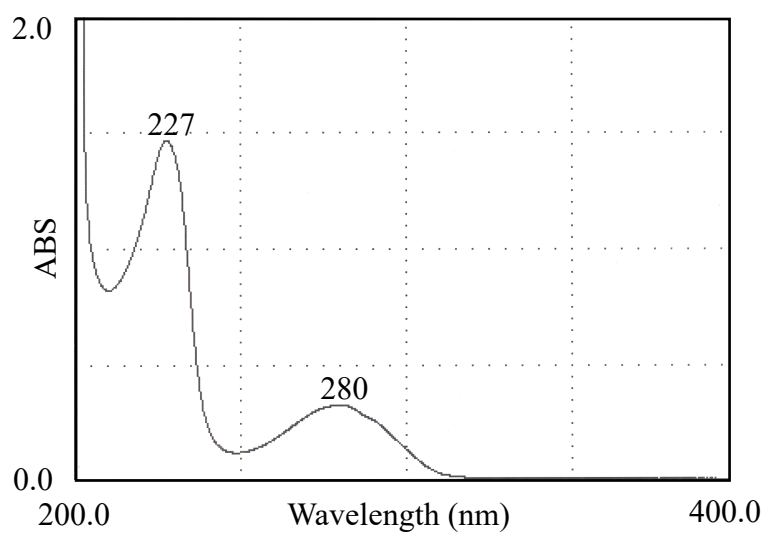
Supplemental Figure 2-23. HMBC spectrum of terpendole N (**5**) taken in DMSO- d_6



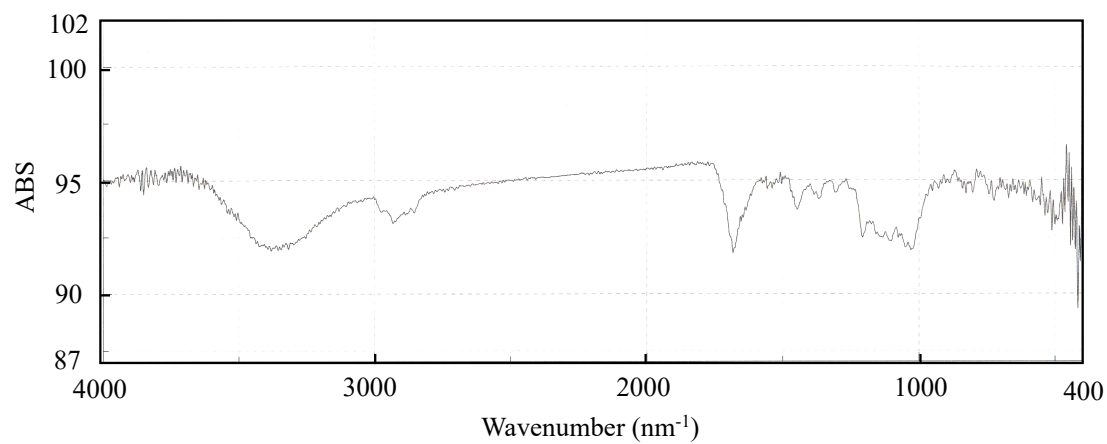
Supplemental Figure 2-24. ROESY spectrum of terpendole N (5) taken in DMSO- d_6



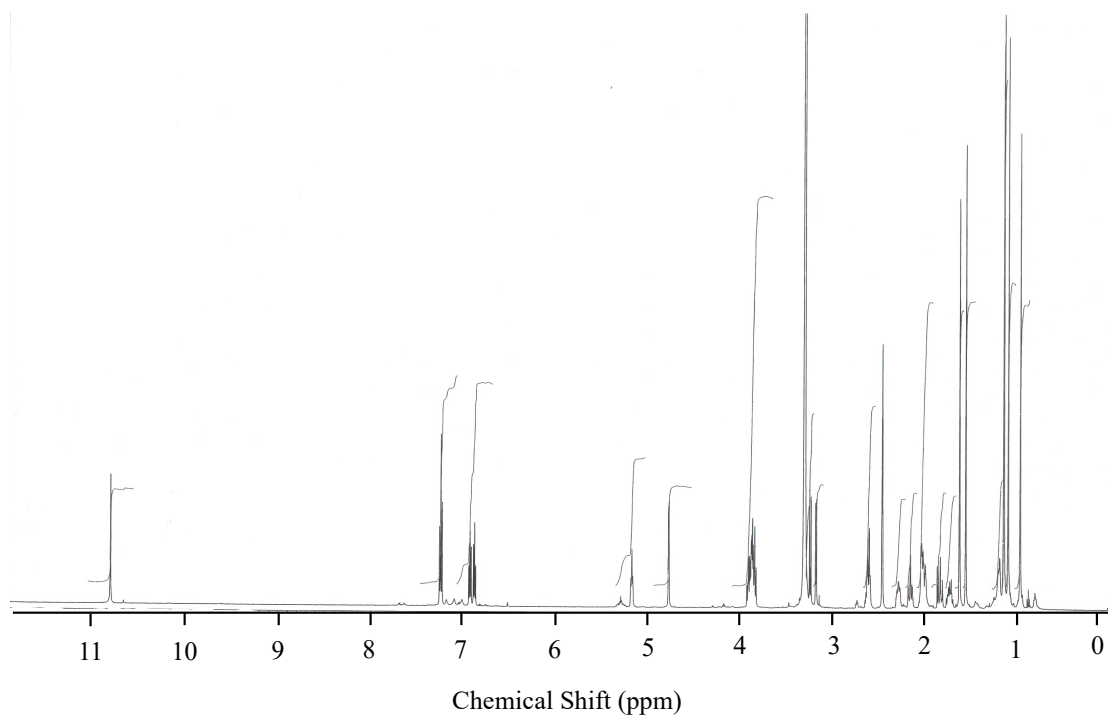
Supplemental Figure 2-25. MS spectrum of terpendole P (7)



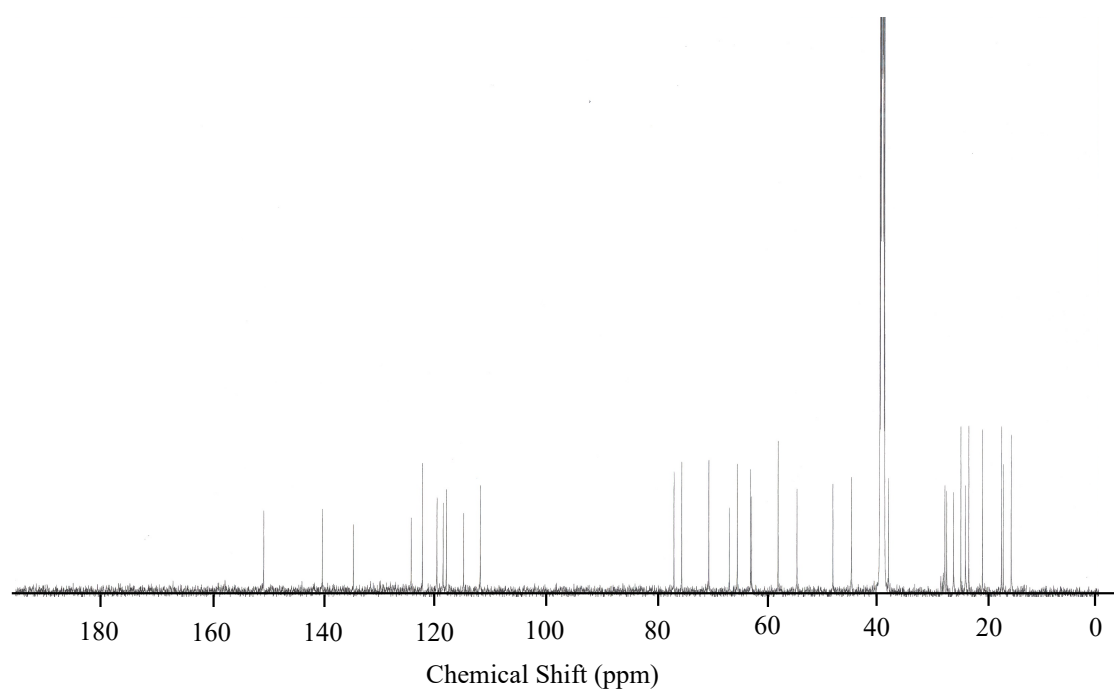
Supplemental Figure 2-26. UV spectrum of terpendole P (7)



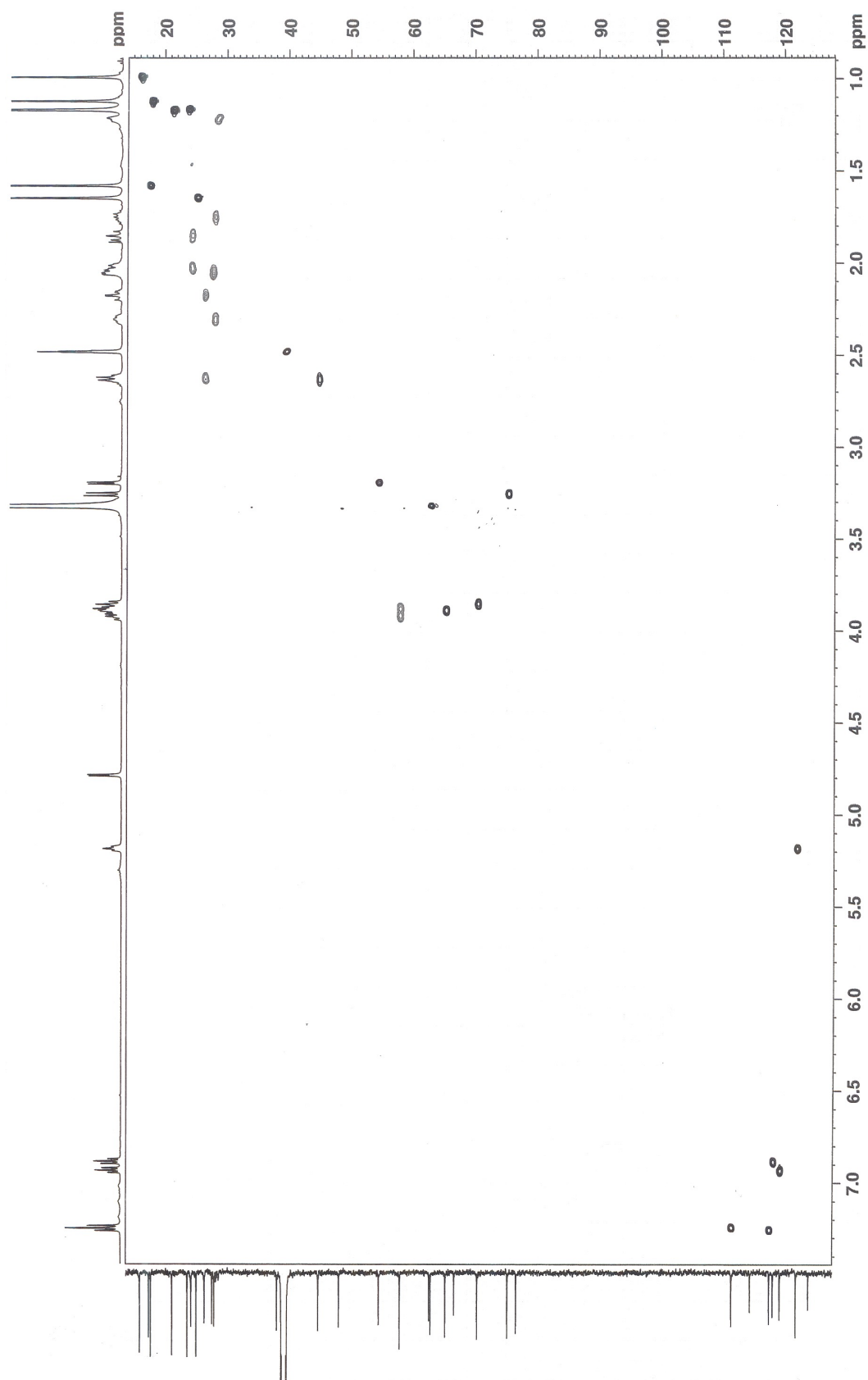
Supplemental Figure 2-27. IR spectrum of terpendole P (7)



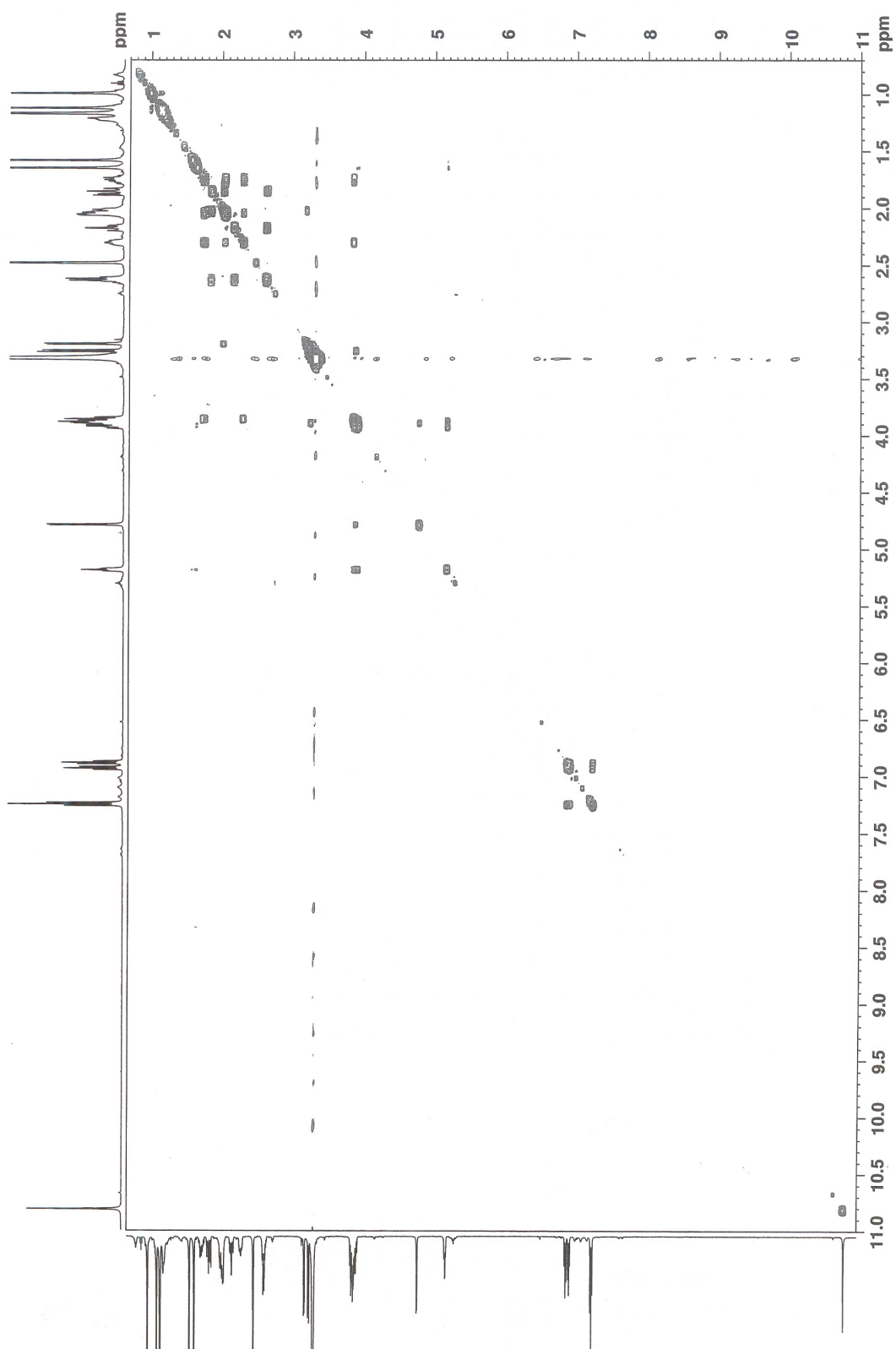
Supplemental Figure 2-28. ¹H-NMR spectrum of terpendole P (7)
(600 MHz in DMSO-*d*₆)



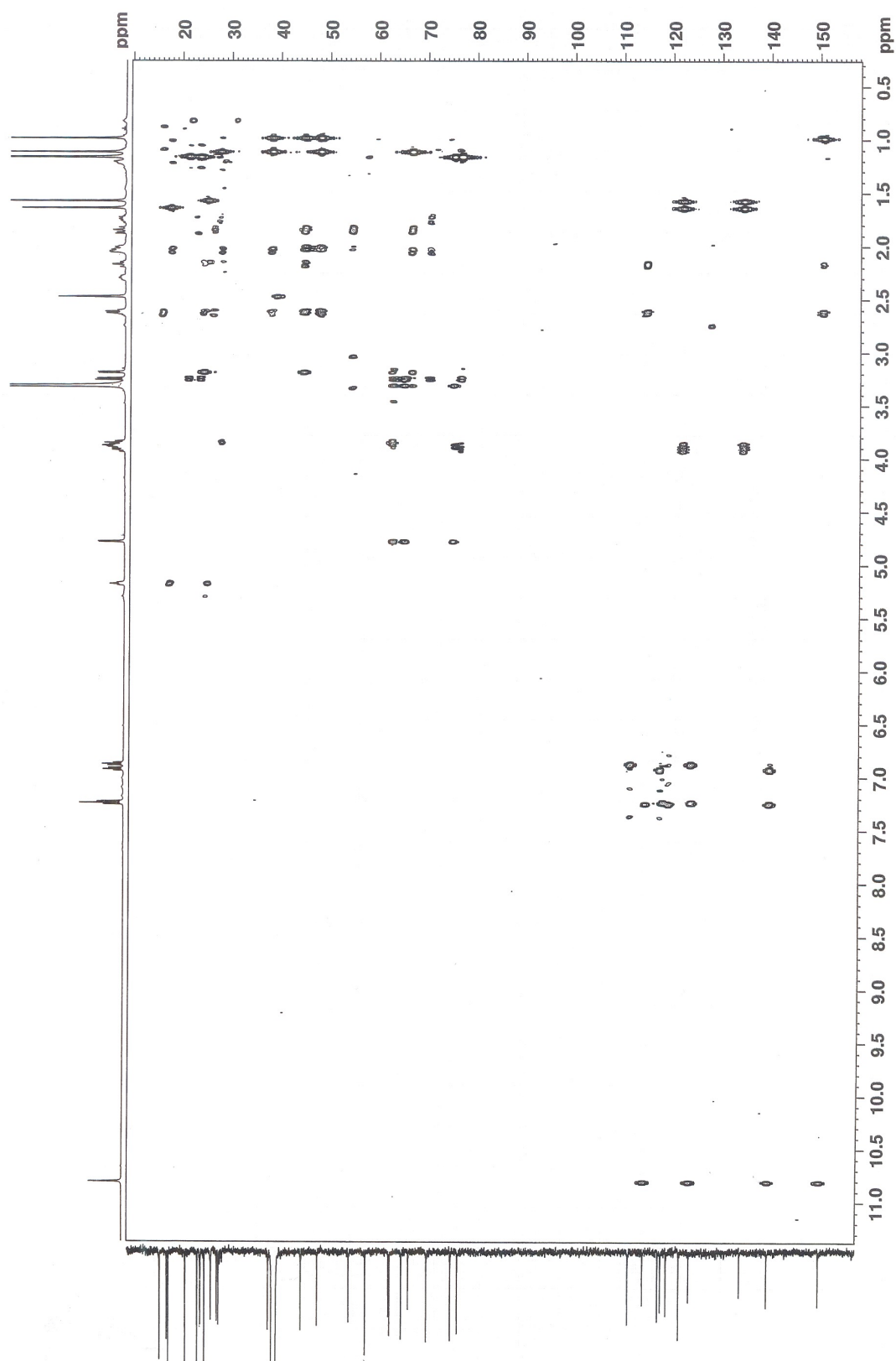
Supplemental Figure 2-29. ^{13}C -NMR spectrum of terpendole P (7)
(150 MHz in $\text{DMSO}-d_6$)



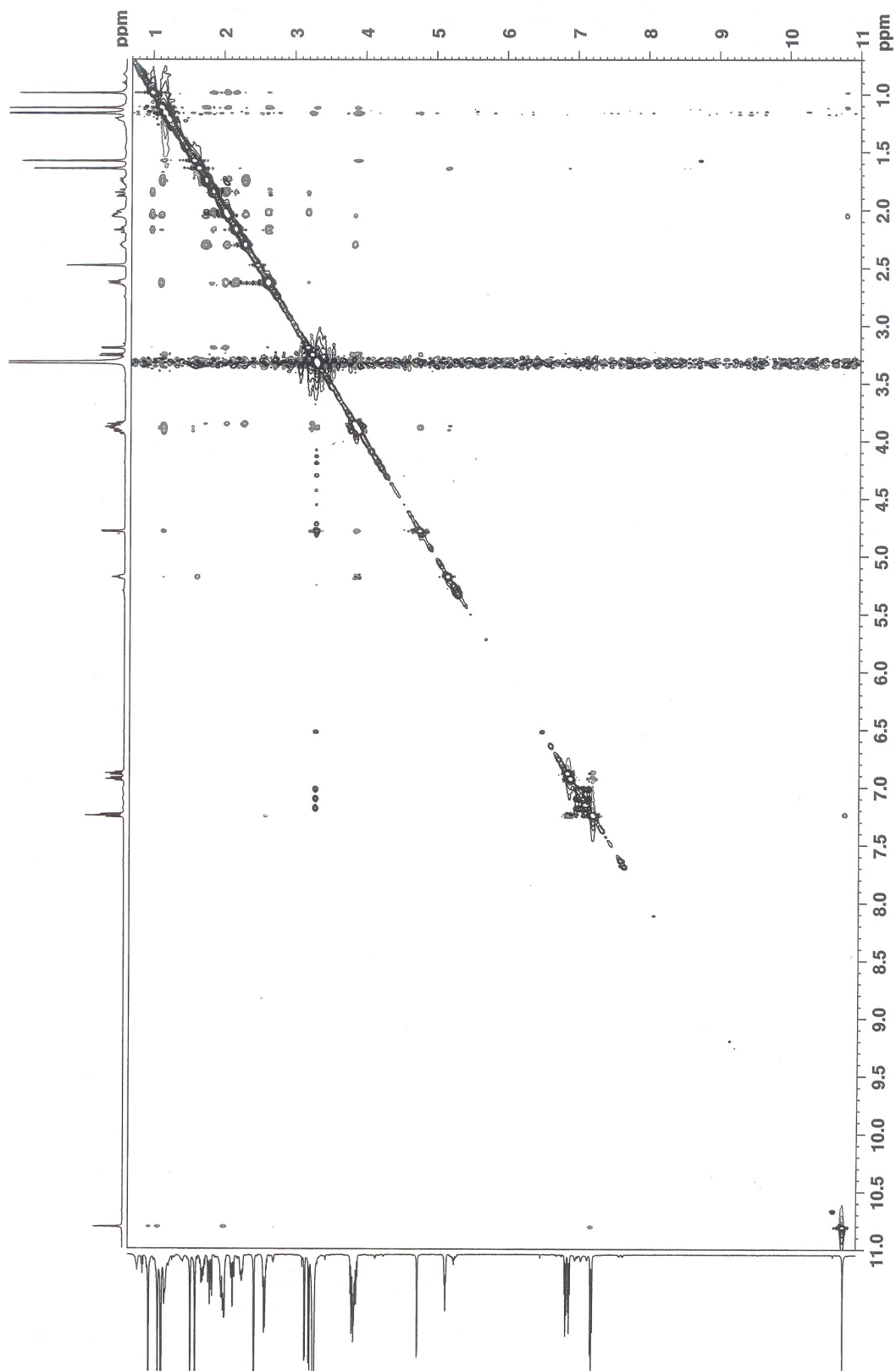
Supplemental Figure 2-30. HSQC spectrum of terpendole P (7) taken in DMSO- d_6



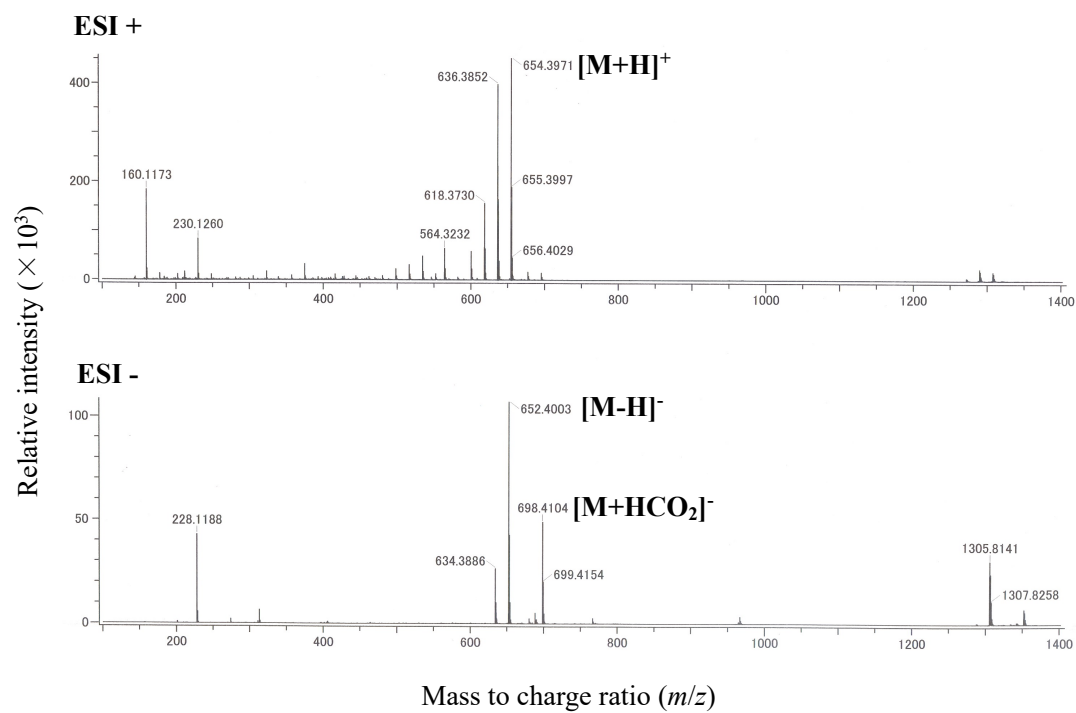
Supplemental Figure 2-31. ^1H - ^1H COSY spectrum of terpendole P (7) taken in $\text{DMSO}-d_6$



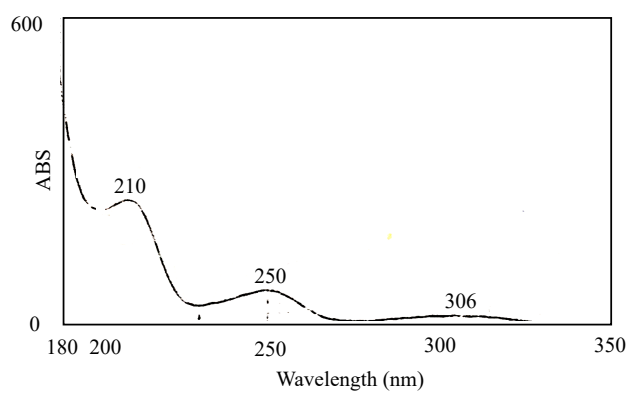
Supplemental Figure 2-32. HMBC spectrum of terpendole P (**7**) taken in $\text{DMSO-}d_6$



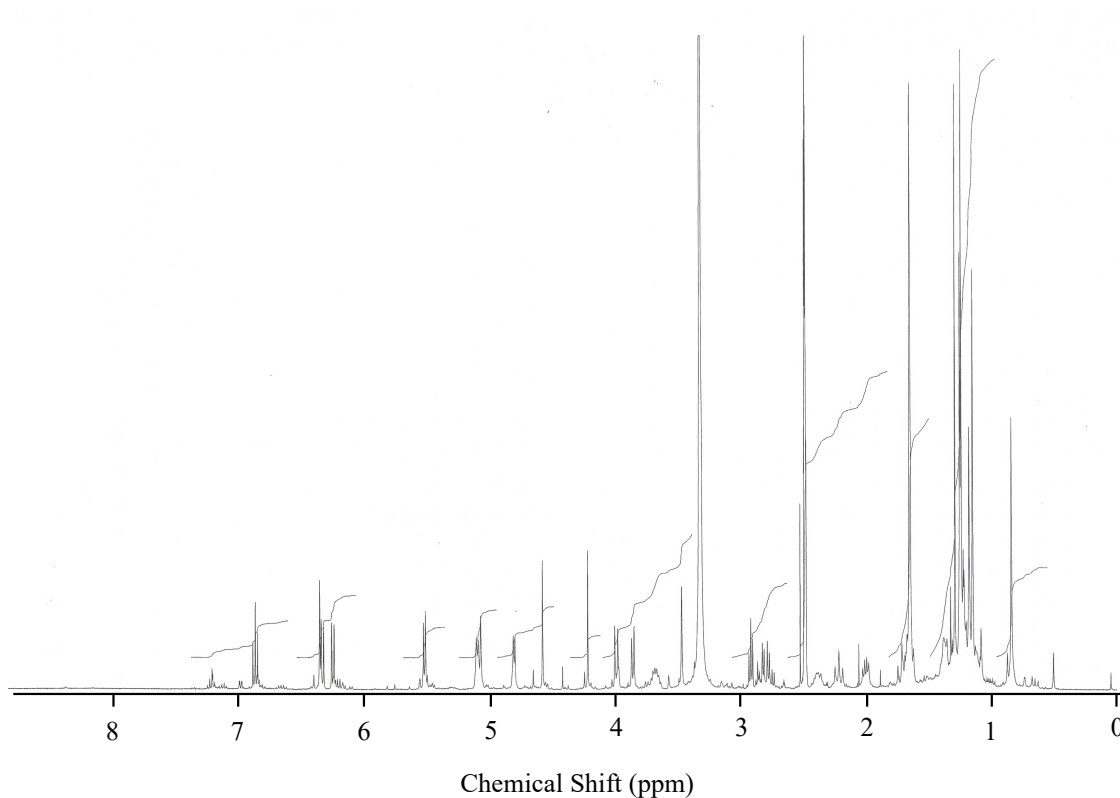
Supplemental Figure 2-33. ROESY spectrum of terpendole P (7) taken in DMSO- d_6



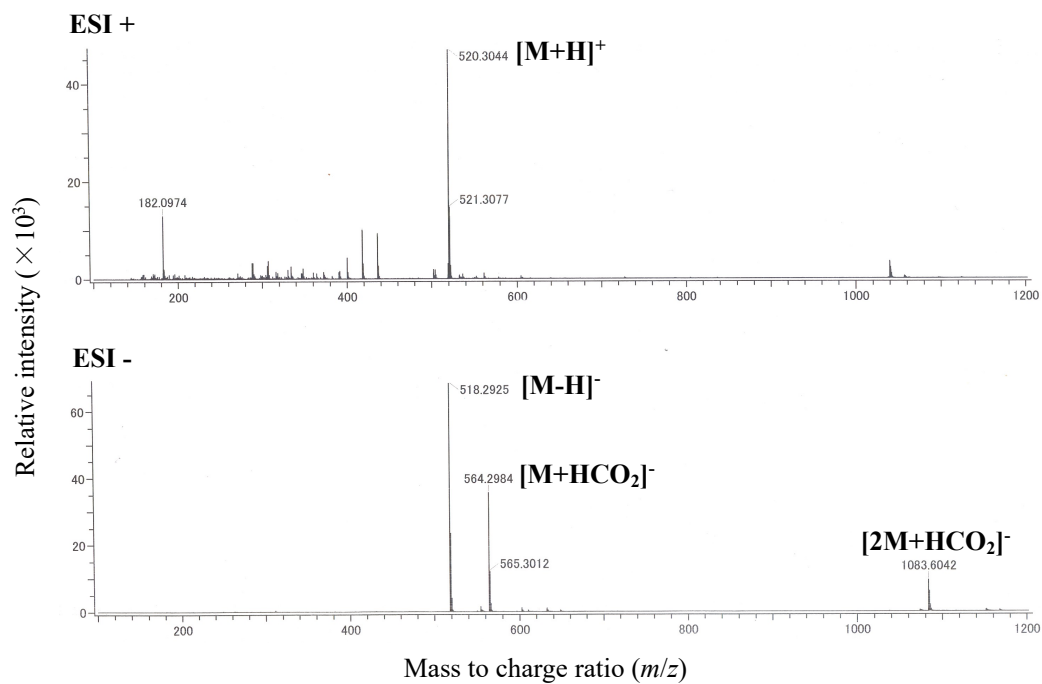
Supplemental Figure 2-34. MS spectrum of NK12838 (**10**)



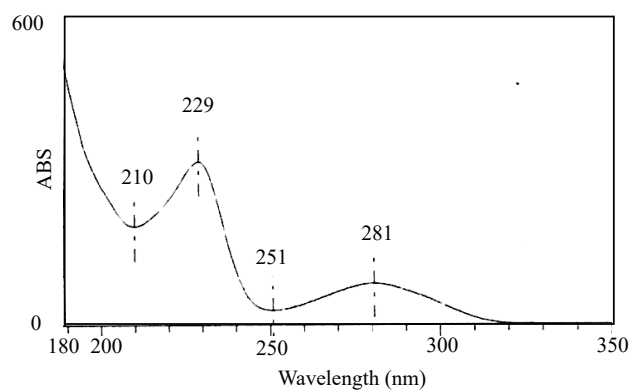
Supplemental Figure 2-35. UV spectrum of NK12838 (**10**)



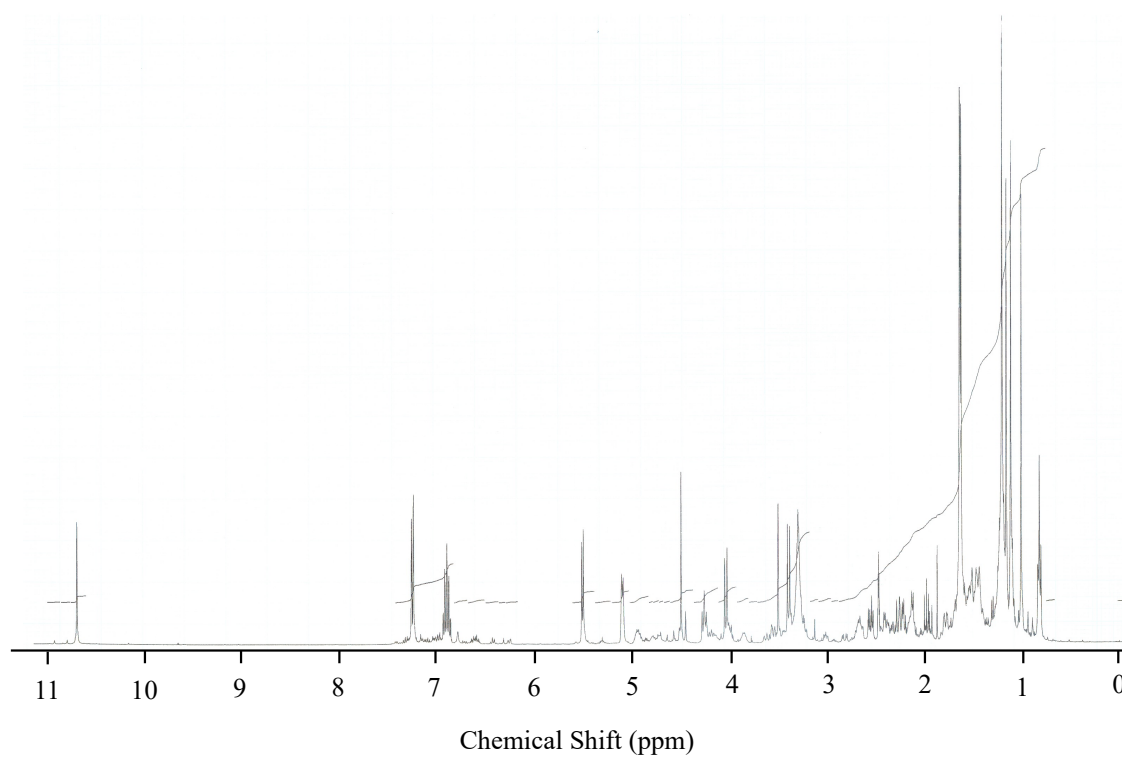
Supplemental Figure 2-36. ^1H -NMR spectrum of NK12838 (**10**) (400 MHz in $\text{DMSO-}d_6$)



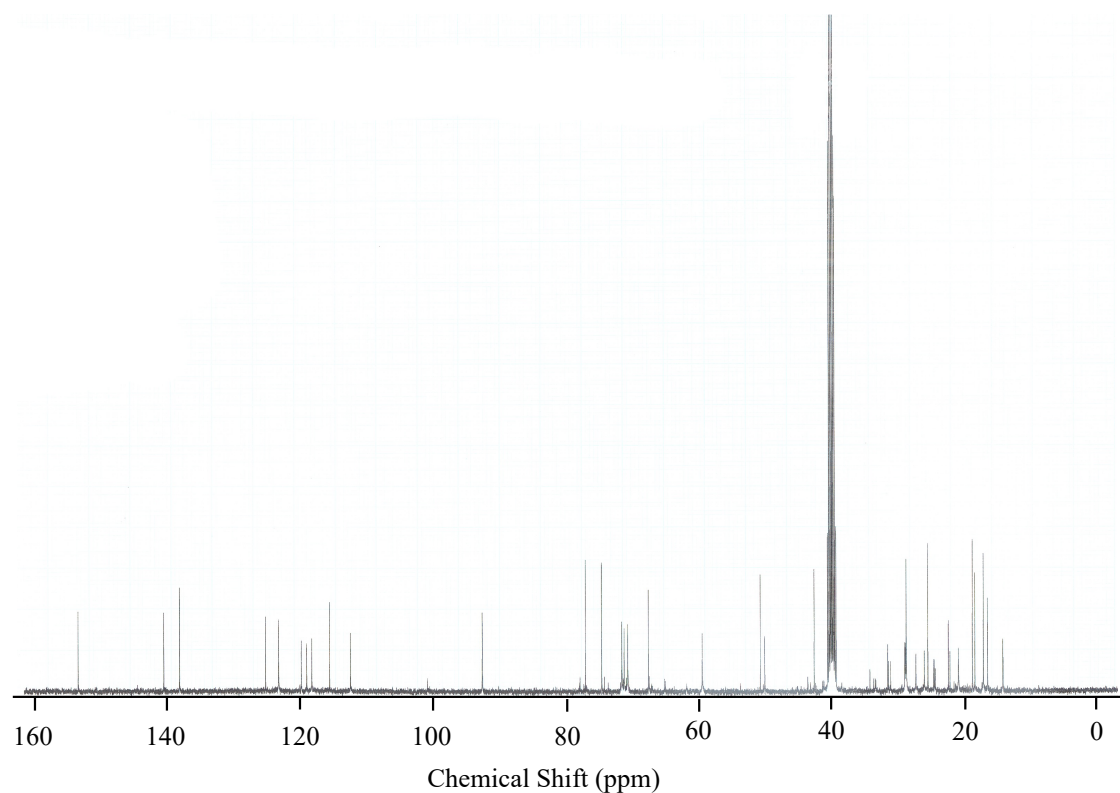
Supplemental Figure 2-37. MS spectrum of terpendole C (**11**)



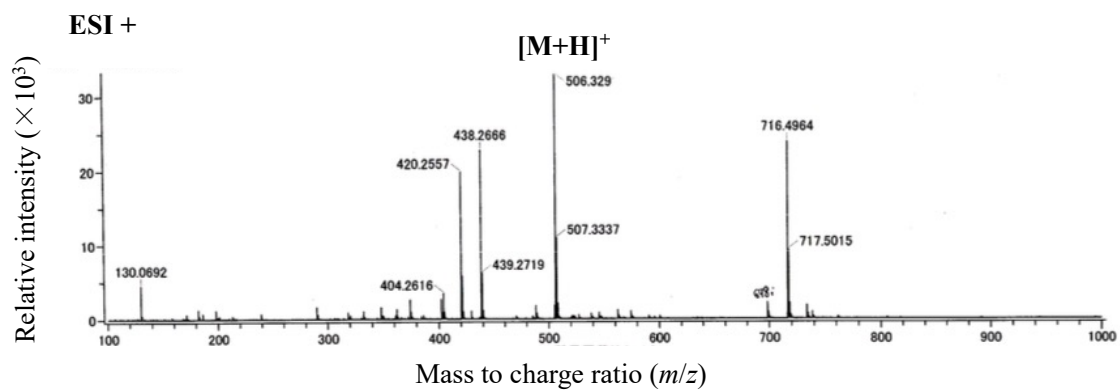
Supplemental Figure 2-38. UV spectrum of terpendole C (**11**)



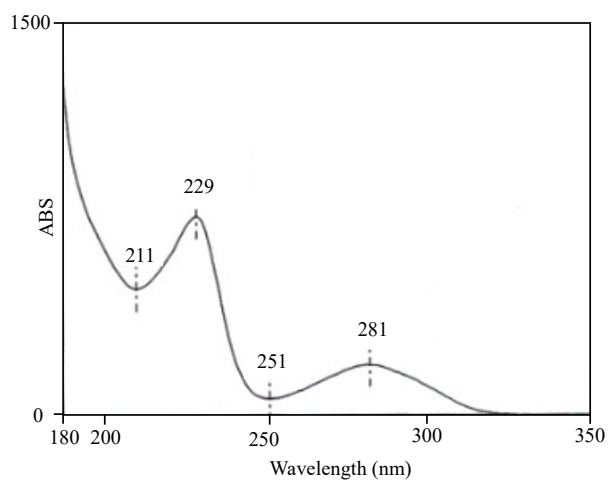
Supplemental Figure 2-39. ¹H-NMR spectrum of terpendole C (**11**)
(400 MHz in DMSO-*d*₆)



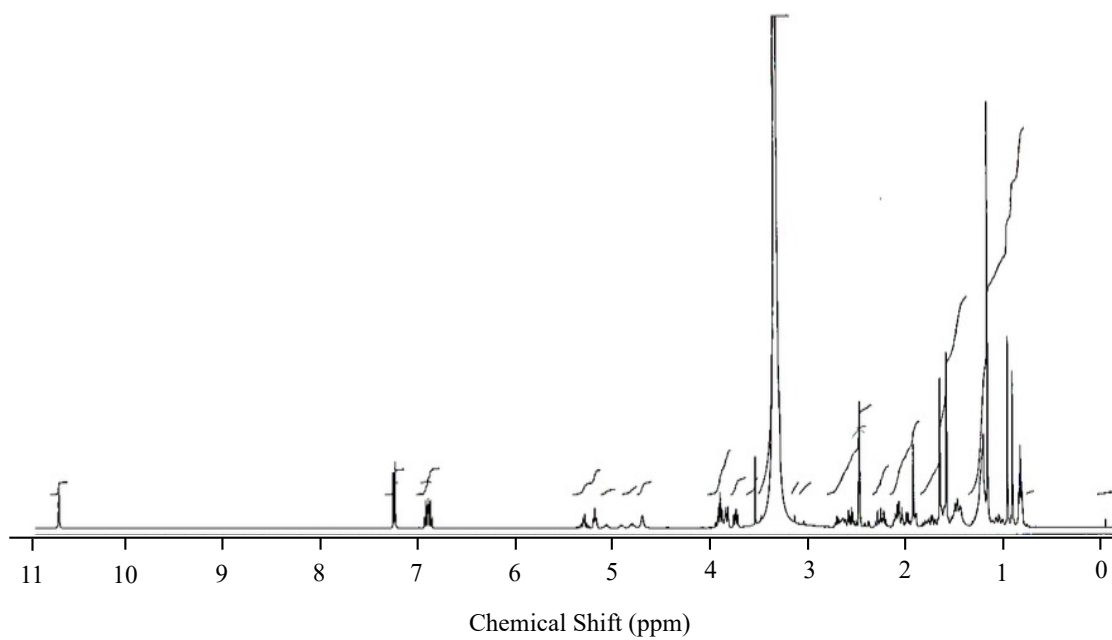
Supplemental Figure 2-40. ^{13}C -NMR spectrum of terpendole C (**11**)
(100 MHz in $\text{DMSO}-d_6$)



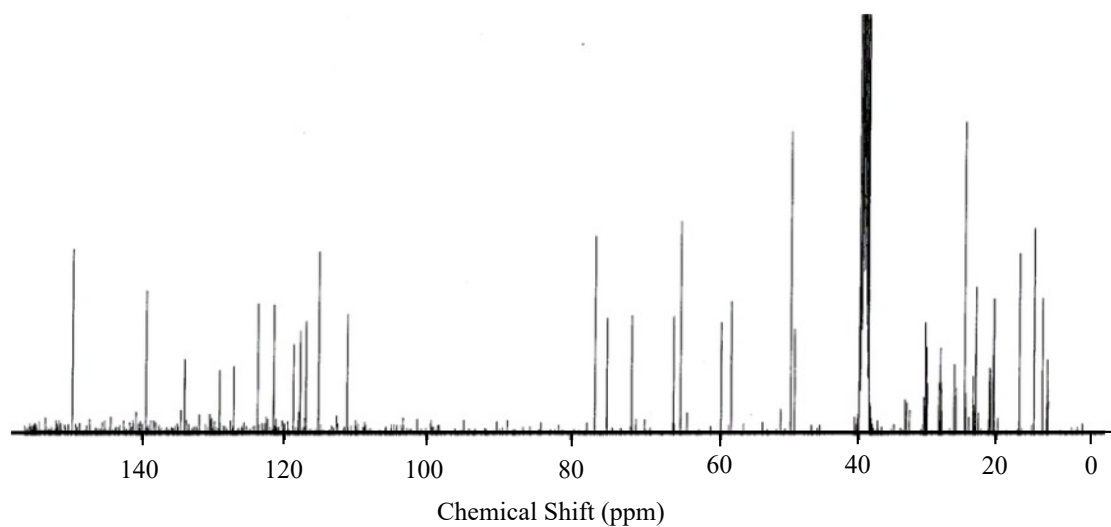
Supplemental Figure 2-41. MS spectrum of terpendole D (**12**)



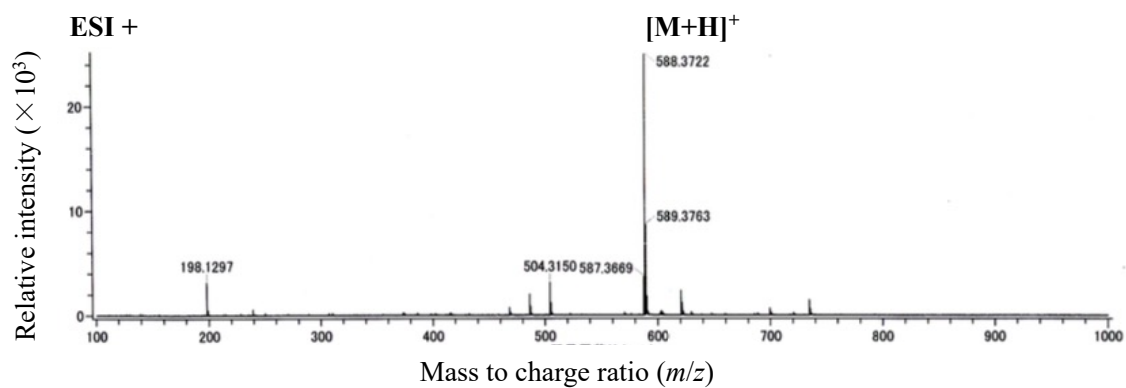
Supplemental Figure 2-42. UV spectrum of terpendole D (**12**)



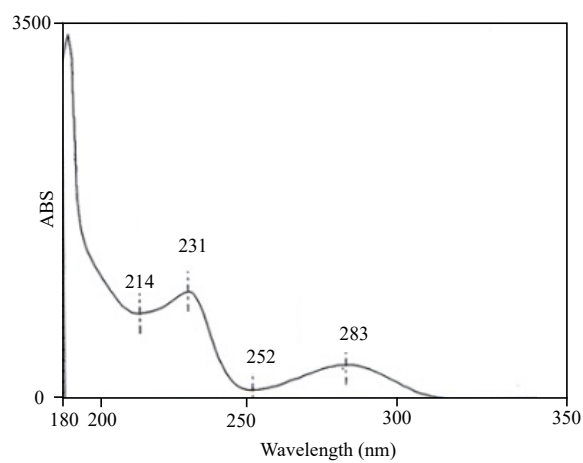
Supplemental Figure 2-43. ¹H-NMR spectrum of terpendole D (**12**)
(400 MHz in DMSO-*d*₆)



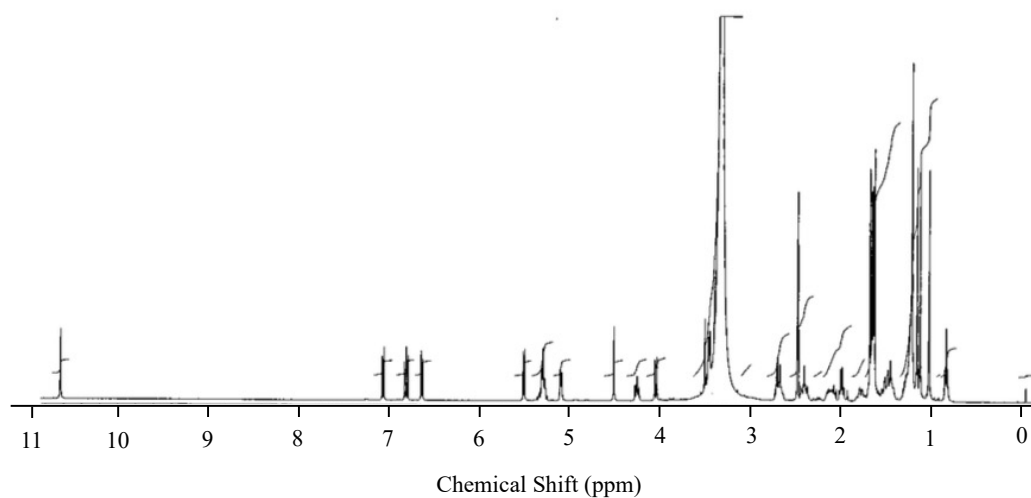
Supplemental Figure 2-44. ^{13}C -NMR spectrum of terpendole D (**12**)
(100 MHz in $\text{DMSO}-d_6$)



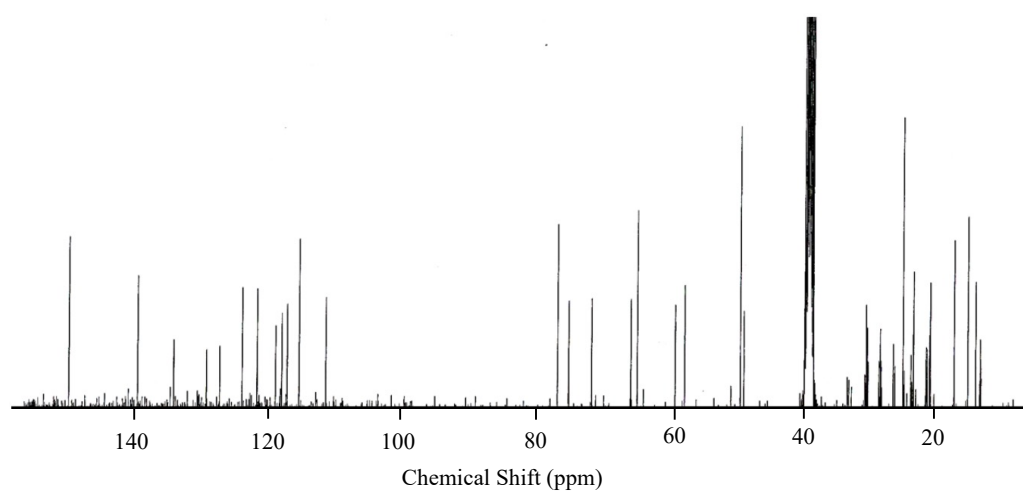
Supplemental Figure 2-45. MS spectrum of terpendole L (**13**)



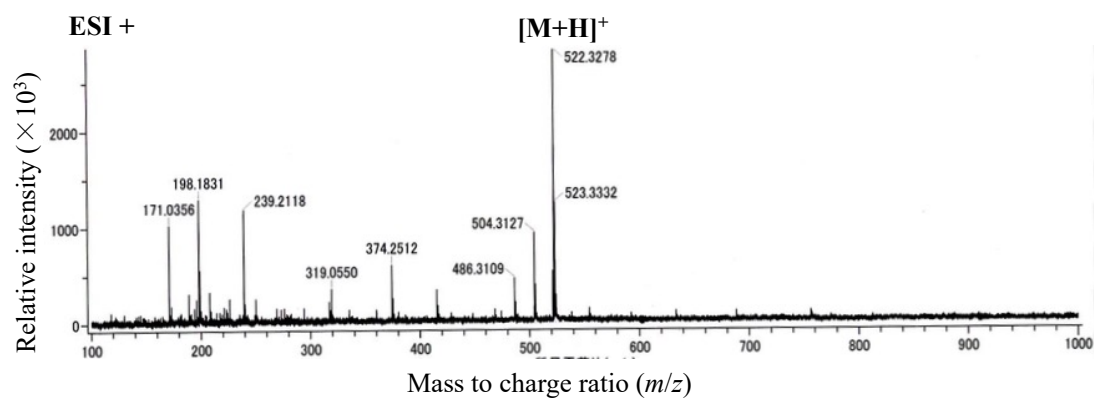
Supplemental Figure 2-46. UV spectrum of terpendole L (**13**)



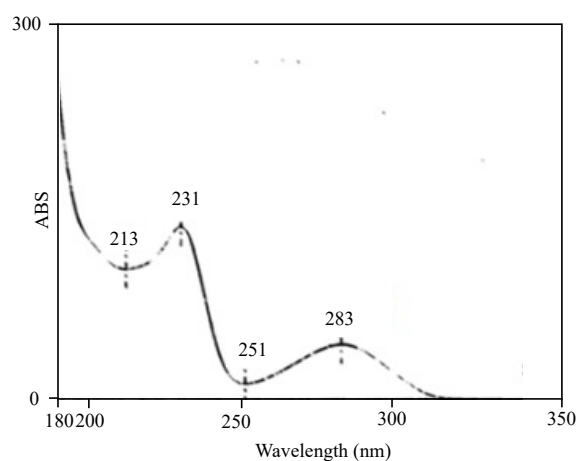
Supplemental Figure 2-47. ¹H-NMR spectrum of terpendole D (**12**)
(400 MHz in DMSO-*d*₆)



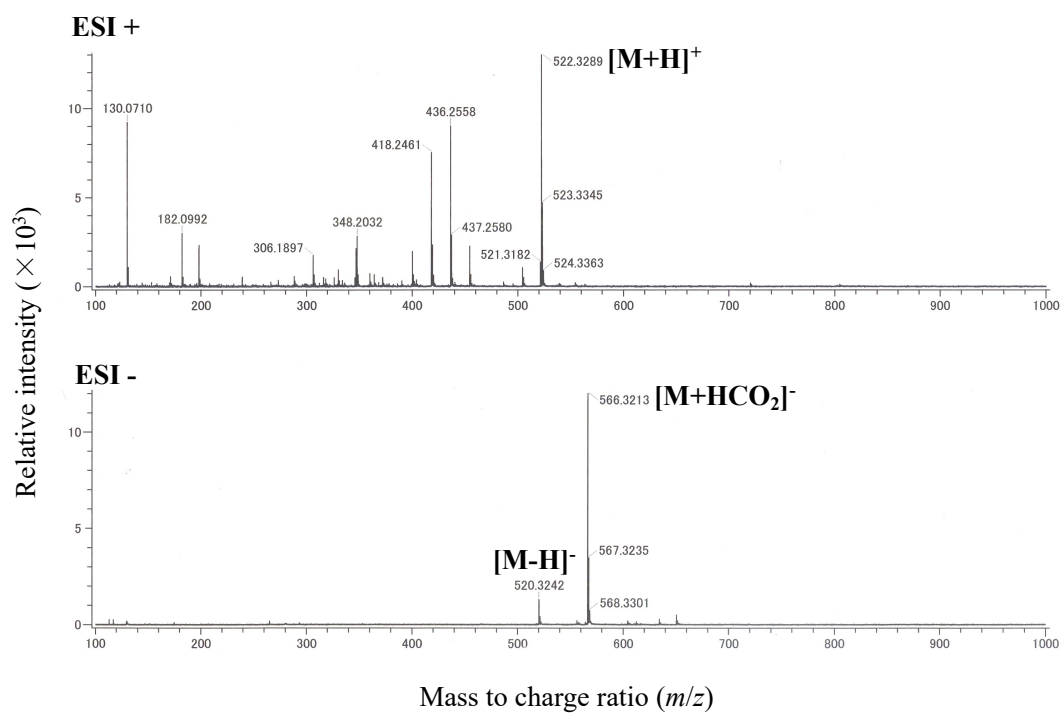
Supplemental Figure 2-48. ¹³C-NMR spectrum of terpendole D (**12**)
(100 MHz in DMSO-*d*₆)



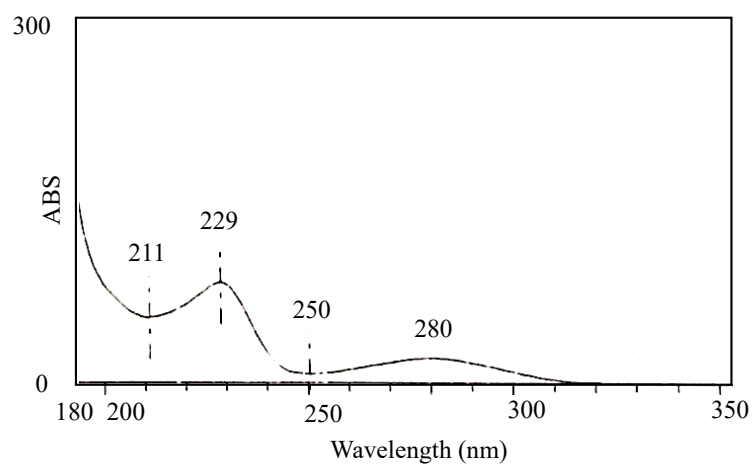
Supplemental Figure 2-49. MS spectrum of tolypocladin A (**14**)



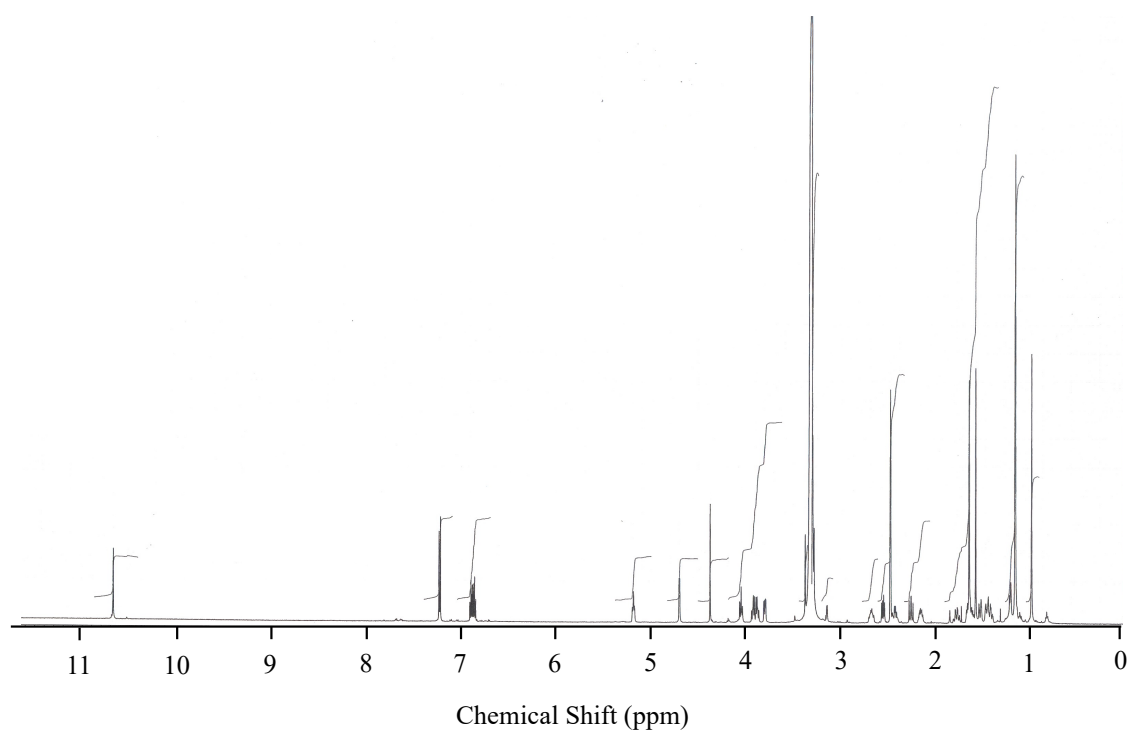
Supplemental Figure 2-50. UV spectrum of tolypocladin A (**14**)



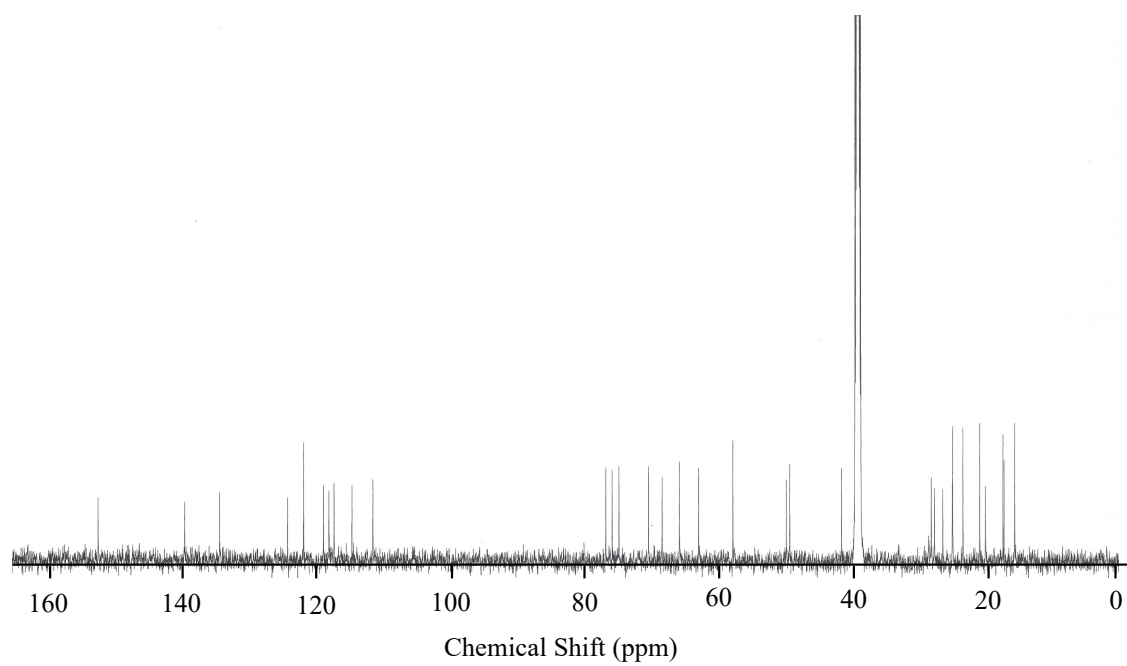
Supplemental Figure 2-51. MS spectrum of terpendole J (**15**)



Supplemental Figure 2-52. UV spectrum of terpendole J (**15**)



Supplemental Figure 2-53. ^1H -NMR spectrum of terpendole J (**15**)
(600 MHz in $\text{DMSO}-d_6$)



Supplemental Figure 2-54. ^{13}C -NMR spectrum of terpendole J (**15**)
(150 MHz in $\text{DMSO}-d_6$)

Chapter III

Screening for the neutral lipid degradation potentiators

This chapter described the assay establishment and the screening for potentiators of neutral lipid degradation. A total of 5,363 microbial cultures from fungi and actinomycetes were screened in cell-based assay. Out of 19 hit samples, 14 fungal cultures contain active brefeldin A (**16**) which potentiated the TG degradation. Beauveriolides I (**17**), III (**18**), beauverolides A (**19**), B (**20**), and K (**21**) from three active fungi cultures exhibited potentiating effect on CE degradation. From two actinomycete cultures, oxohygrolidin (**22**) and hygrolidin (**23**) promoted degradation of CE more preferably than TG.

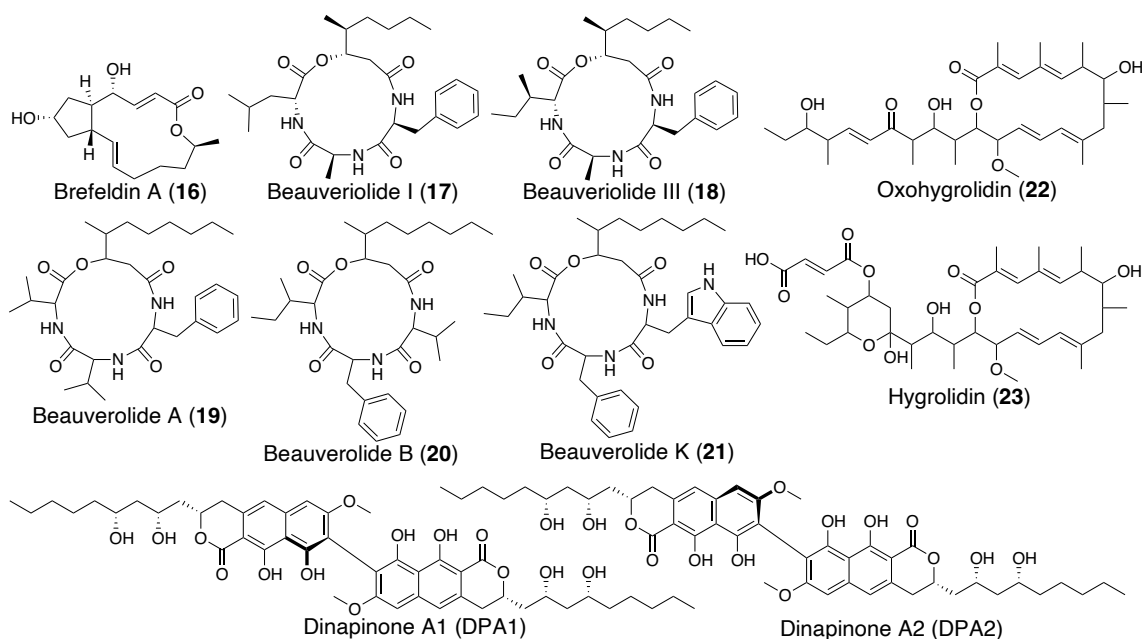


Figure 3-1. Structures of **16–23** and DPAs.

3-1. Establishment of cell-based lipid degradation assay for screening

A cell-based screening method was conducted based on our neutral lipid degradation assay with modification [82]. In the previous study on DPA, three mammalian cell lines, CHO-K1, HeLa, and HepG2 cells, were tested for neutral lipid (TG and CE) accumulation. As a result, CHO-K1 cells were found to have the highest ability to incorporate [^{14}C]oleic

acid into both CE and TG. Accordingly, we chose this cell line in our screening system. CHO-K1 cells were incubated with [^{14}C]oleic acid for 24 hours to accumulate [^{14}C]TG and [^{14}C]CE. After free [^{14}C]oleic acid was removed, cells were treated with a sample and control (in MeOH) (time 0) and incubated for 12 hours. Accumulated [^{14}C]TG and [^{14}C]CE were naturally degraded after 12-hour incubation in the control to 63% and 60% from time 0, respectively [82]. In the screening for lipid degradation potentiators, the amounts of [^{14}C]TG and [^{14}C]CE that remained following 12 hours of incubation were regarded as 100% (control value) (Figure 3-2). Hit samples should promote degradation of [^{14}C]TG and/or [^{14}C]CE to less than 60% of the control with no morphological abnormalities in CHO-K1 cells under microscopy and no effect on phospholipid level ([^{14}C]phospholipid (PL)). EC_{50} values are defined as the effective concentration of a sample causing 50% promotion of each neutral lipid degradation.

First, the effects of DPA (1:1 mixture of DPA1 and DPA2), DPA1, and DPA2 were confirmed in the assay. As shown in Figure 3-3, DPA strongly enhanced the TG degradation with an EC_{50} of 0.07 μM , whereas CE degradation was moderately enhanced with an EC_{50} of >12 μM (approximately 20 μM). Almost no effect on PL degradation implied that DPA affected only neutral lipid degradation without any cytotoxic effect on CHO-K1 cells. DPA2 showed a similar effect on the TG degradation with higher EC_{50} of 1.0 μM (TG) and weak effect on CE degradation (72% of control at 12 μM) (Table 3-3). DPA1 itself showed no effect on neutral lipid degradation. These findings are fundamentally consistent with our previous study [82]. In this screening, DPA was used as a positive control compound.

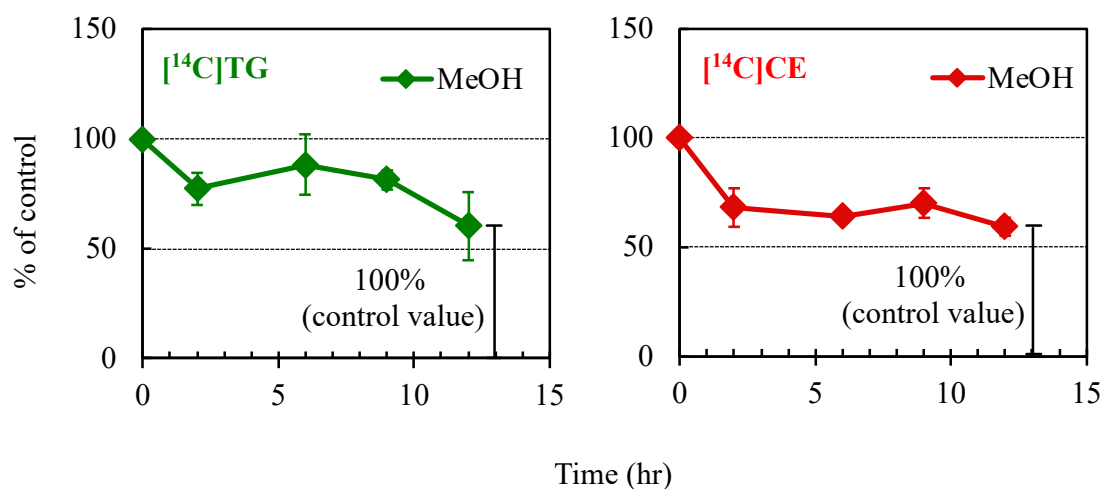


Figure 3-2. Time course on neutral lipid degradation in CHO-K1 cells

CHO-K1 cells were incubated for 24 hours with $[^{14}\text{C}]$ oleic acid to accumulate $[^{14}\text{C}]\text{TG}$ and $[^{14}\text{C}]\text{CE}$. After removing free $[^{14}\text{C}]$ oleic acid, cells were treated with MeOH for 0, 2, 6, 9 and 12 hours. Cells were then lysed. Cellular $[^{14}\text{C}]\text{TG}$ (■), $[^{14}\text{C}]\text{CE}$ (◆), and $[^{14}\text{C}]\text{PL}$ (▲) were separated on TLC and quantified using an image analyzer. The results obtained were plotted as % of control (without MeOH). Values represent means \pm SD ($n = 3$). Data from [82].

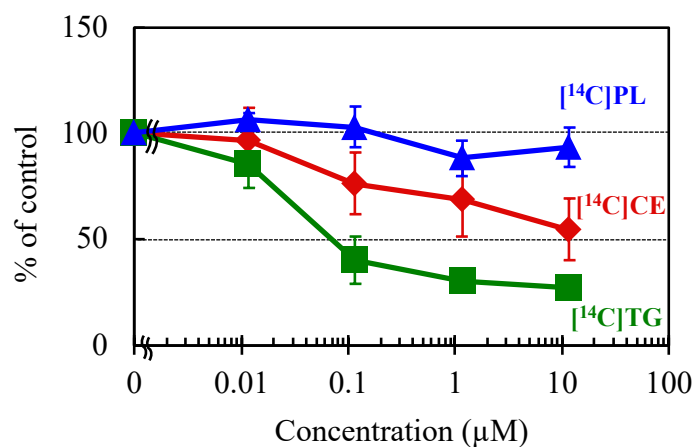


Figure 3-3. Effect of DPA (1:1 mixture of DPA1 and DPA2) on neutral lipid degradation

CHO-K1 cells were incubated for 24 hours with $[^{14}\text{C}]$ oleic acid to accumulate $[^{14}\text{C}]\text{TG}$ and $[^{14}\text{C}]\text{CE}$. After removing free $[^{14}\text{C}]$ oleic acid, cells were treated with DPA 0, 0.12, 1.2, or 12 μM for 12 hours. Cells were then lysed. Cellular $[^{14}\text{C}]\text{TG}$ (■), $[^{14}\text{C}]\text{CE}$ (◆), and $[^{14}\text{C}]\text{PL}$ (▲) were separated on TLC and quantified using an image analyzer. The results obtained were plotted as % of control (without drugs). Values represent means \pm SD ($n = 3$).

3-2. Screening result for neutral lipid degradation potentiators from microbial sources

A total of 5,363 microbial culture broths were screened for neutral lipid degradation potentiators in CHO-K1 cells with only 0.35% of them categorized as hit samples (Table 3-1). The hit rate from fungal cultures (hit rate 0.59%) was 7-fold higher compared to actinomycete cultures (0.08%). Out of 19 active culture broths (Table 3-2), 14 fungal broths promoted degradation of [^{14}C]TG. From these broths, brefeldin A (**16**) [101] was identified as an active compound by database analyses of the retention time and the UV spectrum using UFLC. From one of the fungal cultures, known beauveriolide I (**17**) [102] was identified as a potentiator of [^{14}C]CE degradation. Structurally related beauverolides A, B, and K (**19–21**) [103, 104] were also isolated from the culture broth of soil isolate fungus BF-0452. Two broths from actinomycetes contain hygrolidins that promoted degradation of [^{14}C]CE more preferably than [^{14}C]TG. Known oxohygrolidin (**22**) [105] and hygrolidin (**23**) [106] were isolated from the culture broth of marine-derived actinomycete KM68-21.

Table 3-1. Screening result of microbial potentiators of neutral lipid degradation

Origin	Sample number	Hit sample (rate %)		Hit per-origin (rate %)
		[^{14}C]TG	[^{14}C]CE	
Fungi	2,837	14 (0.49%)	3 (0.10%)	17 (0.59%)
Actinomycetes	2,526	0 (0.00%)	2 (0.08%)	2 (0.08%)
Total	5,363	14 (0.26%)	5 (0.09%)	19 (0.35%)

Table 3-2. Hit strain and microbial potentiators of neutral lipid degradation

Hit strain	Active compounds	Potentiator
Fungal strain		
BF-0398, BF-0460, BF-0487, BF-0546, BF-0562, BF-0586, BF-0589, BF-0626, BF-0763, BF-0808, BF-0899, BF-0938, BF-0939 and BF-0973.	16	TG degradation
BF-0450	17	CE degradation
BF-0452 and BF-0453	19, 20 and 21	CE degradation
Actinomycetes strain		
KM59-1	22	CE degradation
KM68-21	22 and 23	CE degradation

3-3. Purification and identification of active compounds

Compounds **16–18** and dinapinones (DPA, DPA1 and DPA2) were available from our compound library [40, 107, 108] and identified in hit culture broths using our database of UFLC retention time and UV spectrum (Supplemental Figure 3-1). Other compounds (**19–23**) were isolated from hit culture broth and identified from the spectral data, including ¹H-NMR, UV and/or MS data, and the search results of Scifinder scholar and/or Dictionary of Natural Products (Supplemental Figures. 3-1~3-8 and Supplemental Datas 3-1~3-2). These data were also identical with published data [103-106, 109].

3-4. Effect of microbial potentiators on neutral lipid degradation in CHO-K1 cells

A total of eight known compounds (**16–23**, Figure 3-1) were obtained as potentiators of neutral lipid degradation in the screening system. The enhancing activity of neutral lipid (TG and CE) degradation in CHO-K1 cells by these compounds is summarized in Table 3-3. Brefeldin A (**16**), a lactone-containing fungal metabolite, promoted [¹⁴C]TG degradation with an EC₅₀ of 2.6 μM, but had no effect on CE degradation. Thus, **16** is a potentiator selective for TG degradation.

Two beauveriolides and three beauverolides including beauveriolide III (**18**) [40, 108], **17-21** were found to exhibit strong [¹⁴C]CE degradation activity. Compounds **17** and **21** showed the strongest with EC₅₀ of 0.02 μM, followed by **20**, **19**, and **18** with EC₅₀s of 0.06 μM, 0.10 μM, and 0.13 μM, respectively. Sixteen-membered macrolide **23** exhibited

strong potentiation of both [^{14}C]CE (EC_{50} , 0.004 μM) and [^{14}C]TG (EC_{50} , 0.08 μM) degradation, whereas the other macrolide **22** only potentiated [^{14}C]CE degradation with a higher EC_{50} of 0.80 μM .

Table 3-3. Inhibitory activity against neutral lipid synthesis in CHO-K1 cells of **1–4**

Compound	Cell-based lipid degradation EC_{50} (μM) ^a		Cell-based lipid synthesis IC_{50} (μM) ^a		Enzyme-based CE synthesis (SOAT) IC_{50} (μM) ^a
	[^{14}C]TG	[^{14}C]CE	[^{14}C]TG	[^{14}C]CE	[^{14}C]CE
Brefeldin A (16)	2.6	>34	1.6	>34	>34
Beauveriolide I (17)	>2.0	0.02	>2.0	0.01	0.05
Beauveriolide III (18)	>2.0	0.13	>0.2	0.04	0.19
Beauverolide A (19)	>1.8	0.10	>1.8	0.70	0.03
Beauverolide B (20)	>1.8	0.06	>1.8	0.02	0.03
Beauverolide K (21)	>1.5	0.02	>1.5	0.01	0.04
Oxohygroolidin (22)	>1.7	0.80	>1.7	0.63	0.30
Hygroolidin (23)	0.08	0.004	>0.14	0.0002	0.33
DPA1	>12	>12	>12 ^b	>12 ^b	>12
DPA2	1.0	>12	0.65 ^b	>12 ^b	>12
DPA	0.07	>12	0.054 ^b	0.18 ^b	>12

^a n \geq 3. ^b from reference [82]

3-5. Discussion

In this lipid degradation assay, CHO-K1 cells were incubated with [^{14}C]oleic acid overnight to incorporate a high amount of [^{14}C]oleic acid into [^{14}C]TG and [^{14}C]CE accumulated in lipid droplets [82]. After removal of free [^{14}C]oleic acid, the accumulated [^{14}C]TG and [^{14}C]CE still remained at approximately 60% after further 12-hour incubation. This finding indicates that the CHO-K1 cell line is suitable for use in neutral lipid degradation assays.

Fungal brefeldin A (**16**) was identified as a potentiator of [^{14}C]TG degradation in our

screening assay. Bartz *et al.* reported similar findings; in CHO-K2 cells pretreated with [³H]oleic acid, **16** (7 μM) promoted 63% breakdown of stored [³H]neutral lipids after 12-hour incubation [110]. Brefeldin A (**16**) is well known to interfere with protein transport by preventing accumulation of coatamer proteins on the Golgi apparatus, which facilitates vesicle fusion from the endoplasmic reticulum [111, 112]. Accordingly, other studies reported that **16** induced accumulations of neutral lipid [113-115]. However, Bartz *et al.* proposed that the lipid degradation potentiator effect of **16** is not linked to Golgi apparatus disruption and that, instead, **16** inactivates C-terminal-binding protein/brefeldin A-induced ADP-ribosylated substrate (CtBP1/BARS) by stimulating its mono-ADP-ribosylation. CtBP1/BARS works as a gene transcriptional co-repressor in nucleus. Retained CtBP1/BARS function leads to the up-regulation of genes that regulate lipid storage [110].

Fungal beauveriolides I (**17**) and III (**18**) are well known as inhibitors of SOAT enzymes involved in CE synthesis [43]. In the present screening program, beauveriolides and beauverolides (**17–21**) were isolated as potentiators of CE degradation. To investigate CE synthesis (by SOAT activity), **17** to **21** inhibited the synthesis with analogous IC₅₀s (Table 3-3, middle column) to EC₅₀s in the present cell-based degradation assay (Table 3-3, left column). In a SOAT enzyme assay using cells microsomes, **17** to **21** also exhibited potent SOAT inhibition. These data indicated that [¹⁴C]CE is degraded to free cholesterol and [¹⁴C]oleic acid (also provided from [¹⁴C]TG degradation), which are reused to produce [¹⁴C]CE via SOAT during the degradation assay. Beauveriolides and beauverolides may block the [¹⁴C]CE recycling by inhibiting SOAT activity, leading to ostensible potentiation of [¹⁴C]CE degradation. A variety of microbial SOAT inhibitors have been reported [47, 67, 116, 117], but most of them were not discovered in the present screening system.

We evaluated both fungal and actinomycete culture broths in the present screening system and found that fungi were more preferable than actinomycetes as a resource for this screening (Table 3-1). The sole actinomycete-derived potentiators that we found are

hygrolidins, which are members of two diene-containing 16-membered macrolides with diverse chains. Compound **23** with a fumarate-linking tetrahydropyran in the side ring was found to be the strongest potentiator of both CE and TG degradation. Compound **22** with an alkenyl side chain exhibited markedly weaker activity compared to **23**. This group of macrolides is well known as V-ATPase inhibitors that damage the function of lysosomes [118, 119]. The mechanism of lipid droplet degradation in mammalian cells remains elusive; certain proteins located on lipid droplets (such as perilipins) regulate the incorporation of lipase into lipid droplets, and autophagy (lipophagy) is involved in lipid droplet degradation [120-123]. Thus, lysosomes are not directly involved in lipid droplet degradation. Indeed, **22** and **23**, V-ATPase inhibitors, did not inhibit lipid droplet degradation, but conversely potentiated the degradation. The mechanism by which hygrolidins potentiate neutral lipid breakdown requires further investigation. In addition, both compounds exhibited weak SOAT inhibitory activities in the enzyme-based assay (Table 3-3), which may partially contribute to the potentiating effect of lipid degradation in our assay.

In conclusion, we conducted an assay of lipid droplet degradation using CHO-K1 cells and screened for potentiators from microbial cultures. All potentiators identified are known compounds with known mechanism of actions (Figure 3-4). These compounds will help to unveil the incompletely explored mechanism of lipid droplet degradation in mammalian cells.

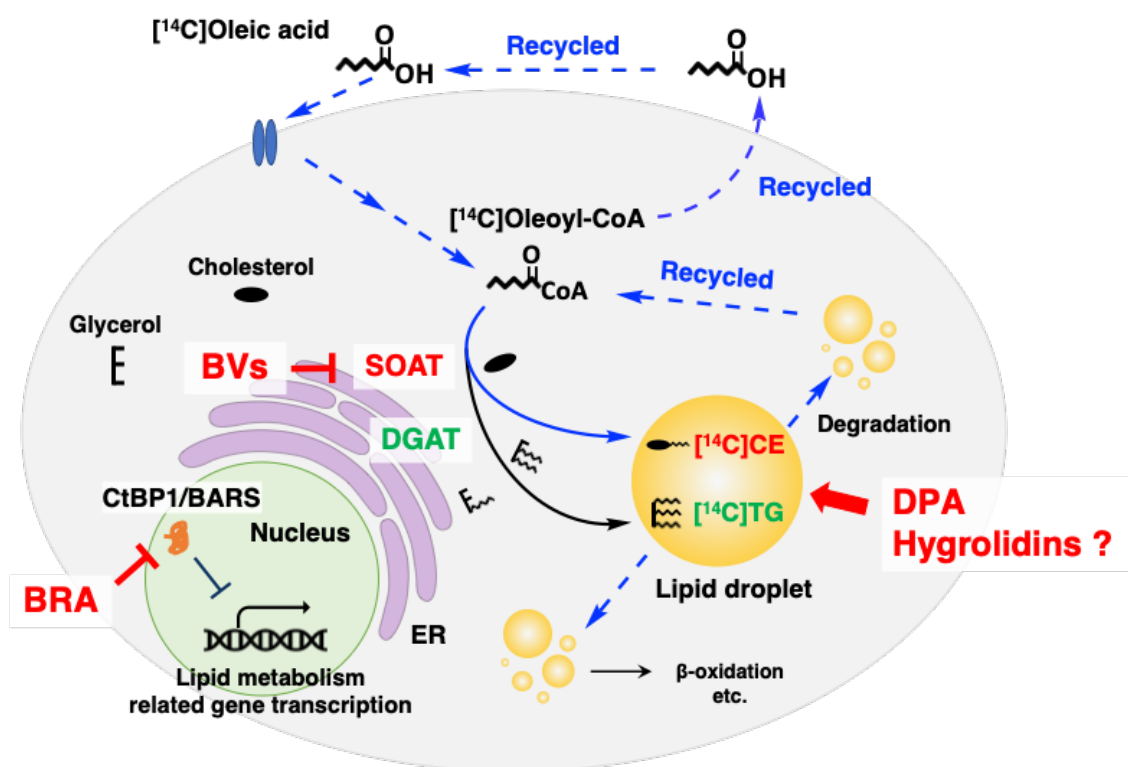
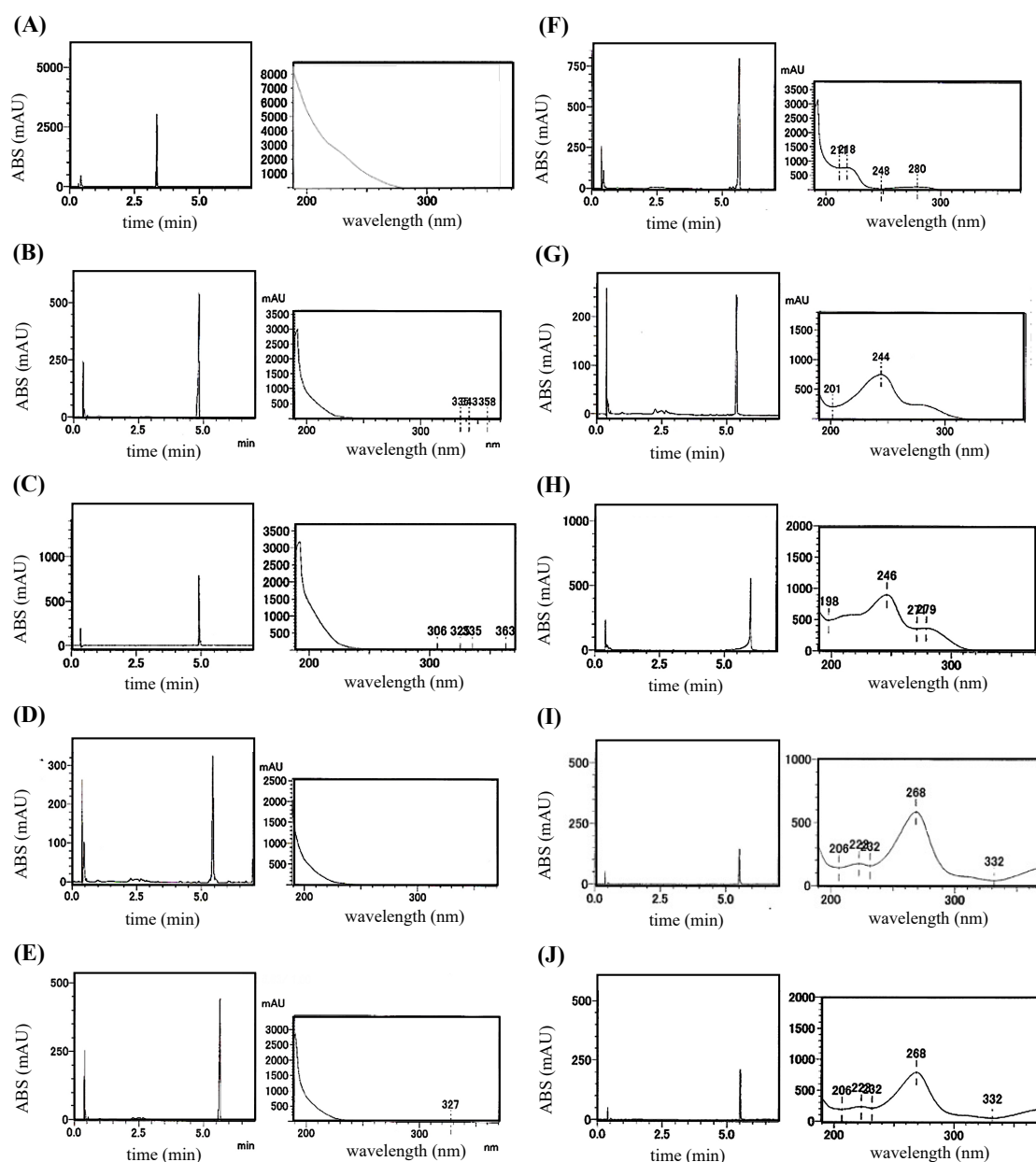


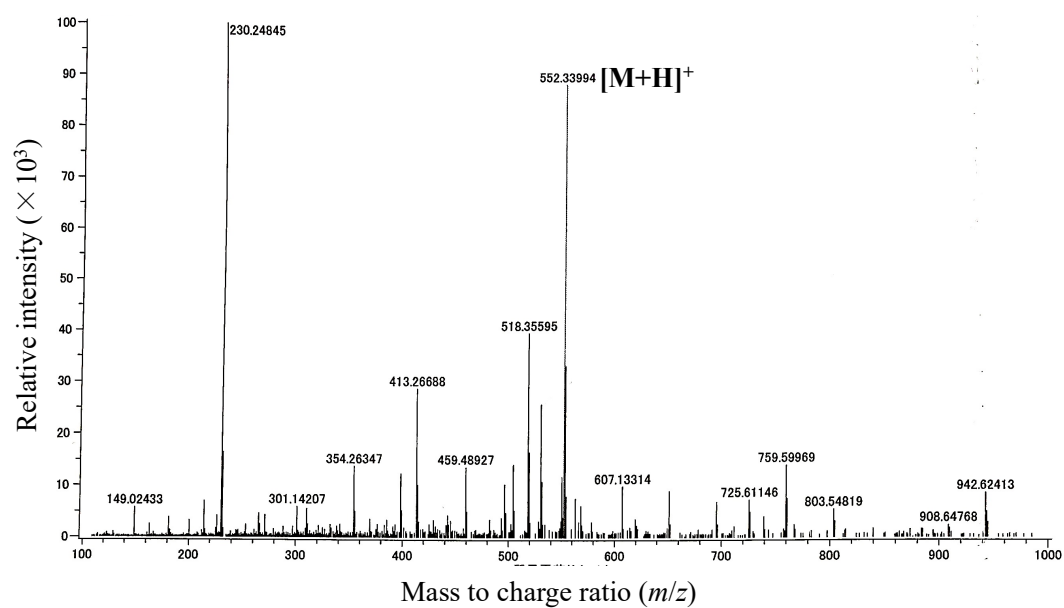
Figure 3-4. Graphical summary of microbial potentiators of neutral lipid degradation. CE; cholesteryl ester, TG; triacylglycerol, SOAT; sterol O-acyltransferase, DGAT; diacylglycerol acyltransferase, ER; endoplasmic reticulum, CtBP1/BARS; C-terminal-binding protein/brefeldin A-induced ADP-ribosylated substrate, BRA; brefeldin A, BVs; beauveriolides, DPA; dinapinone A

3-6. Supplemental data

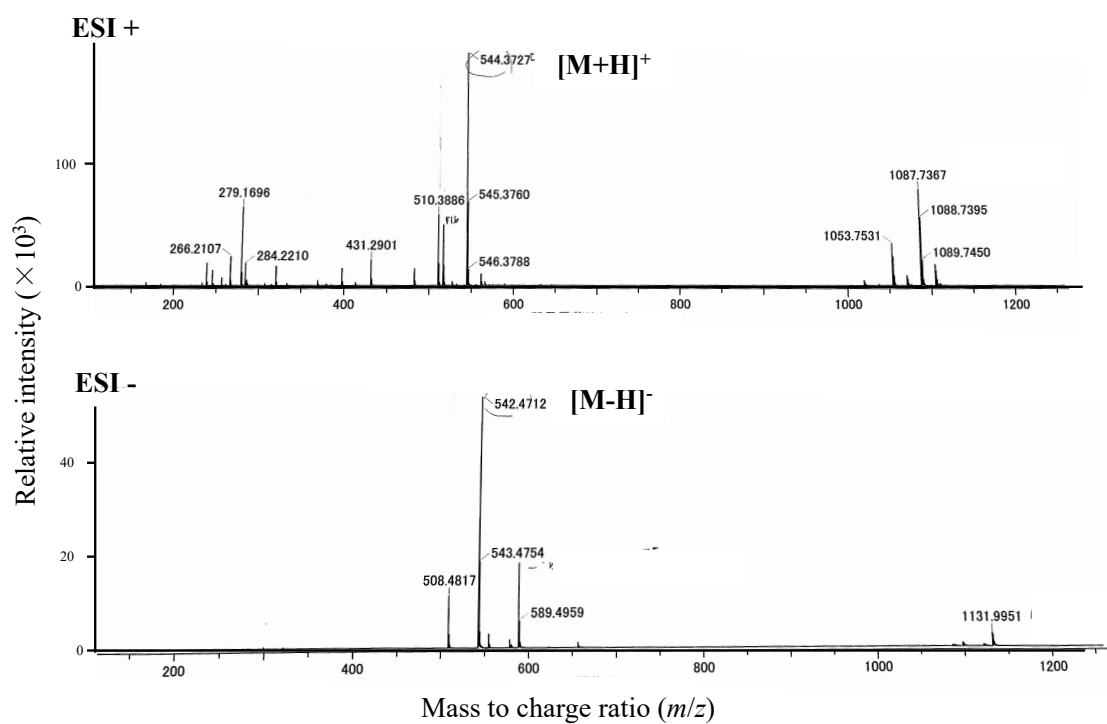


Supplemental Figure 3-1. Chromatogram and spectrogram of active compounds analyzed in UFLC.

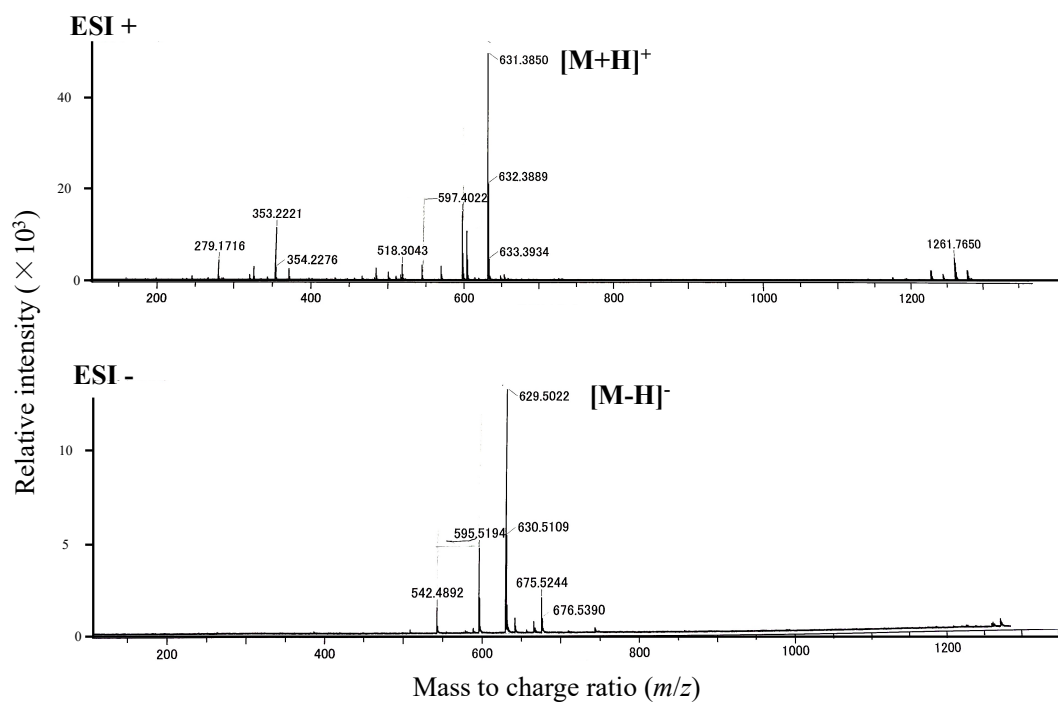
(A) Brefeldin A (**16**) (1 μg), (B) beauveriolide I (**17**) (1 μg), (C) beauveriolide III (**18**) (1 μg), (D) beauveriolide A (**19**) (1 μg), (E) beauveriolide B (**20**) (1 μg), (F) beauveriolide K (**21**) (1 μg), (G) oxohygrolidin (**22**) (1 μg), (H) hygrolidin (**23**) (1 μg), (I) dinapinone A1 (0.2 μg) and (J) dinapinone A2 (0.2 μg) were diluted in MeOH and analyzed in UFLC system under the following condition (column, Shimpak XR-ODS (i.d. 2.0 \times 75 mm); eluent, 6 minutes linear gradient from 5-95% CH₃CN/H₂O-0.1% H₃PO₄ then 1 minute isocratic 95% CH₃CN/H₂O-0.1% H₃PO₄; flow, 0.55 mL min⁻¹; detection, UV at 210 nm).



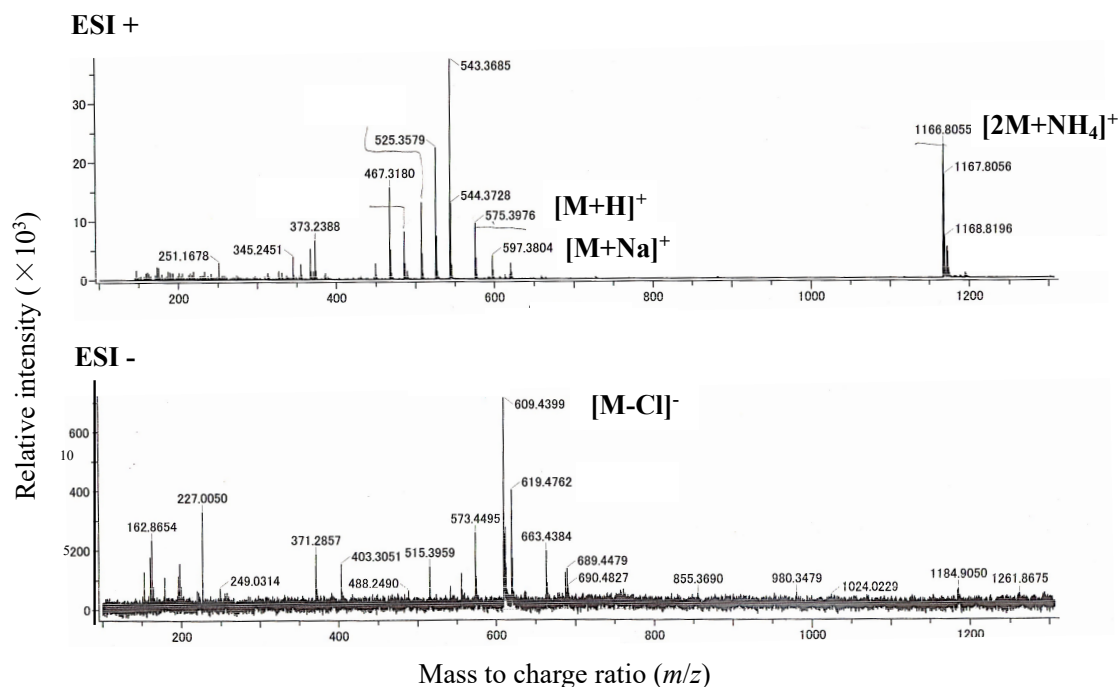
Supplemental Figure 3-2. MS spectra of beauverolide A (19)



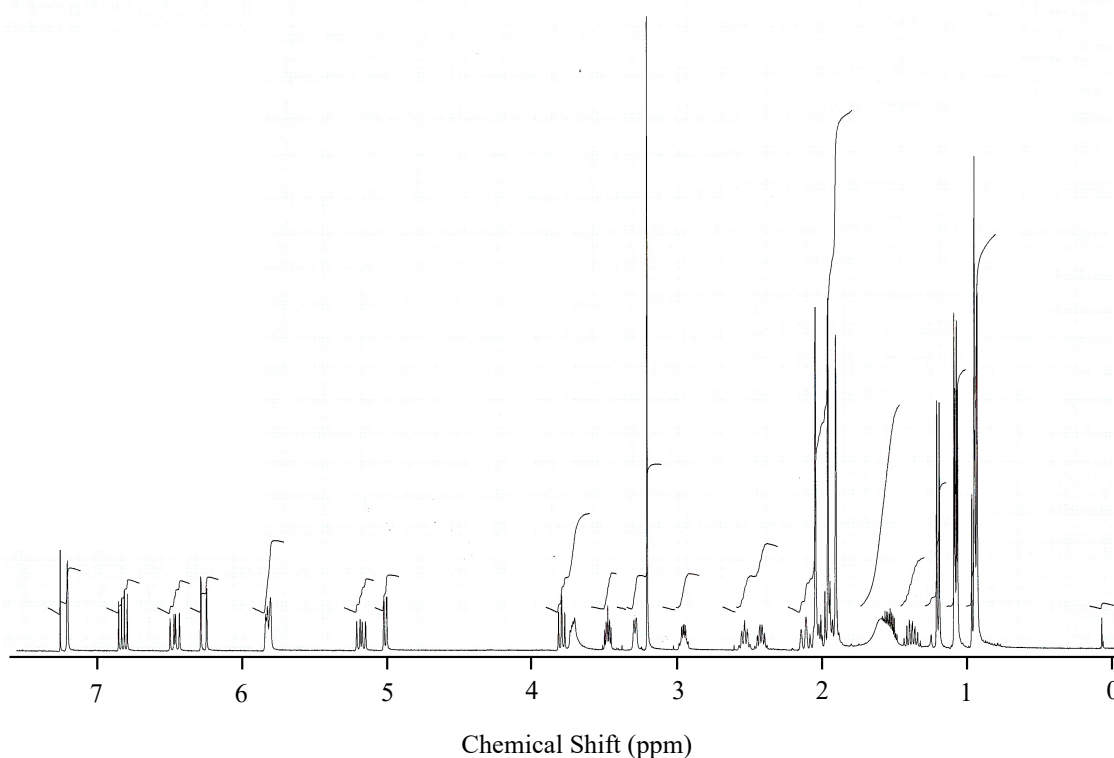
Supplemental Figure 3-3. MS spectra of beauverolide B (20)



Supplemental Figure 3-4. MS spectra of beauverolide K (**21**)



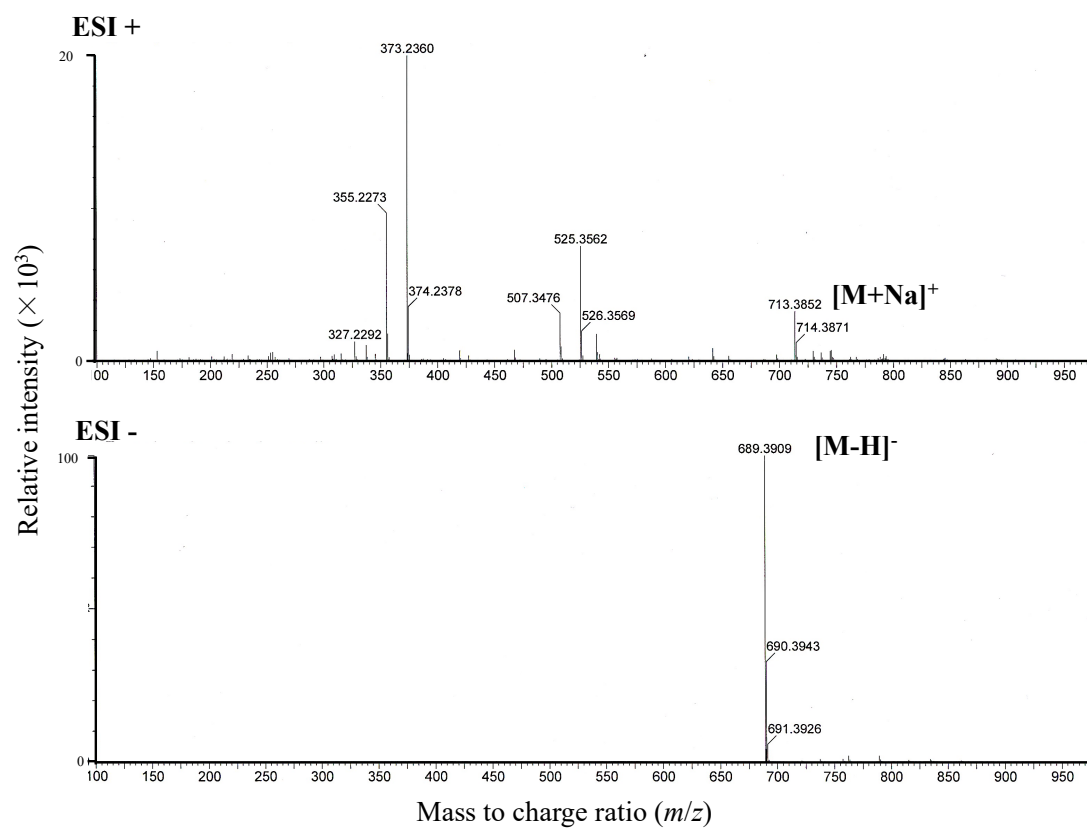
Supplemental Figure 3-5. MS spectra of oxohygrolidin (**22**)



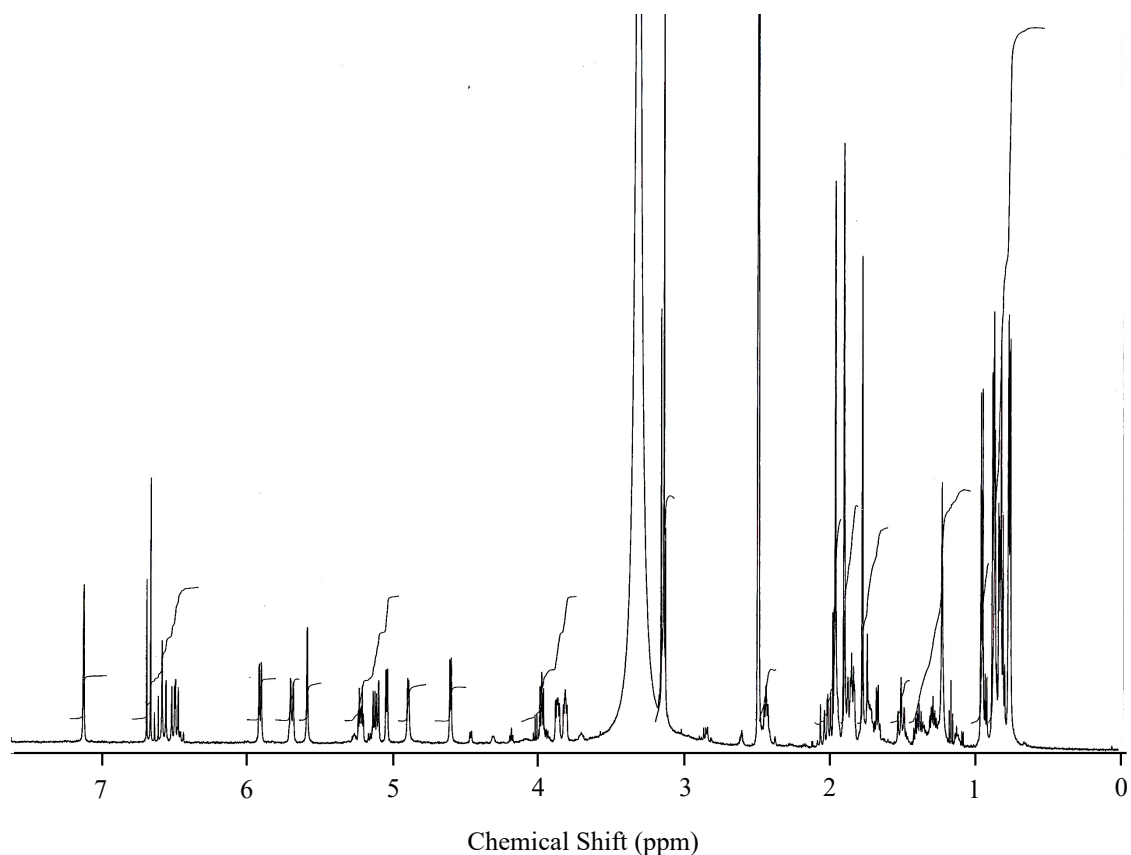
Supplemental Figure 3-6. ^1H -NMR spectrum of oxohygroloidin (**22**)
(400 MHz in CDCl_3)

Supplemental Data 3-1. ^1H -NMR chemical shift of oxohygroloidin (**22**)

^1H -NMR (400 MHz, CDCl_3) δ 0.93 (CH_3 , d), 0.95 (CH_3 , s), 0.95 (CH_3 , s), 1.07 (CH_3 , d), 1.09 (CH_3 , d), 1.20 (CH_3 , d), 1.38~1.54 (CH_2 , m), 1.91 (CH_3 , s), 1.93~1.98 (CH , m), 1.96 (CH_3 , d), 1.95~1.98 (CH_2 -a, m), 1.96~2.10 (CH , m), 2.05 (CH_3 , s), 2.11~2.15 (CH_2 -b, m), 2.42 (CH , m), 2.54 (CH , m), 2.96 (CH , m), 3.21 (CH_3 , s), 3.29 (CH , d), 3.48 (CH , q), 3.73 (CH , q), 3.80 (CH , t), 5.01 (CH , dd), 5.18 (CH , q), 5.80 (CH , br. d), 6.26 (CH , dd), 6.46 (CH , q), 6.82 (CH , q), 7.20 (CH , s).



Supplemental Figure 3-7. MS spectra of hygrolidin (**23**)



Supplemental Figure 3-8. ^1H -NMR spectrum of hygrolidin (**23**) (600 MHz in CDCl_3)

Supplemental Data 3-2. ^1H -NMR chemical shift of hygrolidin (**23**)

^1H -NMR (600 MHz, $\text{DMSO}-d_6$) δ 0.71 (CH_3 , d), 0.74 (CH_3 , d), 0.81 (CH_3 , t), 0.85 (CH_3 , d), 0.86 (CH_3 , d), 0.94 (CH_3 , d), 1.28~1.39 (CH_2 , m), 1.50 (CH_2 -a, t), 1.66 (CH , m), 1.71 (CH , m), 1.76 (CH_3 , s), 1.83 (CH_2 -b, m), 1.83 (CH , m), 1.87~2.00 (CH_2 , m), 1.89 (CH_3 , s), 1.94 (CH , m), 1.95 (CH_3 , s), 2.43 (CH , t), 3.13 (CH_3 , s), 3.14 (CH , t), 3.81 (CH , q), 3.86 (CH , m), 3.97 (CH , t), 4.61 (OH , q), 4.60 (OH , d), 5.04 (CH , dd), 5.11 (CH , dd), 5.22 (CH , m), 5.59 (OH , s), 5.69 (CH , d), 5.91 (CH , d), 6.50 (CH , q), 6.57 (CH , d), 6.68 (CH , d), 7.12 (CH , s).

III. Summary

Cardiovascular diseases contribute to the highest share of death causes in the world with a significant rise in the last 10 years [8]. Underlying the risk factors, excessive accumulation of neutral lipids (CE and TG) has been shown to cause arteriosclerosis and fatty liver [32-34]. For the purpose of lowering blood cholesterol, statin drugs, which are HMG-CoA reductase inhibitors, have been used as first-line drugs. However, it has been reported that only 30% to 40% suppress cardiovascular events (such as myocardial infarction and angina pectoris) [21]. Drugs having other mechanisms of action have been actively developed, for example, PCSK9 inhibitors [26] and CETP inhibitors [27]. Available PCSK9 inhibitors are antibody drugs, the cost is relatively expensive, and the administration route is limited. CETP inhibitors have been shown to have side effects in clinical trials, but the prevention and treatment of atherosclerosis are still insufficient with existing drugs alone. In addition, an abnormal accumulation of CE and TG in the liver caused by obesity termed non-alcoholic fatty liver/non-alcoholic steatohepatitis (NAFLD/NASH) has been increasing worldwide [35]. To this date, the FDA has not approved any therapeutic agents for NAFLD/NASH and pharmacotherapy treatments are relatively limited. Pioglitazone, a PPAR- γ agonist and vitamin E treatment have been used by many clinicians. However, pioglitazone and vitamin E have not been studied further and have been associated with several side effects [39]. Controlling the amounts of neutral lipid prevents or treats these diseases. Our research group has been focusing on this theme for many years. Using various cells and enzyme assay systems, our group discovered small molecules that control lipid metabolism from the secondary metabolites of microorganism. In this study, I focused on the search for neutral lipid synthesis inhibitors and degradation potentiators from natural resources.

1. Screening for the neutral lipid synthesis inhibitors

Using the established cell-based assay of CE and TG synthesis [68, 79], Chapter 1 covers the study of new biological activity of known polyacetylenes isolated from *Atractylodes* rhizome extract and Chapter 2 covers the study of new terpendole congeners isolated from the culture broth of the fungus *Volutella citrinella* BF-0440.

Chapter 1: Polyacetylenes from *Atractylodes* rhizome extract

Traditional herbal medicine, *Atractylodes* rhizome extract was found to inhibit CE synthesis in our established assay using Chinese hamster ovary (CHO-K1) cells. From the extract, four known compounds, one sesquiterpene, atractylenolide III (**1**) and three polyacetylenes, 14-acetoxy-12-seneciolyloxytetradeca-2*E*,8*E*,10*E*-trien-4,6-diyn-1-ol (**2**),

14-acetoxy-12- α -methylbutyl-2*E*,8*E*,10*E*-trien-4,6-diyn-1-ol (**3**) and 14-acetoxy-12- β -methylbutyl-2*E*,8*E*,10*E*-trien-4,6-diyn-1-ol (**4**) were isolated. Structurally similar **3** and **4** (**3/4** mixture) were obtained as a mixture based on ¹H-NMR and ¹³C-NMR data. The separation and purification attempt of **3/4** mixture by several HPLC columns was in vain. Other researchers also reported the difficulty of their purification [87, 93]. Compounds **1**, **2**, and a **3/4** mixture selectively inhibited CE synthesis. Sterol *O*-acyltransferase (SOAT) that catalyzes the synthesis of CE from cholesterol and long chain fatty acid exists as two isozymes, SOAT1 and SOAT2, with distinct functions in human body [50-53]. Selective inhibition of SOAT2 is believed for the prevention of atherosclerosis, hypercholesteremia, and fatty liver disease [54, 55, 60, 61]. The SOAT activity and selectivity of these compounds were tested using human SOAT1- or SOAT2-expressing CHO cells [68]. Polyacetylenes **2** and a **3/4** mixture were found to moderately inhibit both SOAT1 and SOAT2 activity (dual-type inhibitors).

Chapter 2: Terpendoles congeners from *Volutella citrinella* BF-0440

In our screening for SOAT2-selective inhibitors from microorganisms, a culture broth of the fungus *Volutella citrinella* BF-0440 (isolated from soil collected in Shizuoka-shi, Japan) was selected. From the culture broth, new indoline–diterpene-containing compounds, termed voluhemins A (**8**) and B (**9**), and NK12838 (**10**) [95] were discovered [96]. Furthermore, the culture broth of the fungus still contained other structurally related compounds. As a result, new terpendoles N-P (**5–7**), were isolated from the culture broth along with four known terpendole congeners (**11–15**) [97-99]. New terpendole P (**7**) had one while voluhemins (**8–9**) and terpendole O (**6**) had two additional isoprenyl moieties to the indole-diterpene backbone. Only terpendole N (**5**) contained a unique epoxy prenylated-indolinone and 4 consecutive ring system. All compounds except terpendole N (**5**) and tolypocladin A (**14**) showed SOAT inhibitory activity, suggesting the consecutive ring system and additional 2-methyl-2-butene moiety are important for the activity. Intriguingly, only voluhemin B (**9**) exhibited SOAT2 selective inhibition indicating that the *O*-Me moiety is crucial for SOAT2 selectivity.

2. Screening for the neutral lipid degradation potentiators (Chapter 3).

As a challenging screening study, I conducted a cell-based assay system to evaluate neutral lipid (CE and TG) degradation and screened microbial culture broths for potentiators of neutral lipid degradation. Assay for CE and TG degradation using CHO-K1 cells was conducted by modifying the reported method [82]. DPA (a mixture of

atropisomers, dinapinone A1 (DPA1) and dinapinone A2 (DPA2) (1:1 ratio) used as a positive control strongly enhanced TG degradation and moderately enhanced CE degradation. A total of 5,363 microbial cultures from fungi and actinomycetes were screened. Out of 19 hit samples (hit rate 0.35%), 14 fungal cultures contain active brefeldin A (**16**) which potentiated the degradation of TG. Beauveriolides I (**17**), III (**18**), beauveriolides A (**19**), B (**20**), and K (**21**) from three active fungi cultures exhibited potentiating effect on CE degradation. Among beauveriolides, **17** and **21** exhibited the strongest activities. From two actinomycete cultures, oxohygrolidin (**22**) and hygrolidin (**23**) promoted degradation of CE more preferably than TG. All potentiators identified are known compounds with known mechanism of actions.

Through this research, various compounds that regulate neutral lipid synthesis and degradation from natural products, especially microbial resources were discovered (Figure 4). In the future, I hope that these results will lead to the discovery of target molecules and mechanism of actions that will lead to the prevention and treatment of lipid related diseases and the development of new drugs.

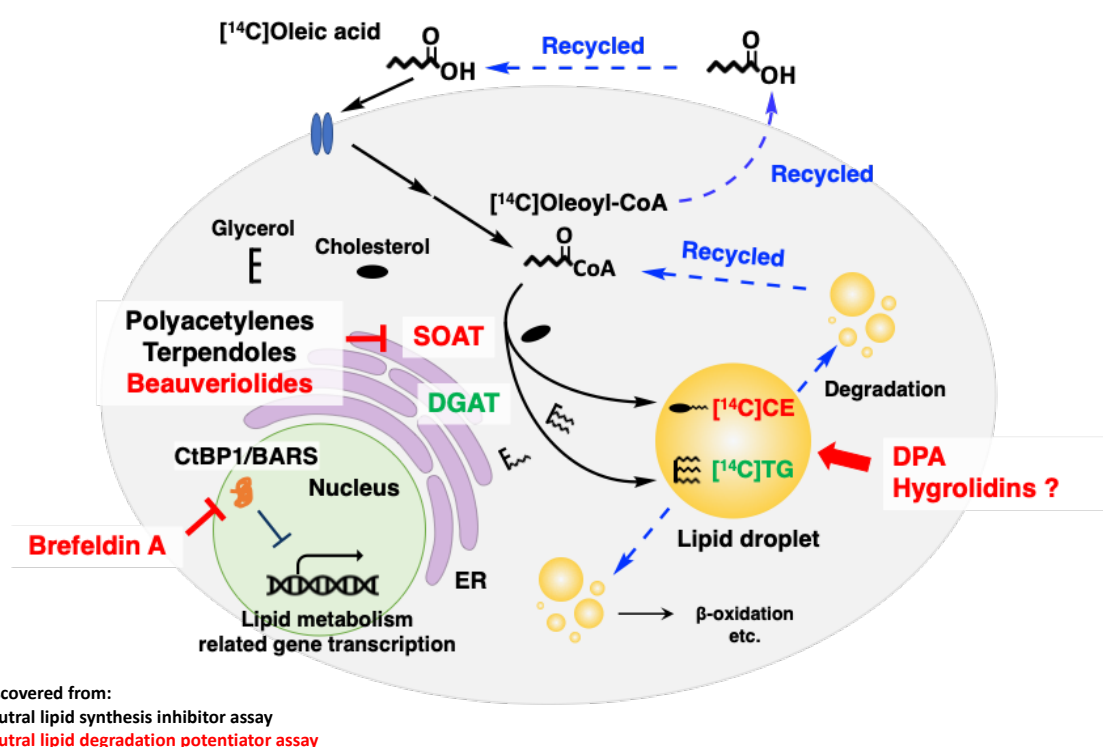


Figure 4. Graphical summary.

CE; cholesteryl ester, TG; triacylglycerol, SOAT; sterol O-acyltransferase, DGAT; diacylglycerol acyltransferase, ER; endoplasmic reticulum, CtBP1/BARS; C-terminal-binding protein/brefeldin A-induced ADP-ribosylated substrate, BRA; brefeldin A, BVs; beauveriolides, DPA; dinapinone A.

IV. Experimental Methods

Chapter I Polyacteylenes from *Atractylodes* rhizome extract

I . Reagents

Chloroform (CHCl_3) (first grade), methanol (MeOH) (first grade) and diethyl ether (special grade) were purchased from Nacalai Tesque. Inc.

Acetic acid (CH_3COOH) (special grade), hexane (special grade), potassium chloride (KCl) (special grade) and hydrochloric acid (HCl) (special grade) were purchased from Kanto Chemical Co., Ltd.

Sodium chloride (NaCl) (special grade), sodium hydrogen phosphate (Na_2HPO_4) (special grade), potassium dihydrogen phosphate (KH_2PO_4) (special grade), ethylenediamine tetraacetic acid tetrasodium salt ($\text{EDTA} \cdot 4\text{Na}$) (special grade), 2-amino-2-hydroxymethyl-1,3-propanediol (Tris) (for biochemistry), sodium dodecyl sulfate (SDS) (for biochemistry), sucrose (special grade), MEM vitamin solution and G418 sulfate (geneticin) were purchased from Wako Pure Chemical Industries, Ltd.

Ethanol (EtOH) (special grade) was purchased from Japan Alcohol Sales Association.

Penicillin ($10000 \text{ units mL}^{-1}$) / streptomycin (10000 mg mL^{-1}) (P/S) solution and 2.5% trypsin solution were purchased from Invitrogen.

Fetal bovine serum (FBS) was purchased from Biowest and used after heat treatment (inactivation) at 56°C for 30 minutes.

HAM's F12 medium and fatty acid-free bovine serum albumin (BSA) were obtained from Sigma-Aldrich.

Radiolabeled [^{14}C]oleic acid ($9.25 \text{ MBq per } 2.5 \text{ mL}$) was purchased from PerkinElmer and diluted 10-fold with PBS (-).

[1- ^{14}C]Oleoyl Coenzyme A ($1.85 \text{ GBq mmol}^{-1}$) was purchased from Moravek.inc.

Oil red O powder was purchased from Merck.

II. Material

Dried *Atractylodes* rhizome was purchased from Jilin Aodong Medicine Industry Group Co., Ltd (Zhejiang Province, China).

100 mm petri dish, 50 mL centrifuge tube and 48-well plate were purchased from Corning.

TLC plate (70F₂₅₄, thickness 0.25 mm) was purchased from Wako Pure Chemical Industries, Ltd.

0.20 μ m syringe filter was purchased from Sartorius.
Silica gel 60 70–230 mm for column chromatography was purchased from Merck.
OptiSeal manufactured by Beckman Coulter manufactured by Hitachi Koki Co., Ltd. was used as ultracentrifugation tubes.

III. Instruments

Refrigerated centrifuge by KUBOTA 2700 (Kubota Corporation).
Micro-refrigerated centrifuge by AX-511 (TOMY®).
Centrifugal evaporator by CVE-200D (EYELA®).
Image analyzer by FLA-7000 (GE Healthcare®).
UFLC by Prominence UFLC system packed with pack XR-ODS column (i.d. 2.0×75 mm).
Kokusan H-700R was used as a refrigerator incubator.
LAQUA twin S010 of Horiba, Ltd. was used as a pH meter.
NMR system 400 MHz spectrometer from Agilent Technologies and 900 MHz spectrometer from Bruker® were used for NMR analyses.
LC-MS analyses were performed using AccuTOF LC-plus JMS-T100LP system from JEOL and analytical column Capcellcore C18 (i.d. 2.1×50 mm) by Osaka soda.
The following HPLC unit from SHIMADZU Corp. was used for high performance liquid chromatography. LC-20AT was used as a pump, SPD-20A as a detector, DGU-20A₅ as a degasser and D-2500 from Hitachi High-Tech Science as a recorder.
The preparative column used was PEGASIL ODS SP100 (i.d. 2.0×250 mm) by Senshu Science.
Centrifuge KUBOTA 3500 from Kubota Corporation was used for centrifuge.
Beckman Coulter Optima Ultracentrifuge and TLA110 as rotor was used for ultracentrifuge.

IV. Cell

CHO-K1 cells were provided by Dr. Kentaro Hanada, National Institute of Infectious Diseases. AC29 cells (SOAT-deficient CHO cells) expressing either the *SOAT1* or *SOAT2* gene from human (hSOAT1-CHO and hSOAT2-CHO cells) were kindly gifted from Professor L. L. Rudel of Wake Forest University [67].

V. Reagent preparation

1. Cell culture medium

For CHO-K1 cells, 500 mL of Ham's F-12 medium was supplemented with 6.3 mL of penicillin ($100 \text{ units mL}^{-1}$)/streptomycin (100 mg mL^{-1}) solution and 55 mL of inactivated FBS. Performed under aseptic condition.

For both hSOAT1- and hSOAT2-CHO cells, 500 mL of Ham's F-12 medium was supplemented with 6.3 mL of MEM vitamin solution, 6.3 mL of penicillin ($100 \text{ units mL}^{-1}$)/streptomycin (100 mg mL^{-1}) solution, 3.75 mL of geneticin solution (dissolved in milliQ water to 50 mg mL^{-1} and sterilized by filtration with $0.20 \mu\text{m}$ syringe filter) and 55 mL of inactivated FBS. Performed under aseptic condition.

2. PBS (-) solution

8.0 g of NaCl, 1.15 g of Na_2HPO_4 , 0.20 g of KCl and 0.20 g of KH_2PO_4 were dissolved in milli Q water to a total volume of 1.0 L and sterilized by autoclaving at 121°C for 15 minutes.

3. 0.0625% trypsin/EDTA • 4Na solution

10 mL of 2.5% trypsin solution, 0.5 mL of 4.0% EDTA • 4Na solution were aseptically added with PBS (-) to a total volume of 100 mL.

4. 1.0 M Tris/HCl (pH 7.5) solution

121.14 g of Tris was dissolved in milli Q water and adjusted to pH 7.5 by HCl addition. The solution then was added with milli Q water to a total volume of 1.0 L.

5. 0.10% SDS-Tris solution

0.10 g of SDS and 1.0 mL of 1.0 M Tris/HCl (pH 7.5) solution were dissolved in milli Q water to a total volume of 1.0 L.

6. Buffer A

Dissolve 17.12 g of sucrose, 1.87 g of KCl, 2.72 g of KH_2PO_4 , and 6.78 g of EDTA • 4Na in milli Q water. A total volume of 500 mL was autoclaved at 121°C for 15 minutes (Fin. 100 mM sucrose, 50 mM KCl, 40 mM KH_2PO_4 , 30 mM EDTA).

7. Sample solution

Compounds **1–4** were obtained isolation from the rhizome extract. The compounds were dissolved in MeOH before used.

VI. Experimental method

1. Extraction and isolation

Dried *Atractylodes* rhizome powder (104 g) was extracted with CHCl₃-MeOH (2:1) and concentrated under reduced pressure to yield a brown oily material (2.49 g). Activity guided isolation was carried out step by step. The extract was applied to a silica gel column (i.d. 4.5 × 17 cm, Silica gel 60, 70–230 mm; Merck, Darmstadt, Germany) previously equilibrated with CHCl₃, and the extract was eluted stepwise with CHCl₃-MeOH solutions (500 mL each; 100:0, 100:1, 100:2, 100:3, 100:4, 100:5, 100:10, 100:50, and 100:100). Four fractions were collected from each eluent. The fourth fraction of 100:1 (17.4 mg) was collected as an active fraction and was concentrated to give brown oily materials. The material from the fourth fraction of 100:1 was purified with preparative high-performance liquid chromatography (HPLC) (column, PEGASIL ODS (i.d. 2.0 × 250 mm); solvent, 57% CH₃CN isocratic; detection, UV at 210 nm; flow rate, 6 mL min⁻¹). Under the conditions, the three active fractions were eluted as peaks with retention times of 29, 48, and 51 min, respectively. Each fraction of peaks was collected, and concentrated *in vacuo* to dryness to yield **1** (3.21 mg), **2** (2.48 mg), a mixture (1.30 mg) of **3** and **4** all as pale-yellow oils.

2. Cell culture method

The cells cultured in a 100 mm Petri dish for 2 days using 10 mL of cell culture medium were washed with 10 mL of PBS (-), added with 1 mL of 0.0625% trypsin / EDTA • 4Na solution, and incubated at 37 ° C in 5.0% CO₂ incubator for 5 minutes. The detached cells were added with 9 mL of fresh medium and collected into a 50 mL centrifuge tube then centrifuged at 1000 rpm for 5 minutes at 4°C. After removing the supernatant, the pellet was then resuspended in 10 mL of cell culture medium and the number of cells were calculated. 250 µL (1.25 × 10⁵ cells) of this cell suspension were plated on a 48-well plate and incubated at 37°C in 5.0% CO₂ incubator for 12 hours or more for assay.

3. Assay for SOAT activity in CHO-K1 cells, hSOAT1- and SOAT2-CHO cells

Cell-based assays for CE, triacylglycerol (TG), and phospholipid (PL) synthesis using CHO-K1 cells and hSOAT1- or hSOAT2-CHO cells were carried out using established methods [124-127]. Cells (1.25×10^5 cells per 250 μ L) were cultured in one well of a 48-well plastic microplate in the culture medium described above and allowed to recover at 37°C overnight in 5% CO₂ with cells that were at least 80% confluent. A sample (2.5 μ L in MeOH) and [¹⁴C]oleic acid (1 nmol, 1.85 kBq, 5.0 μ L in 10% ethanol/PBS solution) were then added to each well of the cell culture. The cells were cultured at 37°C for 6 h in 5% CO₂. Cells in each well were then washed twice with PBS. The cells were lysed by adding 0.25 mL of 10 mM Tris-HCl (pH 7.5) containing 0.1% (w/v) SDS, and the cellular lipids were extracted by the method of Bligh and Dyer[128]. The total lipids were separated on a TLC plate (silica gel F254, 0.5-mm thick, Merck) and the TLC plate was analyzed with a FLA-7000 analyzer (Fuji Film, Tokyo, Japan) to measure the amount of [¹⁴C] lipids. Lipid synthesis activity (%) was defined as ($[\text{¹⁴C}] \text{lipid-drug} / [\text{¹⁴C}] \text{lipid-control}$) x 100. The IC₅₀ value was defined as the drug concentration that causes 50% inhibition of lipid synthesis. Selectivity index was calculated by using this formulation, SI (selectivity index) = log (IC₅₀ for SOAT1)/(IC₅₀ for SOAT2). SOAT2 selective inhibition was defined as $+1.0 \leq \text{SI}$, dual-type inhibition as $-1.0 < \text{SI} < +1.0$ and $\text{SI} \leq -1.0$ means SOAT1-selective inhibition.

4. Preparation of an enzyme source from microsomes prepared from CHO-K1 and hSOAT1-/hSOAT2-CHO cells using a Potter-type homogenizer.

An enzyme source derived from CHO-K1 and hSOAT1-/hSOAT2-CHO cells using a Potter-type homogenizer was prepared using our established method[124-127]. Briefly, CHO-K1 and hSOAT1-/hSOAT2-CHO cells (2.0×10^8 cells) were homogenized in 5 mL cold Buffer A in the Potter-type homogenizer. The microsomal fraction was pelleted by centrifugation at 100,000 g at 4°C for 60 min (TLA110, Beckman Coulter), resuspended in the same buffer at a concentration of 5 mg protein mL⁻¹, and stored at -80°C until used.

5. Enzyme-based assay for CE synthesis microsomes prepared from CHO-K1 and hSOAT1- or hSOAT2-CHO cells.

Enzyme-based assays for CE synthesis using microsomes prepared from CHO-K1 and hSOAT1- or hSOAT2-CHO cells were carried out using established methods[124-127].

SOAT activities were measured using fractionation prepared as described above as an enzyme source. Briefly, an assay mixture was made containing 300 μ M BSA (fatty acid free) and [1- 14 C]oleoyl-CoA (20 μ M, 3.7 kBq). A test sample (1-200 μ M in MeOH solution) and microsomes of CHO-K1 cells or hSOAT1-/hSOAT2-CHO cells in a total volume of 200 μ L Buffer A was incubated at 37°C. The SOAT reaction was started by adding [1- 14 C]oleoyl-CoA. After a 5-min incubation, the reaction was stopped by adding 1.2 mL of 2:1 CHCl₃:MeOH. The product [14 C]CE was extracted using the method of Bligh and Dyer[128]. After the organic solvent was removed by evaporation, lipids were separated on a TLC plate and the radioactivity of [14 C]CE was measured by our established method[125].

Chapter II Terpendole congeners from *Volutella citrinella* BF-0440

I . Reagents

Chloroform (CHCl_3) (first grade), methanol (MeOH) (first grade) and diethyl ether (special grade) were purchased from Nacalai Tesque. Inc.

Acetic acid (CH_3COOH) (special grade), hexane (special grade), potassium chloride (KCl) (special grade) and hydrochloric acid (HCl) (special grade) were purchased from Kanto Chemical Co., Ltd.

Sodium chloride (NaCl) (special grade), sodium hydrogen phosphate (Na_2HPO_4) (special grade), potassium dihydrogen phosphate (KH_2PO_4) (special grade), ethylenediamine tetra acetic acid tetrasodium salt ($\text{EDTA} \cdot 4\text{Na}$) (special grade), 2-amino-2-hydroxymethyl-1,3-propanediol (Tris) (for biochemistry), sodium dodecyl sulfate (SDS) (for biochemistry), magnesium sulfate heptahydrate ($\text{MgSO}_4 \cdot 7\text{H}_2\text{O}$) (special grade), magnesium phosphate octahydrate ($\text{Mg}_3(\text{PO}_4) \cdot 8\text{H}_2\text{O}$) (special grade) and dibasic potassium phosphate (K_2HPO_4) (special grade) were purchased from Wako Pure Chemical Industries, Ltd.

Ethanol (EtOH) (special grade) was purchased from Japan Alcohol Sales Association.

Penicillin ($10000 \text{ units mL}^{-1}$) / streptomycin (10000 mg mL^{-1}) (P/S) solution, 2.5% trypsin solution and MEM vitamin solution were purchased from Thermo Fisher Scientific.

G-418 sulfate (geneticin) was purchased from Merck.

HAM's F12 medium was purchased from Nacalai Tesque, Inc.

Fetal bovine serum (FBS) was purchased from Biowest and used after heat treatment (inactivation) at 56°C for 30 minutes.

Radiolabeled [^{14}C]oleic acid ($9.25 \text{ MBq per } 2.5 \text{ mL}$) and [$1\text{-}^{14}\text{C}$]Oleoyl Coenzyme A ($1.85 \text{ GBq mmol}^{-1}$) were purchased from PerkinElmer and diluted 10-fold with PBS (-).

Polypepton was purchased from Nippon Pharmaceutical Co., Ltd.

Glucose (special grade) was purchased from Kanto Chemical Co., Ltd.

PDA, yeast extract, agar and PDB were purchased from Becton & Dickinson (BD).

Brown rice was purchased from Kakashi rice grain.

II. Material

100 mm petri dish, 50 mL centrifuge tube and 48-well plate were purchased from

Corning.

TLC plate (70F₂₅₄, thickness 0.25 mm) was purchased from Wako Pure Chemical Industries, Ltd.

0.20 µm syringe filter was purchased from Sartorius.

ODS (12 nm, S-150 µM) for liquid chromatography was purchased from YMC Gel.

III. Instruments

Refrigerated centrifuge by KUBOTA 2700 (Kubota Corporation).

Micro-refrigerated centrifuge by AX-511 (TOMY®).

Centrifugal evaporator by CVE-200D (EYELA®).

Image analyzer by FLA-7000 (GE Healthcare®).

UFLC by Prominence UFLC system packed with pack XR-ODS column (φ 2.0 x 75 mm).

TB-5ORVS of Takasaki Scientific Machinery Co., Ltd. was used as a shaking culture machine.

Kokusan H-700R was used as a refrigerator incubator.

LAQUA twin S010 of Horiba, Ltd. was used as a pH meter.

NMR system 400 MHz spectrometer from Agilent Technologies and 600 MHz spectrometer from Bruker® were used for NMR analyses.

LC-MS analyses were performed using AccuTOF LC-plus JMS-T100LP system from JEOL and analytical column Capcellcore C18 (i.d. 2.1 × 50 mm) by Osaka soda.

FT/IR-460 from JASCO Corporation was used for IR spectrum measurement.

UV spectrometer U-2800 from Hitachi High-Tech Science Co., Ltd. was used for UV spectrum measurement.

The following HPLC unit from Hitachi High-Tech Science was used for high performance liquid chromatography. L-2130 was used as a pump, L-2400 as a detector, SSC-3225 from Senshu Scientific Co., Ltd. as a degasser and D-2500 as a recorder.

Another HPLC unit from SHIMADZU Corp. was used for high performance liquid chromatography. LC-20AT was used as a pump, SPD-20A as a detector, DGU-20A5 as a degasser and D-2500 from Hitachi High-Tech Science as a recorder.

The preparative column used was PEGASIL ODS SP100 (i.d. 20 × 250 mm) by Senshu Science and Develosil C30 (i.d. 20 × 250 mm) by Nomura Chemical Co., Ltd.

Centrifuge KUBOTA 3500 from Kubota Corporation was used as centrifuge.

IV. Cell

CHO cells (hSOAT1-CHO and hSOAT2-CHO cells) that selectively expressed human SOAT1 and SOAT2 were kindly gifted from Professor L. L. Rudel of Wake Forest University.

For the reagents, materials, instruments and cells common to the experimental section of Chapter 1, those described in Chapter 1 were used.

V. Reagent preparation

1. Cell culture medium

Prepared according to Chapter I reagent preparation V.1.

2. PBS (-) solution

Prepared according to Chapter I reagent preparation V.2.

3. 0.0625% trypsin/EDTA • 4Na solution

Prepared according to Chapter I reagent preparation V.3.

4. 1.0 M Tris/HCl (pH 7.5) solution

Prepared according to Chapter I reagent preparation V.4.

5. 0.10% SDS-Tris solution

Prepared according to Chapter I reagent preparation V.5.

6. Sample solution

Compounds **5–15** were obtained by culturing and isolation from the producing fungi. The compounds were dissolved in MeOH before used.

VI. Experimental method

1. Fungal BF-0440 strain identification

Fungal strain BF-0440 was isolated from soil collected from Shizuoka-shi, Shizoka, Japan, and was identified as *Volutella citrinella* by TechnoSuruga Laboratory Co., Ltd.

(Shizuoka, Japan) by homology search of the gene based from 28S rDNA-D1/D2 nucleotide sequence, internal transcribed spacer (ITS)-5.8S rDNA and morphological observation.

2. *V. citrinella* BF-0440 strain fermentation and isolation method

A loop-full of strain was inoculated and then cultured with shaking for 3 days at 27°C in 100 mL of seed medium (2.0% glucose, 0.20% yeast extract, 0.050% $\text{MgSO}_4 \cdot 7\text{H}_2\text{O}$, 0.50% polypeptone, 0.10% KH_2PO_4 and 0.10% agar; pH 6.0) in a 500 mL Erlenmeyer flask to obtain a seed culture. The seed culture (10 mL) was inoculated into a 1000 mL culture box containing 50 g of production medium (50 g of brown rice, 5 mL of the following solution; 2.4% PDB, 0.50% $\text{MgSO}_4 \cdot 7\text{H}_2\text{O}$, 0.50% K_2HPO_4 and 0.50% $\text{Mg}_3(\text{PO}_4)_2 \cdot 8\text{H}_2\text{O}$). Fermentation was carried out at 27 °C for 14 days in static conditions.

Culture broth was extracted with 70% EtOH (2.5 L). After concentration to remove EtOH, the aqueous solution was extracted with EtOAc (900 mL). The organic layer was collected and EtOAc was evaporated to give crude extract (brown material, 2.5 g). This crude extract was applied to an ODS column (114 g, i.d. 45 × 200 mm) and eluted stepwise with 40% $\text{CH}_3\text{CN}/\text{H}_2\text{O}$, 60% $\text{CH}_3\text{CN}/\text{H}_2\text{O}$, 80% $\text{CH}_3\text{CN}/\text{H}_2\text{O}$, and 100% $\text{CH}_3\text{CN}/\text{H}_2\text{O}$ solutions (600 mL each, fractionated into two). All fractions were concentrated *in vacuo* and the remaining water layers were extracted with EtOAc. The EtOAc layers of these fractions were collected and evaporated to dryness. Voluhemins A (4) and B (5) were purified from fraction 80%-1. Fraction 60%-2 (brown material, 249 mg) was subjected to preparative high-performance liquid chromatography (HPLC; column, Pegasil ODS SP100 (i.d. 20 × 250 mm); mobile phase, 60% $\text{CH}_3\text{CN}/\text{H}_2\text{O}$ isocratic; flow rate, 6.0 mL min⁻¹; detection, UV at 210 nm). In these conditions, NK12838 (6) and terpendole N (1) were eluted as peaks with retention times of 27 and 29 min, respectively. Purification from fraction 80%-2 (brown material, 214 mg) by preparative HPLC (column, Pegasil ODS SP100 (i.d. 20 × 250 mm); mobile phase, 78% $\text{CH}_3\text{CN}/\text{H}_2\text{O}$ isocratic; flow rate, 6.0 mL min⁻¹; detection, UV at 210 nm) allowed isolation of three peaks, terpendole O (2) eluted at 23 min, terpendole C (7) at 24 min, and a third peak at 26 min. The third peak was, however, found to be a mixture of related compounds from proton NMR analyses. This mixture was also obtained from fraction 100%-1 along with terpendoles C (7), D (8), and L (9), and tolypocladin A (10). By preparative HPLC (column, Pegasil ODS SP100 (i.d. 20 × 250 mm); mobile phase, 35-

min linear gradient 90–95% CH₃CN/H₂O; flow rate, 6.0 mL min⁻¹; detection, UV at 210 nm), **10**, **7**, the mixture, **8**, and **9** were eluted at 16, 18, 22, 31, and 35 min, respectively. The mixture was finally separated in different HPLC conditions (column, Develosil C30 (i.d. 20 × 250 mm); mobile phase, 92% CH₃CN/H₂O isocratic; flow rate, 6.0 mL min⁻¹; detection, UV at 210 nm) to yield a new terpendole P (**3**) and a known terpendole J (**11**) eluted as peaks at 22 and 23 min, respectively. All of these peaks were collected and concentrated to dryness to give **1** (2.1 mg), **2** (21.6 mg), **3** (2.7 mg), **6** (46.6 mg), **7** (29.7 mg and 15.7 mg from 80%-2 and 100%-1, respectively), **8** (8.3 mg), **9** (6.8 mg), **10** (3.8 mg) and **11** (1.6 mg) as white powders.

3. Physicochemical properties measurement

Specific rotation was measured using MeOH at concentration of 1.0 mg mL⁻¹. Compounds **5** and **7** were measured at 25°C and **6** was measured at 23°C.

UV absorption were measured using MeOH at concentration of 0.050 mg mL⁻¹ for compounds **5** and **6**, and 0.030 mg mL⁻¹ for **7**.

IR spectrum were measuby thin film method using KBr as the plate material.

For NMR measurement, DMSO-*d*₆ (¹H; 2.48 ppm, ¹³C; 39.5 ppm) and CDCl₃ (¹H; 7.26 ppm, ¹³C; 77.0 ppm) were used as an internal standard, chemical shifts were expressed in δ (ppm) and coupling patterns were abbreviated as follows. S: singlet, d: doublet, dd: doublet doublet, dt: doublet triplet, br: broad, m: multiplet

4. Cell culture method

Performed according to Chapter I Experimental method VI.2.

5. Assay for SOAT activity in hSOAT1- and SOAT2-CHO cells

Performed according to Chapter I Experimental method VI.3.

Chapter III Screening for the neutral lipid degradation potentiators

I . Reagents

Chloroform (CHCl_3) (first grade), methanol (MeOH) (first grade) and diethyl ether (special grade) were purchased from Nacalai Tesque. Inc.

Acetic acid (CH_3COOH) (special grade), hexane (special grade), potassium chloride (KCl) (special grade), hydrochloric acid (HCl) (special grade), calcium carbonate (CaCO_3) (special grade) and potassium bromide (KBr) (special grade) were purchased from Kanto Chemical Co., Ltd.

Sodium chloride (NaCl) (special grade), sodium hydrogen phosphate (Na_2HPO_4) (special grade), potassium dihydrogen phosphate (KH_2PO_4) (special grade), ethylenediamine tetra acetic acid tetrasodium salt ($\text{EDTA} \cdot 4\text{Na}$) (special grade), 2-amino-2-hydroxymethyl-1,3-propanediol (Tris) (for biochemistry), sodium dodecyl sulfate (SDS) (for biochemistry), magnesium sulfate heptahydrate ($\text{MgSO}_4 \cdot 7\text{H}_2\text{O}$) (special grade), magnesium phosphate octahydrate ($\text{Mg}_3(\text{PO}_4)_3 \cdot 8\text{H}_2\text{O}$) (special grade), dibasic potassium phosphate (K_2HPO_4) (special grade), cobalt(II) chlorate dihydrate ($\text{CoCl}_2 \cdot 2\text{H}_2\text{O}$) (special grade), copper sulfate pentahydrate ($\text{CuSO}_4 \cdot 5\text{H}_2\text{O}$) (special grade), iron(III) sulfate n-hydrate ($\text{Fe}_2(\text{SO}_4)_3 \cdot n\text{H}_2\text{O}$) (special grade), glucose (special grade), magnesium chloride tetrahydrate ($\text{MgCl}_2 \cdot 4\text{H}_2\text{O}$) (special grade), polypeptone, soluble starch, sucrose, zinc sulfate heptahydrate ($\text{ZnSO}_4 \cdot 7\text{H}_2\text{O}$) (special grade), bovine serum albumin (BSA) (fatty acid free) and penicillin (10000 units mL^{-1}) / streptomycin (10000 mg mL^{-1}) (P/S) solution were purchased from Wako Pure Chemical Industries, Ltd.

Ethanol (EtOH) (special grade) was purchased from Japan Alcohol Sales Association. 2.5% trypsin solution was purchased from Thermo Fisher Scientific.

HAM's F12 medium was purchased from Nacalai Tesque, Inc.

Fetal bovine serum (FBS) was purchased from Capricorn Scientific and used after heat treatment (inactivation) at 56°C for 30 minutes.

Radiolabeled [^{14}C]oleic acid (9.25 MBq per 2.5 mL) and [$1\text{-}^{14}\text{C}$]Oleoyl Coenzyme A (1.85 GBq mmol^{-1}) were purchased from PerkinElmer and diluted 10-fold with PBS (-).

Peptone was purchased from Life Technologies Corporation.

Ehrlich meat extract was purchased from Pharmaceutical Industrial.

Agar was purchased from Shimizu Food.

Solulys was purchased from Oriental Yeast.

Yeast extract was purchased from Becton Dickinson.

II. Material

100 mm petri dish, 50 mL centrifuge tube and 48-well plate were purchased from Corning.

TLC plate (70F₂₅₄, thickness 0.25 mm) was purchased from Wako Pure Chemical Industries, Ltd.

0.20 µm syringe filter was purchased from Sartorius.

ODS (12 nm, S-150 µM) for liquid chromatography was purchased from Fuji Silysia Chemical Ltd.

III. Instruments

Refrigerated centrifuge by KUBOTA 2700 (Kubota Corporation).

Micro-refrigerated centrifuge by AX-511 (TOMY®).

Centrifugal evaporator by CVE-200D (EYELA®).

Image analyzer by FLA-7000 (GE Healthcare®).

UFLC by Prominence UFLC system packed with pack XR-ODS column (i.d. 2.0 × 75 mm).

TB-5ORVS of Takasaki Scientific Machinery Co., Ltd. was used as a shaking culture machine.

Kokusan H-700R was used as a refrigerator incubator.

LAQUA twin S010 of Horiba, Ltd. was used as a pH meter.

NMR system 400 MHz spectrometer from Agilent Technologies and 600 MHz spectrometer from Bruker® were used for NMR analyses.

LC-MS analyses were performed using AccuTOF LC-plus JMS-T100LP system from JEOL and analytical column Capcellcore C18 (i.d. 2.1 × 50 mm) by Osaka soda.

The following HPLC unit from Hitachi High-Tech Science was used for high performance liquid chromatography. L-2130 was used as a pump, L-2400 as a detector, SSC-3225 from Senshu Scientific Co., Ltd. as a degasser and D-2500 as a recorder.

Another HPLC unit from SHIMADZU Corp. was used for high performance liquid chromatography. LC-20AT was used as a pump, SPD-20A as a detector, DGU-20A5 as a degasser and D-2500 from Hitachi High-Tech Science as a recorder.

The preparative column used was Capcell pak C18 (i.d. 4.6 × 250 mm) by Osaka Soda

Co., Ltd., and Develosil C30 (i.d. 20 × 250 mm) by Nomura Chemical Co., Ltd.

Centrifuge KUBOTA 3500 from Kubota Corporation was used as centrifuge.

OptiSeal manufactured by Beckman Coulter manufactured by Hitachi Koki Co., Ltd. was used as ultracentrifugation tubes.

IV. Cell

CHO-K1 cells were provided by Dr. Kentaro Hanada, National Institute of Infectious Diseases.

For the reagents, materials, instruments and cells common to the experimental section of Chapter 1, those described in Chapter 1 were used.

V. Reagent preparation

1. Cell culture medium

Prepared according to Chapter I reagent preparation V.1.

2. PBS (-) solution

Prepared according to Chapter I reagent preparation V.2.

3. 0.0625% trypsin/EDTA • 4Na solution

Prepared according to Chapter I reagent preparation V.3.

4. 1.0 M Tris/HCl (pH 7.5) solution

Prepared according to Chapter I reagent preparation V.4.

5. 0.10% SDS-Tris solution

Prepared according to Chapter I reagent preparation V.5.

6. Buffer A

Dissolve 17.12 g of sucrose, 1.87 g of KCl, 2.72 g of KH₂PO₄, and 6.78 g of EDTA • 4Na in milli Q water. A total volume of 500 mL was autoclaved at 121°C for 15 minutes (Fin. 100 mM sucrose, 50 mM KCl, 40 mM KH₂PO₄, 30 mM EDTA).

6. Buffer B

Dissolve 8.766 g of NaCl and 50 mL of 1.0 M Tris/HCl (pH 7.4) solution in milli Q water. A total volume of 1000 mL was autoclaved at 121°C for 15 minutes (Fin. 150 mM NaCl, 50 mM Tris-HCl, pH 7.4).

6. Buffer C

Dissolve 2.0 mg mL⁻¹ of BSA (fatty acid free) in buffer B.

6. Sample solution

Brefeldin A, beauveriolides I and III, and dinapinones (A1, A2, and DPA) were available from our compound library [40, 107, 108]. Other beauveriolides A, B, and K and hygrolidins were isolated from our culture broths. The compounds were dissolved in MeOH before used.

VI. Experimental method

1. Purification of active compounds from culture broth

Beauveriolides (**19–21**): Fungal BF-0452 strain was seeded in medium containing 2.0% glucose, 0.2% yeast extract, 0.5% polypeptone, 0.1% KH₂PO₄, 0.05% MgSO₄ · 7H₂O, 0.1% agar, and tap water, pH 6.0 for 3 days at 27°C in a rotary shaker. The seed culture was then inoculated into production medium containing 2.0% sucrose, 1.0% glucose, 0.5% solulys, 0.5% Ehrlich meat extract, 0.1% KH₂PO₄, 0.3% CaCO₃, 0.05% Mg₃(PO₄)₂ · 8H₂O, 0.1% agar, 1.0% trace metal solution (1 mg mL⁻¹ of each FeSO₄ · 7H₂O, MgCl₂ · 4H₂O, ZnSO₄ · 7H₂O, CuSO₄ · 5H₂O, and CoCl₂ · 2H₂O in water), and tap water, pH 6.0. Fermentation was performed at 27°C for 14 days under static condition. The culture broth (1.8 L) was extracted with ethanol (1.8 L). Ethanol extracts were concentrated to remove ethanol, and the aqueous solution was extracted with ethyl acetate (3.6 L), yielding crude materials (227 mg). The extracts were then dissolved in a small volume of methanol, applied to an ODS column (11 g, i.d. 15 × 150 mm, 100-200 mesh, Fuji Silysia Chemical Ltd., Aichi, Japan) and eluted stepwise with 40%, 60%, 80%, and 100% CH₃CN/H₂O solvents (2 fractions per 150 mL each). The 80%-2 CH₃CN/H₂O eluents containing active materials were evaporated *in vacuo* to yield brownish materials (18 mg). The materials were purified by high performance liquid chromatography (HPLC) under the following conditions: column, Develosil C30 UG5 (Nomura Chemical

Co., Ltd., Aichi, Japan) (i.d. 20×250 mm); eluent, 90% CH₃CN/H₂O; flow, 6.0 mL min⁻¹; detection, UV at 210 nm. Compounds **19–21** were eluted as a peak with retention times of 16.8 min, 18.8 min, and 18.1 min, respectively. Each peak fraction was collected and concentrated to yield **19** (0.6 mg), **20** (3.2 mg), and **21** (1.1 mg) as white powders.

Hygrolidins (22–23): Actinomycete KM68-21 strain was grown in medium containing 1.0% soluble starch, 0.4% yeast extract, 0.2% peptone, and tap water, pH unadjusted at 27°C for 7 days in a rotary shaker. The culture was inoculated into new medium with additional 0.1% CaCO₃, 0.004% Fe₂(SO₄)₃·nH₂O and 0.01% KBr at 27°C for 7 days in a rotary shaker. Culture broth (3 L) was centrifuged (3,000 rpm, 10 min) and the mycelia was collected and then extracted with 70% EtOH (3 L). EtOH extracts were filtered to remove mycelia and then concentrated to remove ethanol. The remaining aqueous solution was extracted with ethyl acetate (1.8 L). The organic layer was collected and dried under pressure to produce a brownish crude extract (388 mg). This crude extract was dissolved in a small amount of MeOH, applied to an ODS column (17.5 g, i.d. 30×130 mm, 100-200 mesh, Fuji Silysia Chemical Ltd.), and eluted stepwise with 0%, 20%, 40%, 60%, 80%, and 100% CH₃CN/H₂O solvents (120 mL each). The 80% and 100% CH₃CN/H₂O eluents containing active materials were evaporated *in vacuo* to yield pale brown materials (38 mg and 44 mg, respectively). The materials from the 80% fraction were subjected to HPLC under the following conditions: column, Capcell pak C18 (Osaka Soda Co., Ltd., Osaka, Japan) (i.d. 4.6×250 mm); eluent, 20 minutes linear gradient from 75%-95% CH₃CN/H₂O; flow, 1.0 mL min⁻¹; detection, UV at 210 nm. Compounds **22** and **23** were eluted as a peak with retention times of 10.0 min and 16.4 min, respectively. Each peak fraction was collected and concentrated to yield **22** (6.3 mg) and **23** (2.0 mg) as white powders. The 100% fraction was subjected to HPLC (column, Capcell pak C18 (i.d. 4.6×250 mm); eluent, 88% CH₃CN/H₂O; flow, 1.0 mL min⁻¹; detection, UV at 210 nm). Under these HPLC conditions, **23** was eluted as a peak with retention time of 10.0 min, collected, and concentrated to yield **23** (4.6 mg) as a white powder.

2. Cell culture method

Performed according to Chapter I Experimental method VI.2.

3. Assay of neutral lipid degradation in CHO-K1 cells

Assays for CE and TG degradation using CHO-K1 cells were performed according to

established methods with some modifications [82]. Cells (1.25×10^5 cells) were seeded in a 48-well plastic microplate in 250 μ L of maintained medium and allowed to recover overnight in 37°C and 5.0% CO₂; 5.0 μ L of [¹⁴C]oleic acid (1 nmol, 1.85 kBq in 10% ethanol/ phosphate-buffered saline (PBS) solution) was then added to each well of the cell culture. The cells were incubated for 24 hours at 37°C and 5.0% CO₂ to allow for accumulation of [¹⁴C]TG and [¹⁴C]CE within the cells. Medium were then removed and cells were washed twice with 250 μ L of Buffer C (150 mM NaCl and 50 mM Tris-HCl, pH 7.4) containing 2.0 mg/mL BSA (fatty acid free) and then washed once with 250 μ L of Buffer B (Buffer C without BSA) to remove the remaining [¹⁴C]oleic acid. Fresh medium (250 μ L) was then added along with 2.5 μ L of sample and control (in MeOH). After 12-hour incubation in 37°C and 5.0% CO₂, cells were washed twice with 250 μ L of PBS. The cells were then lysed using 250 μ L of 10 mM Tris-HCl (pH 7.5) containing 0.1% (w/v) SDS, and neutral lipids were extracted following the method of Bligh and Dyer [128]. [¹⁴C]TG and [¹⁴C]CE were separated on a TLC plate (silica gel F254, 0.5-mm thick, Merck KGaA, Darmstadt, Germany) and then analyzed with a bioimaging analyzer (FLA7000; Fujifilm, Tokyo, Japan). Neutral lipid degradation activity (%) was defined as ($[\text{¹⁴C]TG or [¹⁴C]CE of sample} / [\text{¹⁴C]TG or [¹⁴C]CE of control}) \times 100$. The EC₅₀ value was defined as the sample concentration causing 50% degradation of neutral lipids (TG or CE).

4. Assay for neutral lipid synthesis in CHO-K1 cells

Performed according to Chapter I Experimental method VI.3.

5. Preparation of an enzyme source from microsomes prepared from CHO-K1 cells using a Potter-type homogenizer.

Performed according to Chapter I Experimental method VI.4.

6. Enzyme-based assay for CE synthesis from microsomes prepared from CHO-K1 cells.

Performed according to Chapter I Experimental method VI.5.

V. Acknowledgment

I would like to express my deep and sincere gratitude to my mentor, Professor Hiroshi Tomoda and Professor Taichi Ohshiro of Microbial Chemistry Laboratory, Graduate School of Pharmaceutical Sciences, Kitasato University, for giving me the opportunity and providing me invaluable guidance and encouragement throughout my time in Japan. I also would like to thank assistant professor Dr. Keisuke Kobayashi and Lecturer Dr. Satoshi Ohte of Microbial Chemistry Laboratory, Graduate School of Pharmaceutical Sciences, Kitasato University, for their generous guidance in my study.

I would like to thanks Mrs. Noriko Sato, Dr. Kenichiro Nagai, and Ms. Reiko Seki of Kitasato University for thoughtful advises and various NMR and mass spectrometry measurement. Prof. L. L. Rudel (Wake Forest Univ.,USA) for providing the cells and Technosuruga Lab, Inc. for conducting mycological study. Professor Hirokazu Kawagishi and Dr. Jing Wu from Shizuoka University, Professor Chiaki Imada from Tokyo University of Marine Science and Technology and Professor Kentaro Hanada from National Institute of Infection Disease for their contribution in this study. Professor Fumiaki Hayashi and Dr. Huiping Zhang from RIKEN for NMR measurement. Dr. Tadashi Yasuhara, specially appointed researcher, Mr. Kanji Hosoda, and Mr. Satoru Shigeno of Microbial Chemistry Laboratory, Graduate School of Pharmaceutical Sciences, Kitasato University, for all the support during my study in the lab. I would like to thank all graduate students and undergraduate students of Microbial Chemistry Laboratory, Graduate School of Pharmaceutical Sciences, Kitasato University. Ms. Haruka Morita and Ms. Ai Amagai, School of Pharmacy, Kitasato University for their contribution in this research. I am thankful to and fortunate enough to get financial support from Ministry of Education, Culture, Sports, Science and Technology (MEXT) Japan as one of their scholarship awardees. Finally, I heartily thank my family for all the pray and support throughout everything.

February, 6th 2023

Elyza Aiman Azizah Nur

VI. References

- 1 Hanson JR. In: Abel EW (ed). *Natural Products: The Secondary Metabolites*, vol. 17. The Royal Society of Chemistry, 2003.
- 2 Dias DA, Urban S, Roessner U. A historical overview of natural products in drug discovery. *Metabolites* 2012; 2: 303-336.
- 3 Alberts AW, Chen J, Kuron G, Hunt V, Huff J, Hoffman C *et al.* Mevinolin: a highly potent competitive inhibitor of hydroxymethylglutaryl-coenzyme A reductase and a cholesterol-lowering agent. *Proc Natl Acad Sci U S A* 1980; 77: 3957-3961.
- 4 Dreyfuss M, Härri E, Hofmann H, Kobel H, Pache W, Tschertter H. Cyclosporin A and C. *Eur J Appl Microbiol* 1976; 3: 125-133.
- 5 Burg RW, Miller BM, Baker EE, Birnbaum J, Currie SA, Hartman R *et al.* Avermectins, new family of potent anthelmintic agents: producing organism and fermentation. *Antimicrob Agents Chemother* 1979; 15: 361-367.
- 6 Feher M, Schmidt JM. Property Distributions: Differences between drugs, natural products, and molecules from combinatorial chemistry. *J Chem Inf Comput Sci* 2003; 43: 218-227.
- 7 Newman DJ, Cragg GM. Natural Products as Sources of New Drugs over the Nearly Four Decades from 01/1981 to 09/2019. *J Nat Prod* 2020; 83: 770-803.
- 8 Roth Gregory A, Mensah George A, Johnson Catherine O, Addolorato G, Ammirati E, Baddour Larry M *et al.* Global Burden of Cardiovascular Diseases and Risk Factors, 1990–2019. *J Am Coll Cardiol* 2020; 76: 2982-3021.
- 9 Indonesian Ministry of Health Information Center. Indonesian Health Profile 2016. Ministry of Health Republic of Indonesia (2016).
- 10 Grundy SM. Metabolic syndrome update. *Trends Cardiovasc Med* 2016; 26: 364-373.

- 11 Saklayen MG. The Global Epidemic of the Metabolic Syndrome. *Curr Hypertens Rep* 2018; 20: 12-12.
- 12 Noubiap JJ, Nansseu JR, Lontchi-Yimagou E, Nkeck JR, Nyaga UF, Ngouo AT *et al*. Global, regional, and country estimates of metabolic syndrome burden in children and adolescents in 2020: a systematic review and modelling analysis. *Lancet Child Adolesc Health* 2022; 6: 158-170.
- 13 Witztum JL, Steinberg D. Role of oxidized low density lipoprotein in atherogenesis. *J Clin Invest* 1991; 88: 1785-1792.
- 14 Ross R. The pathogenesis of atherosclerosis: a perspective for the 1990s. *Nature* 1993; 362: 801-809.
- 15 Libby P. Molecular bases of the acute coronary syndromes. *Circulation* 1995; 91: 2844-2850.
- 16 Bansal AB, Cassagnol M. HMG-CoA Reductase Inhibitors. *StatPearls*. StatPearls Publishing LLC.: Treasure Island (FL), 2022.
- 17 Schachter M. Chemical, pharmacokinetic and pharmacodynamic properties of statins: an update. *Fundam Clin Pharmacol* 2005; 19: 117-125.
- 18 Ginter E, Simko V. Statins: the drugs for the 21st century? *Bratisl Lek Listy* 2009; 110: 664-668.
- 19 Stein EA, Lane M, Laskarzewski P. Comparison of statins in hypertriglyceridemia. *Am J Cardiol* 1998; 81: 66b-69b.
- 20 Endo A, Kuroda M, Tanzawa K. Competitive inhibition of 3-hydroxy-3-methylglutaryl coenzyme A reductase by ML-236A and ML-236B fungal metabolites, having hypocholesterolemic activity. *FEBS Lett* 1976; 72: 323-326.

- 21 Libby P. The forgotten majority: unfinished business in cardiovascular risk reduction. *J Am Coll Cardiol* 2005; 46: 1225-1228.
- 22 Van Itallie TB, Hashim SA, Crampton RS, Tennent DM. The treatment of pruritus and hypercholesteremia of primary biliary cirrhosis with cholestyramine. *N Engl J Med* 1961; 265: 469-474.
- 23 Altmann SW, Davis HR, Jr., Zhu LJ, Yao X, Hoos LM, Tetzloff G *et al.* Niemann-Pick C1 Like 1 protein is critical for intestinal cholesterol absorption. *Science* 2004; 303: 1201-1204.
- 24 Kastelein JJ, Akdim F, Stroes ES, Zwinderman AH, Bots ML, Stalenhoef AF *et al.* Simvastatin with or without ezetimibe in familial hypercholesterolemia. *N Engl J Med* 2008; 358: 1431-1443.
- 25 Kastelein JJ, Bots ML. Statin therapy with ezetimibe or niacin in high-risk patients. *N Engl J Med* 2009; 361: 2180-2183.
- 26 Giugliano RP, Sabatine MS. Are PCSK9 Inhibitors the Next Breakthrough in the Cardiovascular Field? *J Am Coll Cardiol* 2015; 65: 2638-2651.
- 27 Bochem AE, Kuivenhoven JA, Stroes ES. The promise of cholesteryl ester transfer protein (CETP) inhibition in the treatment of cardiovascular disease. *Curr Pharm Des* 2013; 19: 3143-3149.
- 28 Robinson JG, Farnier M, Krempf M, Bergeron J, Luc G, Aversa M *et al.* Efficacy and safety of alirocumab in reducing lipids and cardiovascular events. *N Engl J Med* 2015; 372: 1489-1499.
- 29 Tall AR, Rader DJ. Trials and Tribulations of CETP Inhibitors. *Circ Res* 2018; 122: 106-112.

- 30 Lao KH, Zeng L, Xu Q. Endothelial and smooth muscle cell transformation in atherosclerosis. *Curr Opin Lipidol* 2015; 26: 449-456.
- 31 Chistiakov DA, Orekhov AN, Bobryshev YV. Endothelial Barrier and Its Abnormalities in Cardiovascular Disease. *Front Physiol* 2015; 6: 365-365.
- 32 Ratzliff V. Novel Pharmacotherapy Options for NASH. *Dig Dis Sci* 2016; 61: 1398-1405.
- 33 Konerman MA, Jones JC, Harrison SA. Pharmacotherapy for NASH: Current and emerging. *J Hepatol* 2018; 68: 362-375.
- 34 Katsiki N, Mikhailidis DP, Mantzoros CS. Non-alcoholic fatty liver disease and dyslipidemia: An update. *Metabolism* 2016; 65: 1109-1123.
- 35 Younossi Z, Anstee QM, Marietti M, Hardy T, Henry L, Eslam M *et al.* Global burden of NAFLD and NASH: trends, predictions, risk factors and prevention. *Nat Rev Gastroenterol Hepatol* 2018; 15: 11-20.
- 36 Kojima S, Watanabe N, Numata M, Ogawa T, Matsuzaki S. Increase in the prevalence of fatty liver in Japan over the past 12 years: analysis of clinical background. *J Gastroenterol* 2003; 38: 954-961.
- 37 Anstee QM, Targher G, Day CP. Progression of NAFLD to diabetes mellitus, cardiovascular disease or cirrhosis. *Nat Rev Gastroenterol Hepatol* 2013; 10: 330-344.
- 38 Takahashi Y, Fukusato T. Histopathology of nonalcoholic fatty liver disease/nonalcoholic steatohepatitis. *World J Gastroenterol* 2014; 20: 15539-15548.
- 39 Harrison SA. NASH, from diagnosis to treatment: Where do we stand? *Hepatology* 2015; 62: 1652-1655.

- 40 Namatame I, Tomoda H, Si S, Yamaguchi Y, Masuma R, Omura S. Beauveriolides, Specific Inhibitors of Lipid Droplet Formation in Mouse Macrophages, Produced by *Beauveria* sp. FO-6979. *J Antibiot* 1999; 52: 1-6.
- 41 Tomoda H, Namatame I, Si S, Kawaguchi K, Masuma R, Namikoshi M *et al.* Phenochalasin, inhibitors of lipid droplet formation in mouse macrophages, produced by *Phomopsis* sp. FT-0211. *J Antibiot* 1999; 52: 851-856.
- 42 Uchida R, Kim Y-P, Namatame I, Tomoda H, Ōmura S. Suspendole, a new inhibitor of lipid droplet synthesis in macrophages, produced by *Pseudobotrytis terrestris* FKA-25. *J Antibiot* 2006; 59: 93-97.
- 43 Namatame I, Tomoda H, Ishibashi S, Ōmura S. Antiatherogenic activity of fungal beauveriolides, inhibitors of lipid droplet accumulation in macrophages. *Proc Natl Acad Sci U S A* 2004; 101: 737-742.
- 44 Tomoda H, Ohyama Y, Abe T, Tabata N, Namikoshi M, Yamaguchi Y *et al.* Roselipins, inhibitors of diacylglycerol acyltransferase, produced by *Gliocladium roseum* KF-1040. *J Antibiot* 1999; 52: 689-694.
- 45 Tomoda H, Ito M, Tabata N, Masuma R, Yamaguchi Y, Omura S. Amidepsines, inhibitors of diacylglycerol acyltransferase produced by *Humicola* sp. FO-2942 I. Production, isolation and biological properties. *J Antibiot* 1995; 48: 937-941.
- 46 Omura S, TOMODA H, KIM YK, NISHIDA H. Pyripyropenes, highly potent inhibitors of acyl-CoA: cholesterol acyltransferase produced by *Aspergillus fumigatus*. *J Antibiot* 1993; 46: 1168-1169.
- 47 Tomoda H, Ōmura S. Potential therapeutics for obesity and atherosclerosis: Inhibitors of neutral lipid metabolism from microorganisms. *Pharmacol Ther* 2007; 115: 375-389.
- 48 Alegret M, Llaverias G, Silvestre JS. Acyl coenzyme A:cholesterol acyltransferase

inhibitors as hypolipidemic and antiatherosclerotic drugs. *Methods Find Exp Clin Pharmacol* 2004; 26: 563-586.

- 49 Reindel JF, Dominick MA, Bocan TM, Gough AW, McGuire EJ. Toxicologic effects of a novel acyl-CoA:cholesterol acyltransferase inhibitor in cynomolgus monkeys. *Toxicol Pathol* 1994; 22: 510-518.
- 50 Chang CC, Huh HY, Cadigan KM, Chang TY. Molecular cloning and functional expression of human acyl-coenzyme A:cholesterol acyltransferase cDNA in mutant Chinese hamster ovary cells. *J Biol Chem* 1993; 268: 20747-20755.
- 51 Anderson RA, Joyce C, Davis M, Reagan JW, Clark M, Shelness GS *et al.* Identification of a form of acyl-CoA:cholesterol acyltransferase specific to liver and intestine in nonhuman primates. *J Biol Chem* 1998; 273: 26747-26754.
- 52 Cases S, Novak S, Zheng YW, Myers HM, Lear SR, Sande E *et al.* ACAT-2, a second mammalian acyl-CoA:cholesterol acyltransferase. Its cloning, expression, and characterization. *J Biol Chem* 1998; 273: 26755-26764.
- 53 Oelkers P, Behari A, Cromley D, Billheimer JT, Sturley SL. Characterization of two human genes encoding acyl coenzyme A:cholesterol acyltransferase-related enzymes. *J Biol Chem* 1998; 273: 26765-26771.
- 54 Rudel LL, Lee RG, Cockman TL. Acyl coenzyme A: cholesterol acyltransferase types 1 and 2: structure and function in atherosclerosis. *Curr Opin Lipidol* 2001; 12: 121-127.
- 55 Chang T-Y, Chang CCY, Lin S, Yu C, Li B-L, Miyazaki A. Roles of acyl-coenzyme A : cholesterol acyltransferase-1 and -2. *Curr Opin Lipidol* 2001; 12: 289-296.
- 56 Willner EL, Tow B, Buhman KK, Wilson M, Sanan DA, Rudel LL *et al.* Deficiency of acyl CoA:cholesterol acyltransferase 2 prevents atherosclerosis in apolipoprotein E-deficient mice. *Proc Natl Acad Sci U S A* 2003; 100: 1262-1267.

- 57 Yagyu H, Kitamine T, Osuga J, Tozawa R, Chen Z, Kaji Y *et al.* Absence of ACAT-1 attenuates atherosclerosis but causes dry eye and cutaneous xanthomatosis in mice with congenital hyperlipidemia. *J Biol Chem* 2000; 275: 21324-21330.
- 58 Accad M, Smith SJ, Newland DL, Sanan DA, King LE, Jr., Linton MF *et al.* Massive xanthomatosis and altered composition of atherosclerotic lesions in hyperlipidemic mice lacking acyl CoA:cholesterol acyltransferase 1. *J Clin Invest* 2000; 105: 711-719.
- 59 Fazio S, Major AS, Swift LL, Gleaves LA, Accad M, Linton MF *et al.* Increased atherosclerosis in LDL receptor-null mice lacking ACAT1 in macrophages. *J Clin Invest* 2001; 107: 163-171.
- 60 Parini P, Pramfalk C, Ahmed O, Larsson L, Karpe F, Neville M *et al.* Soat2 depletion improves insulin sensitivity and hepatic steatosis. *Atherosclerosis* 2016; 252: e240.
- 61 Alger HM, Brown JM, Sawyer JK, Kelley KL, Shah R, Wilson MD *et al.* Inhibition of acyl-coenzyme A:cholesterol acyltransferase 2 (ACAT2) prevents dietary cholesterol-associated steatosis by enhancing hepatic triglyceride mobilization. *J Biol Chem* 2010; 285: 14267-14274.
- 62 Qian H, Zhao X, Yan R, Yao X, Gao S, Sun X *et al.* Structural basis for catalysis and substrate specificity of human ACAT1. *Nature* 2020; 581: 333-338.
- 63 Guan C, Niu Y, Chen S-C, Kang Y, Wu J-X, Nishi K *et al.* Structural insights into the inhibition mechanism of human sterol *O*-acyltransferase 1 by a competitive inhibitor. *Nat Commun* 2020; 11: 2478.
- 64 Long T, Liu Y, Li X. Molecular structures of human ACAT2 disclose mechanism for selective inhibition. *Structure* 2021; 29: 1410-1418. e1414.

- 65 Geng F, Cheng X, Wu X, Yoo JY, Cheng C, Guo JY *et al.* Inhibition of SOAT1 Suppresses Glioblastoma Growth via Blocking SREBP-1-Mediated Lipogenesis. *Clin Cancer Res* 2016; 22: 5337-5348.
- 66 El-Maouche D, Merke DP, Vogiatzi MG, Chang AY, Turcu AF, Joyal EG *et al.* A Phase 2, Multicenter Study of Nevanimibe for the Treatment of Congenital Adrenal Hyperplasia. *J Clin Endocrinol Metab* 2020; 105: 2771-2778.
- 67 Lada AT, Davis M, Kent C, Chapman J, Tomoda H, Omura S *et al.* Identification of ACAT1- and ACAT2-specific inhibitors using a novel, cell-based fluorescence assay: individual ACAT uniqueness. *J Lipid Res* 2004; 45: 378-386.
- 68 Ohshiro T, Rudel LL, Ōmura S, Tomoda H. Selectivity of microbial acyl-CoA : cholesterol acyltransferase Inhibitors toward Isozymes. *J Antibiot* 2007; 60: 43-51.
- 69 Ohshiro T, Kobayashi K, Ohba M, Matsuda D, Rudel LL, Takahashi T *et al.* Selective inhibition of sterol O-acyltransferase 1 isozyme by beauveriolide III in intact cells. *Sci Rep* 2017; 7: 4163.
- 70 Tomoda H, Huang X-H, Nishida H, Masuma R, Kim YK, Omura S. Glisoprenins, New Inhibitors of Acyl-CoA: Cholesterol Acyltransferase Produced by Gliocladium sp. FO-1513 I. Production, Isolation and Physico-Chemical and Biological Properties. *J Antibiot* 1992; 45: 1202-1206.
- 71 Kobayashi K, Tsukasaki N, Uchida R, Yamaguchi Y, Tomoda H. Clonoamide, a new inhibitor of sterol O-acyltransferase, produced by Clonostachys sp. BF-0131. *J Antibiot* 2015; 68: 615-619.
- 72 Kobayashi K, Fukuda T, Terahara T, Harunari E, Imada C, Tomoda H. Diketopiperazines, inhibitors of sterol O-acyltransferase, produced by a marine-derived Nocardiosis sp. KM2-16. *J Antibiot* 2015; 68: 638-641.
- 73 Uchida R, Nakajyo K, Kobayashi K, Ohshiro T, Terahara T, Imada C *et al.* 7-

Chlorofolipastatin, an inhibitor of sterol O-acyltransferase, produced by marine-derived *Aspergillus ungui* NKH-007. *J Antibiot* 2016; 69: 647-651.

- 74 Tomoda H, Nishida H, Masuma R, Cao J, Okuda S, Omura S. Purpactins, new inhibitors of acyl-CoA: Cholesterol acyltransferase produced by *Penicillium purpurogenum* I. Production, isolation and physico-chemical and biological properties. *J Antibiot* 1991; 44: 136-143.
- 75 Huang X-H, Tomoda H, Nisnida H, Masuma R, Omura S. Terpendoles, Novel ACAT Inhibitors Produced by *Albophoma yamanashiensis* I. Production, Isolation and Biological Properties. *J Antibiot* 1995; 48: 1-4.
- 76 Koyama N, Nagahiro T, Yamaguchi Y, Ohshiro T, Masuma R, Tomoda H *et al.* Spyridone, a novel inhibitor of lipid droplet accumulation in mouse macrophages produced by *Phoma* sp. FKI-1840. *J Antibiot* 2005; 58: 338-345.
- 77 Fukuda T, Arai M, Yamaguchi Y, Masuma R, Tomoda H, Omura S. New Beauvericins, Potentiators of Antifungal Miconazole Activity, Produced by *Beauveria* sp. FKI-1366 I. Taxonomy, Fermentation, Isolation and Biological Properties. *J Antibiot* 2004; 57: 110-116.
- 78 Long T, Sun Y, Hassan A, Qi X, Li X. Structure of nevanimibe-bound tetrameric human ACAT1. *Nature* 2020; 581: 339-343.
- 79 Ohte S, Matsuda D, Uchida R, Nonaka K, Masuma R, Ōmura S *et al.* Dinapinones, novel inhibitors of triacylglycerol synthesis in mammalian cells, produced by *Penicillium pinophilum* FKI-3864. *J Antibiot* 2011; 64: 489-494.
- 80 Uchida R, Ohte S, Kawamoto K, Yamazaki H, Kawaguchi M, Tomoda H. Structures and absolute stereochemistry of dinapinones A1 and A2, inhibitors of triacylglycerol synthesis, produced by *penicillium pinophilum* FKI-3864. *J Antibiot* 2012; 65: 419-425.

- 81 Kawaguchi M, Uchida R, Ohte S, Miyachi N, Kobayashi K, Sato N *et al.* New dinapinone derivatives, potent inhibitors of triacylglycerol synthesis in mammalian cells, produced by *Talaromyces pinophilus* FKI-3864. *J Antibiot* 2013; 66: 179-189.
- 82 Kobayashi K, Ohte S, Ohshiro T, Ugaki N, Tomoda H. A mixture of atropisomers enhances neutral lipid degradation in mammalian cells with autophagy induction. *Sci Rep* 2018; 8: 1-11.
- 83 (ed.) OT. Encyclopedia of Natural Medicine *Hirokawa Publishing Co, Tokyo* 1986: 354.
- 84 Wang KT, Chen LG, Wu CH, Chang CC, Wang CC. Gastroprotective activity of atractylenolide III from *Atractylodes ovata* on ethanol-induced gastric ulcer in vitro and in vivo. *J Pharm Pharmacol* 2010; 62: 381-388.
- 85 Wang CC, Chen LG, Yang LL. Cytotoxic activity of sesquiterpenoids from *Atractylodes ovata* on leukemia cell lines. *Planta Med* 2002; 68: 204-208.
- 86 Wang CC, Lin SY, Cheng HC, Hou WC. Pro-oxidant and cytotoxic activities of atractylenolide I in human promyeloleukemic HL-60 cells. *Food Chem Toxicol* 2006; 44: 1308-1315.
- 87 Dong H, He L, Huang M, Dong Y. Anti-inflammatory components isolated from *Atractylodes macrocephala* Koidz. *Nat Prod Res* 2008; 22: 1418-1427.
- 88 Lee JC, Lee KY, Son YO, Choi KC, Kim J, Kim SH *et al.* Stimulating effects on mouse splenocytes of glycoproteins from the herbal medicine *Atractylodes macrocephala* Koidz. *Phytomedicine* 2007; 14: 390-395.
- 89 Endo K, Taguchi T, Taguchi F, Hikino H, Yamahara J, Fujimura H. Antiinflammatory Principles of *Atractylodes* Rhizomes. *Chem Pharm Bull (Tokyo)* 1979; 27: 2954-2958.

- 90 Kang TH, Han NR, Kim HM, Jeong HJ. Blockade of IL-6 secretion pathway by the sesquiterpenoid atractylenolide III. *J Nat Prod* 2011; 74: 223-227.
- 91 Duan J, Wang L, Qian S, Su S, Tang Y. A new cytotoxic prenylated dihydrobenzofuran derivative and other chemical constituents from the rhizomes of *Atractylodes lancea* DC. *Arch Pharm Res* 2008; 31: 9650969.
- 92 Chen Z. The Acetylenes from *Atractylodes macrocephala*. *Planta Med* 1987; 53: 493-494.
- 93 Kano Y, Sakurai T, Komatsu K, Yamada H, Saito K. Polyacetylene Compounds from *Atractylodes* Rhizome. *Chem Pharm Bull* 1990; 38: 1082-1083.
- 94 Chen Z. Chemical constituents of *Atractylodes macrocephala* II: α -methylbutyryl derivatives of atractylentriol. *Acta Chimica Sinica* 1989; 47: 1022-1024.
- 95 Tsuchiya K, Sukenaga Y, Kuroiwa S. Physiological active substance NK12838, its manufacturing method, and a purpose. *Jpn Kokai Tokkyo Koho* 2002; 2002-363184.
- 96 Ohshiro T, Morita H, Nur EAA, Hosoda K, Uchida R, Tomoda H. Voluhemins, new inhibitors of sterol *O*-acyltransferase, produced by *Volutella citrinella* BF-0440. *J Antibiot* 2020; in press.
- 97 Huang XH, Nishida H, Tomoda H, Tabata N, Shiomi K, Yang DJ *et al.* Terpendoles, novel ACAT inhibitors produced by *Albophoma yamanashiensis*. II. Structure elucidation of terpendoles A, B, C and D. *J Antibiot* 1995; 48: 5-11.
- 98 Tomoda H, Tabata N, Yang D-J, Takayanagi H, Omura S. Terpendoles, novel ACAT inhibitors produced by *Albophoma yamanashiensis*. III. Production, isolation and structure elucidation of new components. *J Antibiot* 1995; 48: 793-804.
- 99 Xu L-L, Hai P, Zhang S-B, Xiao J-F, Gao Y, Ma B-J *et al.* Prenylated indole diterpene alkaloids from a mine-soil-derived *Tolypocladium* sp. *J Nat Prod* 2019;

82: 221-231.

- 100 Uchida R, Kim Y-P, Nagamitsu T, Tomoda H, Ōmura S. Structure elucidation of fungal sespendole, an inhibitor of lipid droplet synthesis in macrophages. *J Antibiot* 2006; 59: 338-344.
- 101 Kim H, Kochevar J. Isolation of brefeldin A. *Gen Pharmacol* 1995; 26: 363-364.
- 102 Mochizuki K, Ohmori K, Tamura H, Shizuri Y, Nishiyama S, Miyoshi E *et al.* The Structures of Bioactive Cyclodepsipeptides, Beauveriolides I and II, Metabolites of Entomopathogenic Fungi *Beuveria* sp. *Bull Chm Soc Jpn* 1993; 66: 3041-3046.
- 103 Elsworth JF, Grove JF. Cyclodepsipeptides from *Beauveria bassiana*. Part 2. Beauverolides A to F and their relationship to isarolide. *J Chem Soc, Perkin trans I* (10.1039/P19800001795) 1980: 1795-1799.
- 104 Grove JF. Cyclodepsipeptides from *Beauveria bassiana*. Part 3. The isolation of beauverolides Ba, Ca, Ja, and Ka. *J Chem Soc, Perkin trans I* (10.1039/P19800002878) 1980: 2878-2880.
- 105 Kretschmer A, Dorgerloh M, Deeg M, Hagenmaier H. The Structures of Novel Insecticidal Macrolides: Bafilomycins D and E, and Oxohygrolidin. *Agric Biol Chem* 1985; 49: 2509-2511.
- 106 Seto H, Akao H, Furihata K, Ōtake N. The structure of a new antibiotic, hygrolidin. *Tetrahedron Lett* 1982; 23: 2667-2670.
- 107 Hasumi K, Naganuma S, Koshizawa J, Mogi H, Endo A. Stimulation of acyl-CoA : cholesterol acyltransferase activity by brefeldin A in macrophage J774 cells. *Biochim Biophys Acta* 1993; 1167: 155-158.
- 108 Namatame I, Tomoda H, Tabata N, Si S, Omura S. Structure elucidation of fungal beauveriolide III, a novel inhibitor of lipid droplet formation in mouse macrophages.

J Antibiot 1999; 52: 7-12.

- 109 Kuzma M, Jegorov A, Kačer P, Havlíček V. Sequencing of new beauverolides by high-performance liquid chromatography and mass spectrometry. *J Mass Spectrom* 2001; 36: 1108-1115.
- 110 Bartz R, Seemann J, Zehmer JK, Serrero G, Chapman KD, Anderson RG *et al.* Evidence that mono-ADP-ribosylation of CtBP1/BARS regulates lipid storage. *Mol Biol Cell* 2007; 18: 3015-3025.
- 111 Fujiwara T, Oda K, Yokota S, Takatsuki A, Ikehara Y. Brefeldin A causes disassembly of the Golgi complex and accumulation of secretory proteins in the endoplasmic reticulum. *J Biol Chem* 1988; 263: 18545-18552.
- 112 Soni KG, Mardones GA, Sougrat R, Smirnova E, Jackson CL, Bonifacino JS. Coatamer-dependent protein delivery to lipid droplets. *J Cell Sci* 2009; 122: 1834-1841.
- 113 Stein O, Dabach Y, Hollander G, Ben-Naim M, Stein Y. Dissimilar effects of Brefeldin A on cholesteryl ester and triacylglycerol metabolism in CaCo2 and HepG2 cells as compared to peritoneal macrophages. *Biochim Biophys Acta* 1992; 1125: 28-34.
- 114 Kato N, Dong T, Bailey M, Lum T, Ingram D. Triacylglycerol mobilization is suppressed by brefeldin A in *Chlamydomonas reinhardtii*. *Plant Cell Physiol* 2013; 54: 1585-1599.
- 115 Kim S, Kim H, Ko D, Yamaoka Y, Otsuru M, Kawai-Yamada M *et al.* Rapid induction of lipid droplets in *Chlamydomonas reinhardtii* and *Chlorella vulgaris* by Brefeldin A. *PLoS One* 2013; 8: e81978.
- 116 Ohshiro T, Tomoda H. Isoform-specific inhibitors of ACATs: recent advances and promising developments. *Future Med Chem* 2011; 3: 2039-2061.

- 117 Tomoda H, Namatame I, Omura S. Microbial metabolites with inhibitory activity against lipid metabolism. *Proc Japan Acad B-Phys* 2002; 78: 217-240.
- 118 Bowman EJ, Siebers A, Altendorf K. Bafilomycins: a class of inhibitors of membrane ATPases from microorganisms, animal cells, and plant cells. *PNAS* 1988; 85: 7972-7976.
- 119 Pimentel-Elardo SM, Sørensen D, Ho L, Ziko M, Bueler SA, Lu S *et al.* Activity-independent discovery of secondary metabolites using chemical elicitation and cheminformatic inference. *ACS Chem Biol* 2015; 10: 2616-2623.
- 120 Sztalryd C, Brasaemle DL. The perilipin family of lipid droplet proteins: Gatekeepers of intracellular lipolysis. *Biochim Biophys Acta Mol Cell Biol Lipids* 2017; 1862: 1221-1232.
- 121 Sekiya M, Osuga J, Igarashi M, Okazaki H, Ishibashi S. The role of neutral cholesterol ester hydrolysis in macrophage foam cells. *J Atheroscler Thromb* 2011; 18: 359-364.
- 122 Singh R, Kaushik S, Wang Y, Xiang Y, Novak I, Komatsu M *et al.* Autophagy regulates lipid metabolism. *Nature* 2009; 458: 1131-1135.
- 123 Schott MB, Weller SG, Schulze RJ, Krueger EW, Drizyte-Miller K, Casey CA *et al.* Lipid droplet size directs lipolysis and lipophagy catabolism in hepatocytes. *J Cell Biol* 2019; 218: 3320-3335.
- 124 Ohshiro T, Kobayashi K, Ohba M, Matsuda D, Rudel LL, Takahashi T *et al.* Selective inhibition of sterol O-acyltransferase 1 isozyme by beauveriolide III in intact cells. *Sci Rep* 2017; 7: 4163.
- 125 Ohshiro T, Rudel LL, Omura S, Tomoda H. Selectivity of microbial acyl-CoA: cholesterol acyltransferase inhibitors toward isozymes. *J Antibiot* 2007; 60: 43-51.

- 126 Ohte S, Matsuda D, Uchida R, Nonaka K, Masuma R, Omura S *et al.* Dinapinones, novel inhibitors of triacylglycerol synthesis in mammalian cells, produced by *Penicillium pinophilum* FKI-3864. *J Antibiot* 2011; 64: 489-494.
- 127 Kobayashi K, Ohte S, Ohshiro T, Ugaki N, Tomoda H. A Mixture of Atropisomers Enhances Neutral Lipid Degradation in Mammalian Cells with Autophagy Induction. *Sci Rep* 2018; 8: 12099.
- 128 Bligh EG, Dyer WJ. A rapid method of total lipid extraction and purification. *Can J Biochem Physiol* 1959; 37: 911-917.